مؤتمر ريمار الدولي الرابع للعلوم الصرفة والتطبيقية

IV. International Rimar Congress of Pure, Applied Sciences

IV. Uluslararası Rimar Uygulamalı ve Teknolojik Araştırmalar Kongresi

JANUARY - OCAK - 2025

rimar.science@gmail.com

Rimar Academy
Publishing House

مؤتمر ريمار الدولي الرابع للعلوم الصرفة والتطبيقية

IV. International Rimar Congress of Pure, Applied Sciences

FULL TEXT BOOK

2025

ISBN 978-625-95642-9-6

Publishing House:	دار النشر:	Rimar Academy
Editor:	المحرر:	Prof. Dr. Ghuson H. MOHAMMED
Publication Coordinator:	تنسيق النشر:	AMIR MUAENI
ISBN:	نظام الترميز الدولى لترقيم الكتاب:	'978-625-95642-9-6'
DOI :	رقم معرف الكائن الرقمي:	http://dx.doi.org/10.47832/RimarCongress04
Printing:	تاريخ الطباعة:	05 / 03 / 2025
Date of The Congress:	تاريخ المؤتمر:	24- 25- 26 / 01 / 2025
Pages:	عدد الصفحات:	116
URL:	رابط النشر:	www.rimaracademy.com
Certificate Printing Press Number	رقم شهادة المطبعة:	47843

PREFACE

IV. International Rimar Congress of Pure, Applied Sciences was organized by Igdir University in collaboration with Rimar Academy. The primary objective of this event was to compile and disseminate valuable scientific knowledge and make a meaningful contribution to the future.

A substantial number of researchers from both local and international backgrounds demonstrated their interest in this conference. The scientific committee meticulously reviewed the submissions and ultimately accepted a select group of applicants—**48** in total—of whom **44** were approved by the scientific committee.

The core of this conference was the presentation of **33** full research papers, while the remaining articles and research findings are set to be featured in forthcoming issues of the MINAR Journal.

I would like to extend my sincere appreciation to all the contributors and scholars who played an essential role in making this conference a resounding success. Your dedication and valuable contributions are deeply respected and acknowledged.

Editor-in-Chief
Prof. Dr. Ghuson H. MOHAMMED

الرؤساء الفخريون
HONORARY COMMITTEE

Prof. Dr. Mehmet Hakkı ALMA

Rector of Iğdır University

Türkiye

Prof. Dr. Waad Mahmood RAOOF

Rector of Tikrit University

Iraq

Prof. Dr. Alyaa A. Ali Al-ATTAR

Rector of Northern Technical University

Iraq

Prof. Dr. Tariq Hafdhi Abbd Tawfeeq

President of the University of Al-Farhidi

Iraq

Prof. Dr. Khamis A. ZIDAN

Vice Rector of Al-Iraqia University for Scientific Affairs

Iraq

رئيس المؤتمر
CHAIR OF CONGRESS

Prof. Dr. Ghuson H. MOHAMMED

Baghdad University

Iraq

رئيس الهيئة التحضيرية
Chairman of Organizing Committee

Prof. Dr. Muneer salim TAHA

Vice-president for Scientific Affairs of the University of Mosul

Iraq

الأمين العام للمؤتمر
General Secretary

Prof. Dr. Abdulkareem Dash ALI

Tikrit University

Iraq

الهيئة الاستشارية
CONSULTATIVE COMMITTEE

Prof. Dr. Jamal Naser Abed AL_ Rahman AL _Sadoon
Wasit University
Iraq

Prof. Dr. Nezar Husein Ata Samarah
Jordan university of Science and Technology -Jordan

Prof. Dr. Ebtehag Zeki Sulyman Al Halim
University of Mosul
Iraq

Prof. Dr. Hayajneh, Firas Mahmoud Faleh
Free University, Berlin-Germany
Jordan

Dr. Eman SHARAF
Animal Health Research Institute
Egypt

Dr. Nabil Mohie Abdel–Hamid ALY
Kafrelsheikh University
Egypt

Dr. Bader AL-AİFAN
Kuwait University
Kuwait

Dr. Osman TÜRK
Harran University
Türkiye

Dr. May Ahmed Fakhry Farhat Mousa
Alexandria University
Egypt

الهيئة التحضيرية
ORGANIZING COMMITTEE

Prof. Dr. Lubna Abdulazeem Majeed AL-Bayati
University of Babylon
Iraq

Prof. Dr. Nihad Abdul-Lateef Ali
Al-Qasim Green University
Iraq

Prof. Dr. Mahmood Ahmad Hamood
University of Mosul
Iraq

Prof Dr Najwa Ibrahim Al-Barhawee
University of Mosul
Iraq

Assist. Prof. Iman radha JASIM
University of Mosul
Iraq

Assist. Prof. Jalil Talab ABDULLA
Wasit University
Iraq

Assist. Prof. Dr. Methaq Abd Muslim GUDA
University of Kufa
Iraq

Lec.Dr. Hadeel Salih Mahdi
University of Misan
Iraq

Lect. Dr. Bassim Kareem Mihsin
General Directorate of Education in Karbala
Iraq

Dr. Haleemah Jaber MOHAMMED
Uruk university
Iraq

Dr. Riyam Adnan Hammudi Al inizi
College of Medicine, Wasit University
Iraq

Dr. Ihab Qays Ali Aldalawi
f Ibn Sina university for medical and pharmaceutical sciences
Iraq

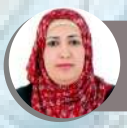

Dr. Esraa Habeeb Khaleel
Tikrit university
Iraq

الهيئة العلمية
SCIENTIFIC BODY

Prof. Dr. Israa Abdul Razzaq Majed Al-Dobaissi
University of Baghdad
Iraq

Prof. Dr. Nawras Abdelah Alwan
Basrah University
Iraq

Prof. Dr. Baida Muhsen Ahmed
Mustansiriyah University
Iraq

Assist. Prof. Dr. Alaa Yaseen Taha Taqa
University of Mosul
Iraq

Assist. Prof. Dr. Rasha jawad kadhim
University of Sumer
Iraq

Assist. Prof. Dr. Fatima Rammadan ABDUL
Mustansiriyah University
Iraq

Assist. Prof. Dr. Ali faisal alsaad
Southern Technical University
Iraq

Assist. Prof. Dr. Intisar Ghanim Taha
Damascus University
Syria

Assist. Prof. Dr. Nihad Taha Mohammed JADDOA
University of Baghdad
Iraq

Assist . Prof . Dr. Ielaf O Abdul Majjed
University of Mosul
Iraq

Assoc. Prof. Dr. Eda M. A. Alshailabi
Omar Almukhtar University
LIBYA

Assist. Prof. Dr. Raghad Mukdad Mahmood AL.Hamdani
Tikrit University
Iraq

Lect. Dr. Sabah Noori HAMMOODİ
AShur University Collage
Iraq

Lect. Dr. Hadeel Waleed Abdulmalek AlJirjees
Baghdad University
Iraq

Lect. Dr. Shayma Muhsen Ahmad
Al-Nahrain University
Iraq

Lect. Dr. Eslah shakir rajab
Al-Karkh University of Science
Iraq

Lect. Dr. Aseel younis Khalaf Alnaimy
University of Babylon
Iraq

Lect. Dr. Mohammed Ali Hassan albeayaty
Al-Karkh University of Science
Iraq

Dr. Muslim Muhsin ALI
University of Missouri
USA

Dr. May Ahmed Fakhry Farhat Mousa
Alexandria University
Egypt

Dr. Abeer Saleem AbduKreem Almamury
University of Babylon
Iraq

Dr. Husam R. ABED
Ministry of Education
Iraq

Dr. Raja'a Al-Naimi
University of Petra
Jordan

Dr. Batool Abd Al Ameer Baqer ALSAFAR
Al Mustansiriyah University
Iraq

Dr. Mutasim Ali Mohamed ELAGAB
Gezera University
Sudan

Lect. Dr. Hind Abdulrazzaq Mohammed Ali
University of Technology
Iraq

Assist. Prof. Dr. Zina Bakir Al-Hilli
Al-Qasim Green University
Iraq

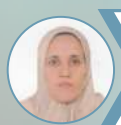

Dr. FOUZIA Youcef
University of Kasdi Merbah Ouargla
Algeria

Lect. Dr. shahbaa fayadh bdewi
University of Anbar
Iraq

Assist. Prof. Dr. Najat Jalil Noon
Ministry of Education
Iraq

Assist. Prof. Dr. Liqaa Zeki Hummady
University of Baghdad
Iraq

Prof. Dr. Sundus Nsaif Abed Alhuchaimi
University of Kufa
Iraq

INDEX

INDEX


150

Elucidation of some morphological features in chaste tree and yellow bells

Lamiaa A. Gharb [1]

Lubab G. Ali [2]

Abstract

By examining many exterior aspects, morphology offers crucial classification criteria for plants. Vitex agnus-castus L. (Chaste tree) and Tecoma stans (Yellow bells) which are fantastic for the landscaping of the house were chosen in the current study. Some parts of these two plants were examined to investigate morphological features to facilitate their recognition in our gardens and not be confused with other plants. Important morphological variations appeared in chaste tree flowers colors. This plant appeared to have different varieties which have flowers (white, Pink. Purple) in colors. The morphology of flowers. fruits and seeds for the two plants revealed an important taxonomical feature. On the other hands. Trichomes appeared in the male reproductive organ for the two plants. Despite the modern approach in botany the morphology represents the basic and important study to identify different plants species and varieties.

Keywords: Lamiaceae, Chaste Tree, Cultivated Plants, Tecoma Stans.

http://dx.doi.org/10.47832/RimarCongress04-1

[1] Department of Biology, College of Science, University of Baghdad, Iraq lamya.gharb@sc.uobaghdad.edu.iq

[2] Department of Biology, College of Science, University of Baghdad, Iraq lobab.ali1102@sc.uobaghdad.edu.iq

Introduction

Morphological studies, which focused on vegetative and reproductive characteristics create a profile of the plant that can be used to identify species, varieties, cultivars and make broad comparisons. Adding beauty and intrigue to any environment is one of the main advantages of ornamental plants. In gardens and parks, ornamental plants can be used to create colorful displays that attract visitors and provide a peaceful and relaxing atmosphere. Ornamental plants may enhance indoor spaces in houses by adding color and texture. They can also help to improve indoor air quality and purify the air [1]. Vitex agnus –castus L. which is called (Monk pepper,chaste tree) belongs to order lamiales and lamiaceae family is a lovely deciduous tree with a maximum height of (6 -7) meters, and spreads over River banks in southern Europe, the countries of the Mediterranean, Central Asia and the Middle east [2].

For over 2500 years, the fruits of this plant have been used to treat a range of gynecologic issues in ancient Egypt, Greece, Iran, and Rome. Additionally, it has been used for its purported ability to lower libido [3]. The leaves and fruits of V. agnus castus are suitable candidates to be used in food as flavor and spice, and the berries can be used in place of pepper in traditional Persian medicine [4,5]. The fruit has been suggested as a hormone-like treatment for menstruation problems, as well as for digestive diseases, antiepileptic, carminative, energizer, sedative, anticonvulsant, and tranquilizer [6,7]. According to various countries' traditional medical practices, this plant is used to cure eye conditions, spasmodic dysmenorrhea, inadequate lactation, acne, snakebites, scorpion stings, stomachaches, and as an antispasmodic [8, 9].

Tecoma stans L. is a common upright shrub belongs to the Bignoniaceae family and the Lamiales order. Other English names for this plant include trumpet flower, yellow bells, yellow elder, and Piliya in India [10]. This significant medicinal plant has long been used to cure a wide range of illnesses. It has been utilized in South and Latin America to lower blood sugar levels. This plant's roots, leaves, and bark have all been utilized in herbal medicine for a number of reasons. Bark exhibits modest cardiac tonic and smooth muscle relaxing properties. Applications include the experimental management of yeast infections, diabetes, digestive issues, and other medical conditions. It has a number of substances that are known to have catnip-like effects on cats. This plant's root is said to have strong diuretic and tonic properties. To treat snake and rat bites, the root is ground and used externally, a small amount are also consumed internally [11,12].

Since the morphology of medicinal plants which are cultivated in gardens represent an important field for identification the proper species so this research aimed to describe some parts of these plants.

Material and methods

Samples of Vitex agnus-castus and Tecoma Stans which were investigated in this study were collected from gardens. This research was done by using (Dissecting Microscope, Light, needles, forceps and graph paper).

Results and discussion

1.Vitex agnus-castus (chaste tree):

Leaves:

The leaves are light aromatic and arranged oppositely. Leaves are usually Palmately compound which consist from (5-6) leaflets. The leaflets shape is lanceolate with entire margins, have dark green color in the upper surface and light green to gray color in the lower surface. (fig.1).

Figure 1: Leaf shape of Vitex agnus-castus

The inflorescence is axillary, raceme consist from numerous opposite florets with cymose arrangement (mixed inflorescence) (fig. 2 A). Corolla shape is tubular to funnel. The color is lilac to purple. It consists from 5 petals (one large and the others are small) The corolla is bilabiate, the outside surface is pubescent and the calyx is shorter than corolla with hairy or woolly surface consist from 5 teeth (fig. 2 B).

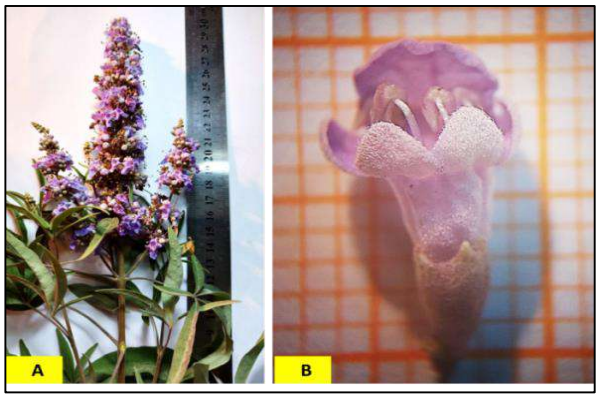

Figure 2: Shape of Vitex agnus-castus: A: inflorescence and B:flower

On the other hand one of an important morphological variations appeared in chaste tree flowers colors. This plant may have different varieties with flowers (white, Pink. Purple) in colors (fig.3).

Figure 3: Different colors in chaste tree flowers

On the other hand Adamov and Rendyuk (13), point out that earlier researches that described the varieties and forms of chaste trees based on bloom color had a new perspective in current taxonomy that took into account the ancient infra species rankings as being equivalent to V. agnus-castus.

Androecium consist from four stamens didynamous. Filament base contains long hairs at the point of corolla attachment (fig.4 A)The anther is oblong to elliptic with violet color contains glandular hairs at the edge. (fig.4 B)

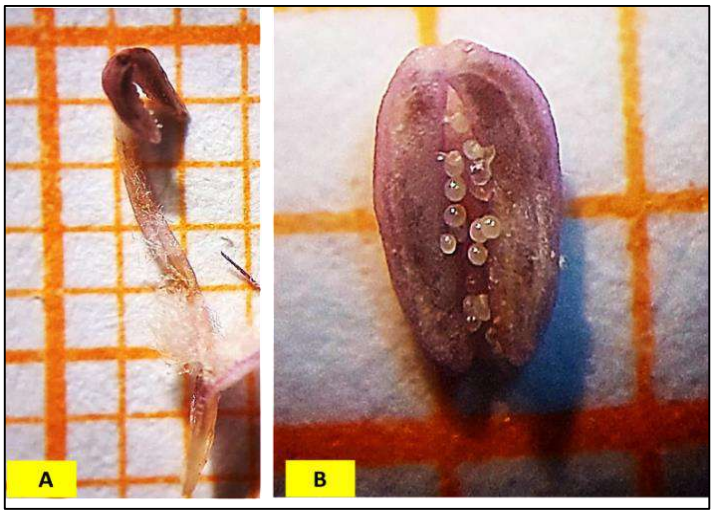

Figure 4: Shape of Vitex agnus-castus:A: hairy filament base and B:glandular hair in anther

Gynoecium: consist from round yellow ovary and the style is elongated and purple in color, the stigma is divided into two parts from the anterior end (fig.5).

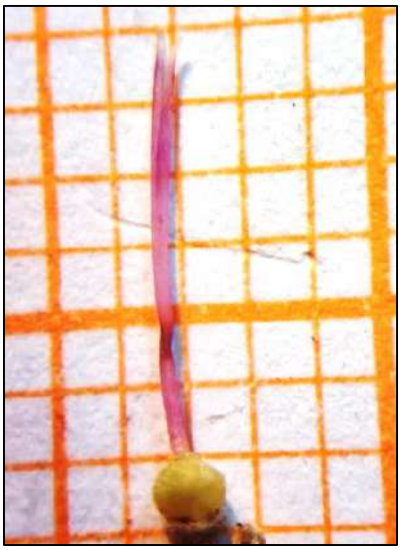

Figure 5: Shape of Vitex agnus-castus pistil

Fruit: the shape of fruit is ubovate to globular (fig.6), the color is dark brown to black and it has a persistent grey calyx that is delicately hairy with small terminal teeth. The chaste tree's fruit contains a number of secondary metabolites that are crucial to human health, including flavonoids, phenol carboxylic acids, and terpenoids, which are the primary constituents of essential oil..[13]

Figure 6: Shape of Vitex agnus-castus fruit

2. Tecoma stans:

An evergreen tree with compound leaves that are bright green all year round. Phyllotaxy is opposite and it is pinnately compound **(**imparipinnate) made up of (5 to 11) leaflets, the leaf margin is serrate and the venation is pinnate, the shape of each leaflet is lanceolate to ovate (fig.7).

Figure 7: Shape of Tecoma stans leaf.

Inflorescence is raceme (fig 8 A). The flowers have five lobed petals and a bell to funnel shape (fig.8 C).The Corolla color is bright yellow with vertical crimson stripes along the inner throat. The corolla, which has five petals and resembles a trumpet, emerges from the calyx. The calyx is uniformly long and 5-dentate (figure 8 B) .

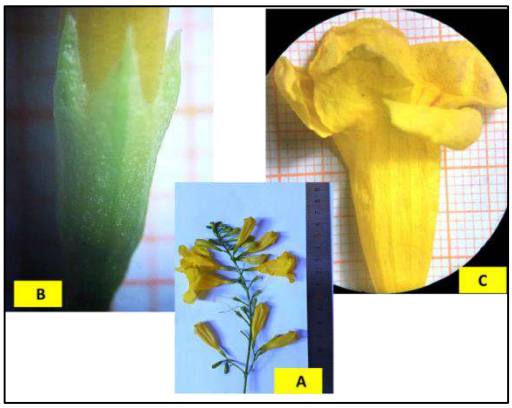

Figure 8: Shape of Tecoma stans: A:Inflorescence, B:Calyx, C:Corolla

Androecium: four stamens with a sagittate anther and a didynamous form (fig. 9 A).There are glandular hairs at the base of the filaments. The petals are connected to this foundation..(fig.9 B).

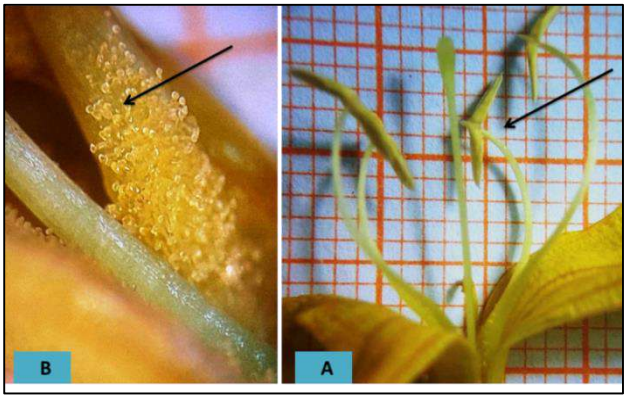

Figure 9: Shape of Tecoma stans: A:anther, B: hairs in the base of the filament.80X

Gynoecium: ovary slightly elongate with long filiform style and stigma consists of the two lobes (figure 10).

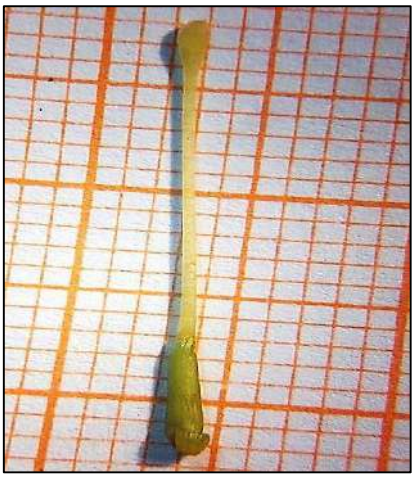

Figure 10: Shape of Tecoma stans Pistil

Fruit and seeds:

The fruit is Capsule (linear and tapering) at the ends, surface lenticellate (fig.11A). These pods contain seeds with wings hyaline- membranaceous, sharply appear from the seed body.(fig.11 B)

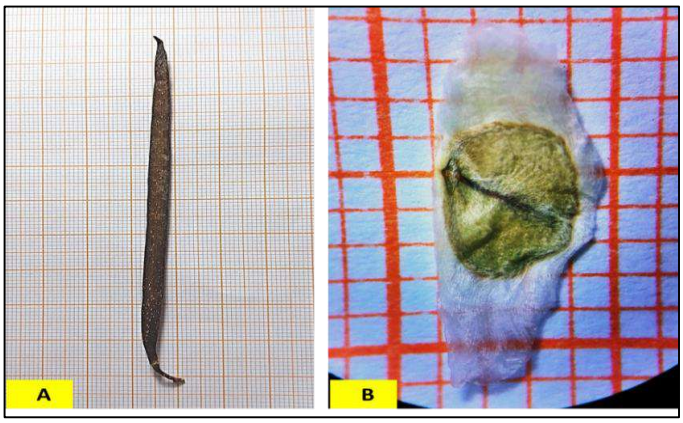

Figure 11: Shape of Tecoma stans: A:Fruit , B:Seed

Tecoma stans is taxonomically complicated, due to its morphological variability critical morphological study determined two sub species; T. stans var. angustata and var. stans. Stem anatomical characters are also found important to distinguish the varieties within the species [14]. It is crucial to understand the morphological characteristics and even common names of ornamental plants, which can serve as significant living elements in urban areas.

For instance, Vitex agnus-castus L. is a fragrant tree that is widely used as a medicinal plant in the Middle East and Europe. [15]. In Iraq, this plant is commonly referred to as "Maryam's palm" because of its complex palmate leaves, which have several leaflets that resemble an open hand numbering system (5-7) and uneven leaflets that resemble fingers while according to local herbalists and even certain studies [16] ; the common name of the plant Anastatica hierochuntica is Mary hand (fig.12)

Figure 12: Anastatica hierochuntica

Conclusions

Cultivated and ornamental plants represent significant living components of urban environments, and if the right species are employed, they can provide important ecosystem services like shade, beauty and preserve soil and air quality.Despite the modern approach in botany the morphology represent the basic and important study to identify different plants species and varieties.

References:

[1] Wallace JG, Bradbury PJ, Zhang N, Gibon Y, Stitt M, Buckler ES.2014. Association mapping across numerous traits reveals patterns of functional variation in maize. PLoS Genet. 10(12):e1004845

[2] Anonymous Chaste Tree. In: Dombek C, editor. Lawerence.1998. Review of Natural Products. St. Louis: Facts and Comparisons.

[3] Roemheld-Hamm B.2005. Chasteberry. Am Fam Physician .72 :821-824.

[4] Li S, Qiu S, Yao P, Sun H, Fong HH and Zhang H.2013. Compounds from the fruits of the popular European medicinal plant Vitex agnus-castus in chemoprevention via NADP (H):Quinone oxidoreductase type 1 induction. Evid Based Complement Alternat Med : 432829.

[5] Amin, G.R.1991.Popular Medicinal Plants of Iran. Iranian Research Institute of Medicinal Plants, Tehran, 1-66. (In Persian).

[6] Ghannadi A, Bagherinejad M, Abedi D, Jalali M, Absalan B, Sadeghi N, et al. 2012.Antibacterial Activity and composition of essential oils from Pelargonium graveolens L'her and Vitex agnus-castus L. Iran J Microbiol .4:171-176.

[7] Khalilzadeh E, Vafaei Saiah G, Hasannejad H, Ghaderi A, Ghaderi S, Hamidian G.2015. Antinociceptive effects, acute toxicity and chemical composition of Vitex agnus-castus essential oil. Avicenna J Phytomed ;5(3) :218- 30.

[8] Zhou J, Hu H, Long J, Wan F, Li L, Zhang S, Shi YE, Chen Y.2013. 5-11 Vitexin 6, a novel lignan, induces autophagy and apoptosis by activating the Jun N-terminal kinase pathway. Anticancer Drugs . 24(9) :928 -936.

[9] Tandon S, Mittal AK, Pant AK.2008. Insect growth regulatory activity of Vitex trifolia and Vitex agnus-castus essential oils against Spilosoma obliqua. Fitoterapia 79(4): 283-286

[10] Liogier HA.1990. Plantas medicinales de Puerto Rico y del Caribe, Iberoamericana de Ediciones, Inc., San Juan, PR; 566.

[11] Sharma P.C., Dennis T. J.2000. Data Base on Medicinal Plants used in Ayurveda.Vol- I . CCRAS, New Delhi : 378-83.

[12] Jadhav D. 2006.Ethanomedicinal plants used By Bhil tribe of Bibdod, Madhya Pradesh. Indian Journal of Traditional Knowledge ; 5(2):263-267.

[13] Adamov G. V., T. D. Rendyuk , O. L. Saybel , T. D. Dargaeva , A. N. Tsitsilin , D. O. Bokov.2022. Vitex agnus-castus : Botanical features and area, chemical composition of fruit, pharmacological properties, and medicinal uses Journal of Applied Pharmaceutical Science Vol. 12(03), pp 034-044.

[14] Anish Babu V B and V T Antony.2018.Comparative Morphology and Stem Anatomical Studies of Tecoma stans (Bignoniaceae) in Kerala. International Journal of Vol. 7(2):1033-1035.

[15] Gökbulut, A., Özhan, O., Karacaoğlu, M., & Şarer, E.2010. Radical scavenging activity and vitexin content of Vitex agnus castus leaves and fruits FABAD J. Pharm. Sci., 35, 85-91.

[16] Siti Rosmani Md Zin , Normadiah M. Kassim, Mohammed A. Alshawsh, Noor Eliza Hashim,Zahurin Mohammed.2017. Biological activities of Anastatica hierochuntica L.: A systematic review .Biomedicine & Pharmacotherapy.Vol. 91, Pages 611-620.

Histological Effect of RAD 140 Supplement on testis of Rats

Ban Jasim Mohamad [1]

Faiza Kadhim Emran [2]

Bassam Kareem Abdul ameer [3]

Abstract

bind to androgen receptors and function either as agonists, partial agonists, or antagonists. One of them is a new brand known as (RAD-140). There are limited clinical studies evaluating the pharmacokinetics profile, adverse effects, and drug interactions of RAD 140 on body organs. This task aims to evaluate the histological effect of this supplement on testes of albino rats. **Methods:** eighteen of albino rats were randomized into 2sets; the control set of 3 rats, and the test set which contained 15 rats, scattered into 5 subsets of 3 animals for each, individually got a daily mouth dosage of 0.3 ml of the following concentrations of drug (1.25 mg/ml, 2.5 mg/ml, 5 mg/ml, 10 mg/ml, 20 mg/ml) respectively. After 45 days of dosing, the animals were sacrificed, testes had been isolated, fixed in formalin, dehydrated in ethanol, and cleared in xylol. The fixed tissues were embedded in wax and cut into thin section of 5 µm which then were attached to glass slides and stained with routine stain(H&E) and being ready for microscopic examination. **Results:** The current outcome showed that after 45 days of RAD 140 doses, there were dose-dependent alterations in the morphology and histology of the testes. The study found that different concentrations of Rad 140 were associated with different degrees of structural alterations in the testes tissue. **Conclusion**: the result of this study provides a proof of testes toxicity due to RAD140 usage. This leads us to suggest the using of the lowest possible amount of RAD140 to minimize its harmful effect. Extra investigation is needed to understand the mechanisms behind rad 140's effects on other body organs and to validate these findings in human. Overall, caution is advised in RAD 140 use, especially concerning testes health.

Keywords: *Androgenic Steroids, Anabolic, RAD 140, Toxicity, Selective Androgen Recep*

http://dx.doi.org/10.47832/RimarCongress04-2

[1] Department of Biology, College of science, University of Baghdad, Iraq ban.jasim@sc.uobaghdad.edu.iq

[2] Department of Biology, College of science, University of Baghdad, Iraq

[3] Department of Biology, College of science, University of Baghdad, Iraq

Introduction

RAD140 is a member of the class of new androgenic medicines known as selective androgen receptor modulators (SARMS). As its term infers, SARM encourages the development of flexible bones and muscles while having less of an effect on the receptors found in tissues that are dependent on testosterone, such as the skin, prostate, and testis. SARMs brands vary in structure and are primarily they are non-steroidal in origin.

The agonistic action on the androgen receptor (AR) is a characteristic shared by all SARMs. Despite being tissue selective, SARMs have attracted profuse concern in the medical field over 20 years ago because they are thought to be a potential therapeutic avenue for conditions involving bone damage, weakness, or muscle atrophy because they promote muscle growth and strength, which is advantageous for those seeking for performance-enhancing ingredients, especially in resistance sporting such as weightlifting or bodybuilding [1 , 2].

Similar to androgens, SARMs enter the cytoplasm and displace heat shock proteins' androgen receptor. After they bonded, they travel to the nucleus where they bind to androgen response elements (ARE) to function as transcription factors. Different co-regulatory proteins assist in shaping and modifying the transcriptional response, depending on the tissue type and the cell's regulatory environment [3].

SARMs have been investigated as possible therapies for multiple sclerosis, Alzheimer's illness, osteoporosis, cancer, sexual dysfunction, and muscle atrophy, and recently they have been included in a number of supplements targeted in athletes. Potential adverse outcomes including erythrocytosis, prostate enlargement, hepatotoxicity, aromatization to estrogen, and testicular atrophy, frequently limit their therapeutic usage [4, 5].

SARMs have also been shown to change liver function, lower endogenous testosterone, and impact cholesterol levels. According to recent pharmacological reports, SARMs offer a wide range of potential clinical uses and show promise for the safe treatment of breast cancer, prostate cancer, benign prostatic hyperplasia, cachexia, and hypogonadism [6, 7].

The new brand RAD 140 is found to have many advantages for the fact that it is tissue selective, but little is known about its disadvantages since its mechanism is not well understood[8].

In breast cancer, oral prescription of RAD140 significantly repressed the growth of AR/ER^{+} breast cancer patient-derived xenografts (PDX). Stimulation of AR and suppression of

ER trail, together with the *ESR1* gene, were noticed during RAD140 treatment. Co-dosage of RAD140 and Palbociclib showed enhanced efficiency in the AR/ER$^+$ PDX models. In line with efficacy, a subset of AR-repressed genes associated with DNA replication is suppressed with RAD140 treatment, an effect apparently enhanced by concurrent administration of Palbociclib. This leads to a conclusion that RAD140 is a potent AR agonist in breast cancer cells with a distinct mechanism of action including the AR-mediated repression of *ESR1*, it impedes the growth of multiple AR/ER$^+$ breast cancer PDX models as a single agent, and in combination with Palbociclib [9].

SARMs products cannot however be sold to the general public as dietary supplements, and no claims about their advantages may be made. It is uncertain how SARMs in general interact with other substances, such as alcohol and other narcotics, especially when used in high doses over an extended period of time. Even though it is known that the treatment of RAD140 may be associated with side effects on body organs, but the effects on testes tissue are not determined precisely [10, 11]. Therefore, this assignment has been designed to evaluate the consequence of different concentrations of one of these brands; the RAD140, on testis tissues of rats.

Materials and Methodology

A cluster of eighteen, six-week-old male albino rats, weighting (250-350gm) were selected and reserved under optimal environmental conditions. They were randomized into 2sets; the control set of 3 rats, received regular lab nutrients without treatment. And the test set which contained 15 rats, scattered into 5 subsets of 3 animals for each, individually got a daily mouth dosage of 0.3 ml of the following concentrations of drug (1.25 mg/ml, 2.5 mg/ml, 5 mg/ml, 10 mg/ml, 20 mg/ml) respectively. After 45 days of dosing, the residual rats sacrificed and testes had been isolated, fixed in 4% formaldehyde solution, dehydrated in growing sequences of ethanol, and cleared in xylol, the fixed tissues were embedded in wax and cut into thin section of 5 μm which then were attached to slides and stained with routine stain and being ready for microscopic examination.

Results

Control animals: The microscopic appearance of the testes in control group showed normal structure of seminiferous tubules that appear with normal Sertoli cells, with cytoplasm that extends between the germ cells, numerous germ cells, small basophilic oblong spermatozoa are

seen toward the center lumen of the tubules. Also, there is an active spermatogenesis that appear

with normal Leydig cells which seen as pink in color in the interstitial tissue (figure1).

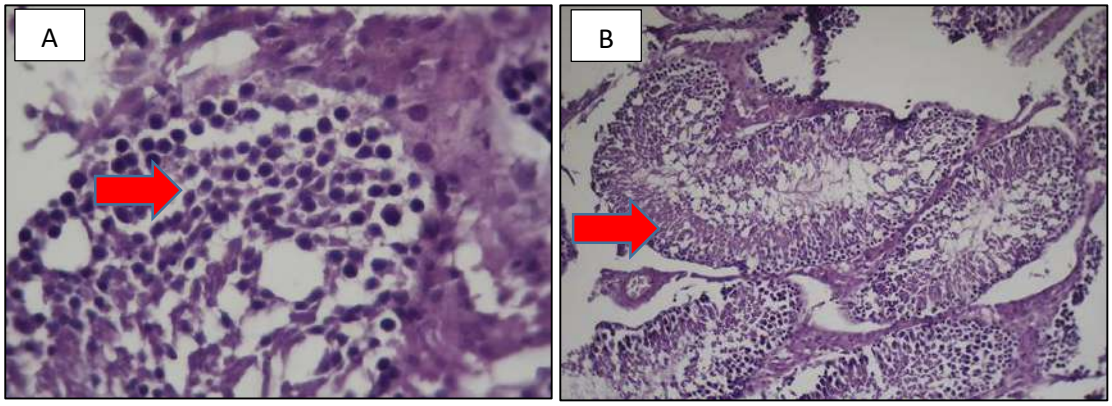

Figure 1: section in testes of control animals showing normal structure of seminiferous tubules.

A: active spermatogenesis that appear with normal Leydig cells **(H&E stain, 40X).**

B: normal structure of seminiferous tubules that appear with normal sertoli cells. **(H&E stain, 10X).**

1. Effect of 1.25 mg/ml and 2.5 mg/ml doses of drug on testes tissues:

The histopathological changes in these subgroups were identical and characterized by focal atrophy of testicular tubules, and mild area of orchitis that seen with atrophy spermatogonia (figure 2 A). In some sections we recorded loss of germ cells, with remaining tall pinkish (eosinophilic) color of sertoli cells (figure 2 B).

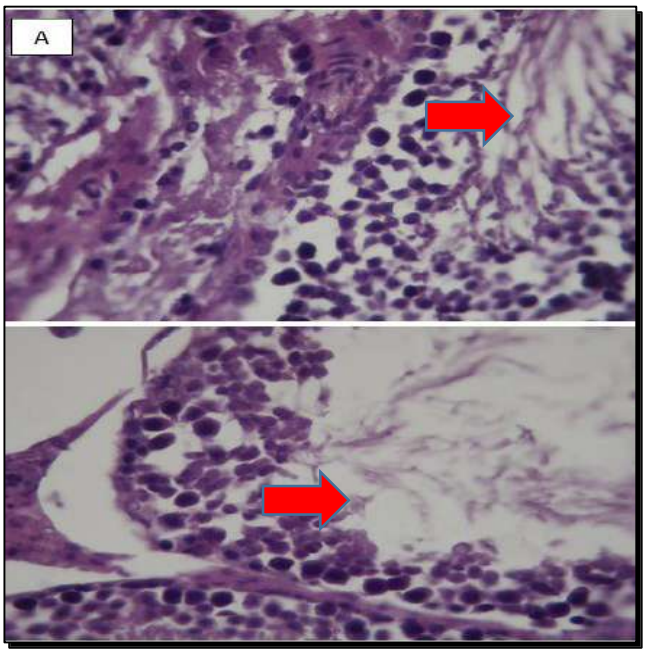

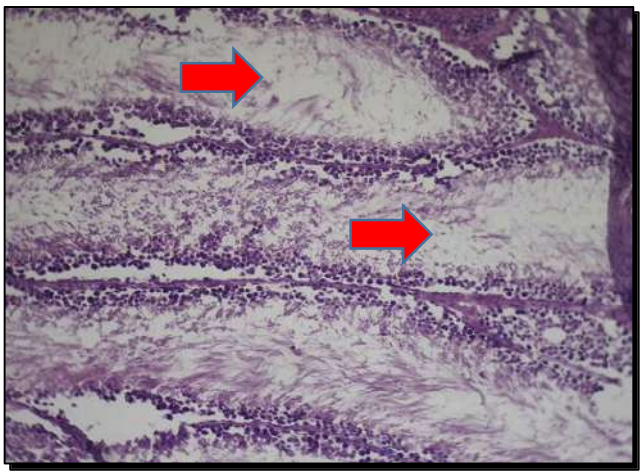

Figure 2A: sections of testes of subgroups 1 and 2 showing focal atrophy of testicular tubules, and mild area of orchitis that seen with atrophy spermatogonia(H&E stain, 40X).

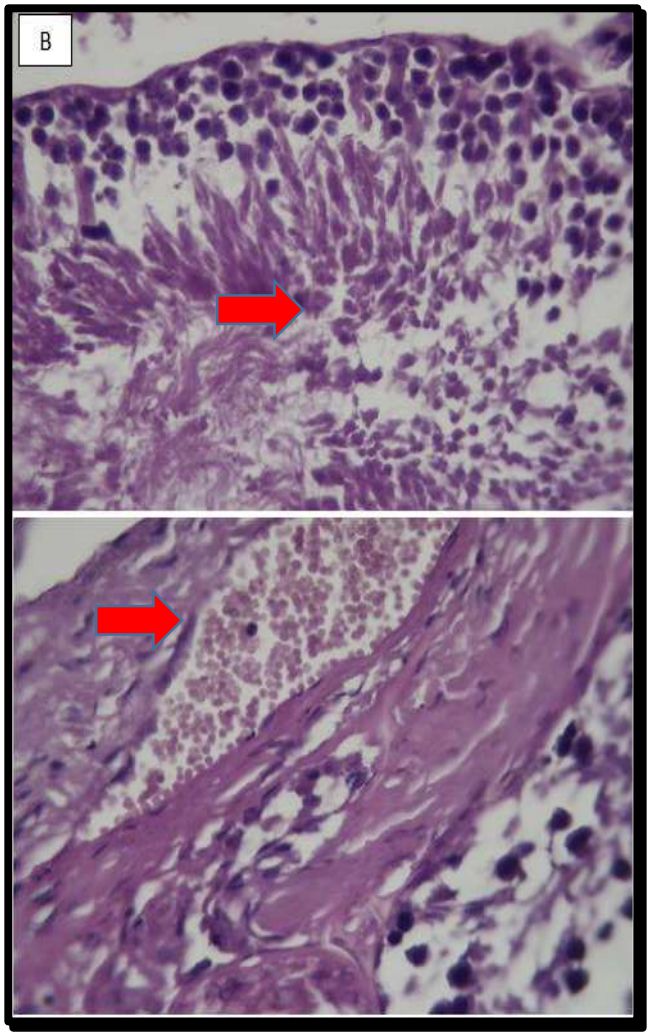

Figure 2B: sections of testes of subgroups 1 and 2 showing loss of germ cells, with remaining tall pinkish (eosinophilic) color of sertoli cells (H&E stain, 40X).

2. Effect of 5 mg/ml dose of drug on testes tissues:

histopathological changes in this group showed atrophic testicular tissue demonstrated with loss of germ cells and orchitis with pinkish color of sertoli cells associated with fibrocytes′ infiltration in the peritubular and interstitial regions. In other section there is a mild desquamation of the epithelial lining that generated the spermatids (figure 3 A, B & C).

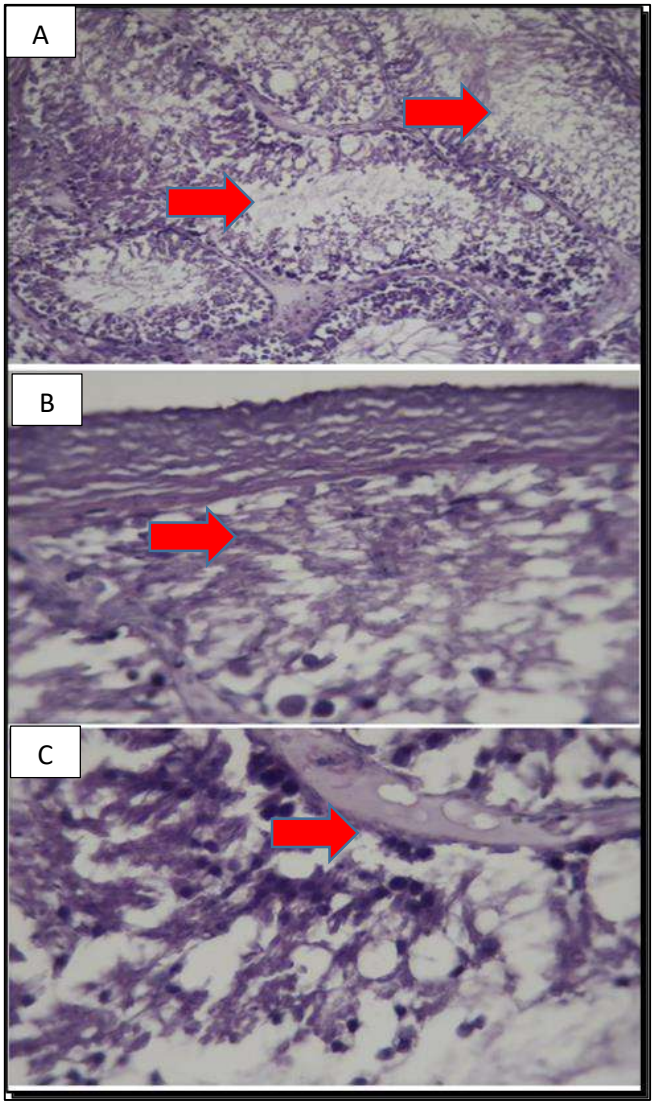

Figure 3: sections of testes of subgroups 3 showing: A: atrophic testicular tissue that monstrated with loss of germ cells. B: orchitis with still remaining pinkish color of sertoli cells associated ith fibrocyte infiltration in the peritubular and interstitial regions. C: mild desquamation of the epithelial lining that generated the spermatids. (H&E stain, 40X).

3. Effect of 10 and 20 mg/ml doses of drug on testes tissues:

The histopathological changes in these subgroups were similar but with severe pattern in subgroup5 (20mg/ml). The changes included severe desquamation and loss of the epithelial

lining that generated the spermatid, severe infiltration of inflammatory cell within interstitial tissue and congestion of blood vessels (figure 4 A and B). other section revealed epithelial metaplasia of epithelial lining to give shape near from cuboidal to flatted like cell. In some sections spermatocyte appeared large with vesicular nuclei, and pale watery cytoplasm (Figure4 C and D).

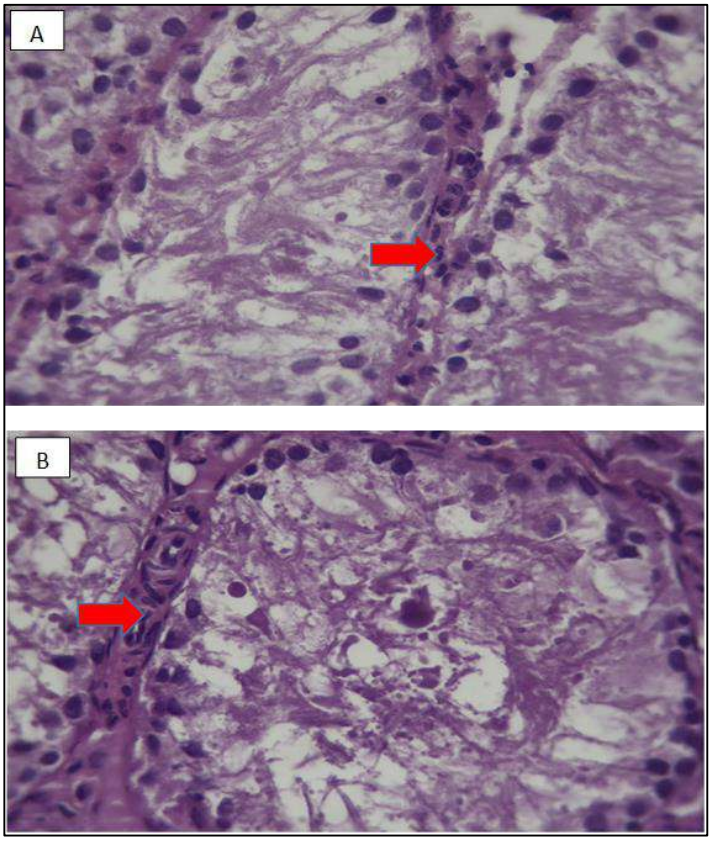

Figure 4: sections of testes of subgroups 4&5 showing: A: severe desquamation and loss of the epithelial lining that generated the spermatid. B: severe infiltration of inflammatory cell within interstitial tissue and congestion of blood vessels (H&E stain, 40X).

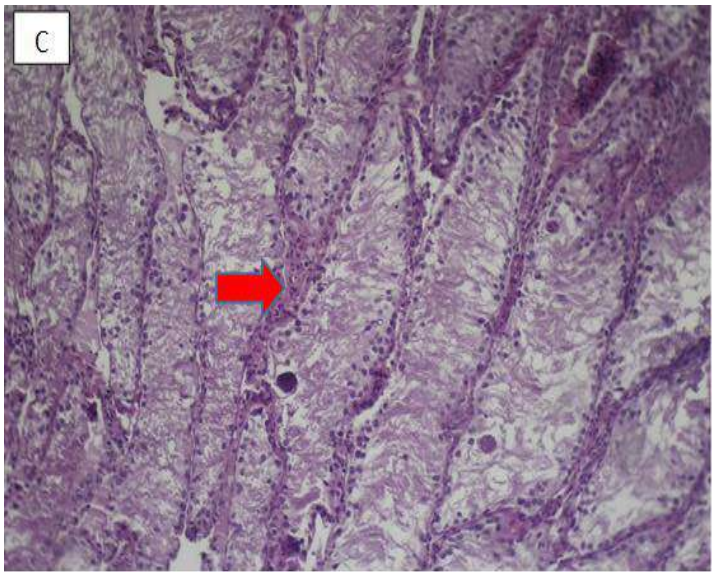

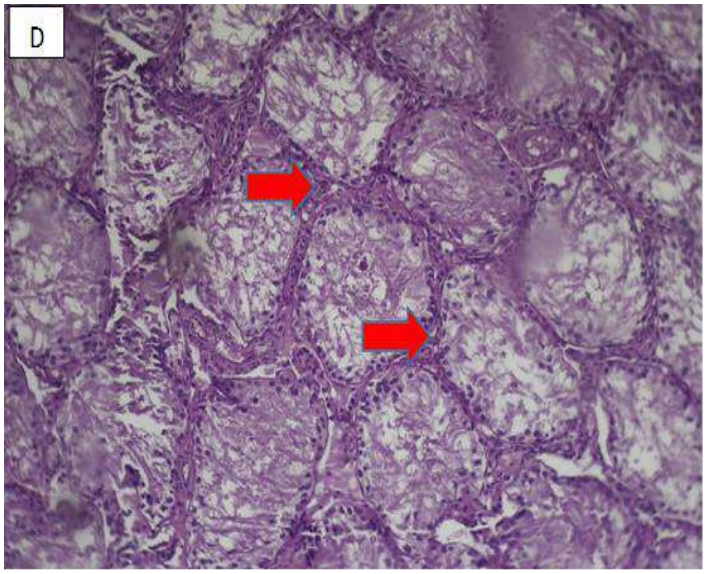

Figure 4: C and D showing epithelial metaplasia of epithelial lining to give shape near from cuboidal to flatted like cell. (H&E stain, 10X).

Discussion

Over the past ten years, there has been an increasing public health concern about the increased recreational use of performance-enhancing drugs (PEDs), such as SARMs and GH secretagogues, which are marketed as commercially available supplements. This is due to a lack of knowledge about the negative effects of these drugs. The majority of PEDs are currently used by non-athletes in the form of these supplements, despite the fact that their use has historically been linked to elite athletes. These supplements frequently include unapproved and unreported ingredients, which raises the possibility of unfavorable side effects [12].

In this work, different concentrations of one of these supplements; RAD 140 were examined and how it affected the testis tissue of male albino rats. Our findings showed that after 45 days of RAD 140 doses, there were dose-dependent alterations in the morphology and histology of the testes. The study found that different concentrations of Rad 140 were associated with different degrees of structural alterations in the testes tissue. Higher doses produced more noticeable effects, whereas lower doses had lesser effects. The observed histological changes suggest that the testes′ cellular composition and structural integrity changed in response to RAD 140 exposure. Comparing our results with existing researches can deepen our understanding of RAD 140's impact on testes health and inform clinical decisions [13]. A study by Budaya *et al* 2024, found no differences in testosterone levels, prostate mass, or the ratio of fibromuscular stroma to epithelium area in rats undergoing bilateral orchiectomy and placebo surgery with the administration of SARM RAD140[14].

The FDA has not approved selective androgen receptor modulators (SARMs), and it is against the law to get SARMs for personal use. However, the usage of SARMs by recreational sportsmen is growing in popularity. The safety of recreational SARM users is seriously threatened by recent case reports of tendon rupture and drug-induced liver damage (DILI) [15]. In the past two to three years, there have been numerous instances of severe adverse effects that could endanger life or limb. Younger men in particular have been using SARMs more frequently, perhaps as a result of the rise in popularity of numerous fitness influencers on social media [16]. Healthcare providers should be aware of the possible adverse effects on health and advice individuals accordingly, especially those using SARMs without medical supervision [17]. Since the negative effects of using SARMs, including possible impacts on fertility, have not been investigated, the growing interest in these medications is worrying and more research is required [18].

One of our case study's limitations is that we were incapable to make extra discussion down to the shortage of former tasks about the effect of RAD140 on testes, this limited the interpretation of the current outcome.

Conclusion

The result of this study provides a proof of testes toxicity due to RAD140 usage. This leads us to suggest the using of the lowest possible amount of RAD140 to minimize its harmful effect. Extra investigation is needed to understand the mechanisms behind rad 140's effects on other body organs and to validate these findings in human. Overall, caution is advised in RAD 140 use, especially concerning prostate health.

References:

[1] Miklos, a., tero-vescan, a., vari, c. E., ősz, b. E., filip, c., rusz, c. M., & muntean, d. L. (2018). Selective androgen receptor modulators (sarms) in the context of doping. *Farmacia*, *66*(5), 758-762. [link]

[2] Wagener, f., euler, l., görgens, c., guddat, s., & thevis, m. (2022). Human in vivo metabolism and elimination behavior of micro-dosed selective androgen receptor modulator rad140 for doping control purposes. *Metabolites*, *12*(7), 666. [link]

[3] Solomon, z. J., mirabal, j. R., mazur, d. J., kohn, t. P., lipshultz, l. I., & pastuszak, a. W. (2019). Selective androgen receptor modulators: current knowledge and clinical applications. Sexual medicine reviews, 7(1), 84-94. [link]

[4] Thevis, m., piper, t., beuck, s., geyer, h., & schänzer, w. (2013). Expanding sports drug testing assays: mass spectrometric characterization of the selective androgen receptor modulator drug candidates rad140 and acp-105. Rapid communications in mass spectrometry, 27(11), 1173-1182.[link]

[5] Hoffmann, d. B., derout, c., müller-reiter, m., böker, k. O., schilling, a. F., roch, p. J., ... & komrakova, m. (2023). Effects of ligandrol as a selective androgen receptor modulator in a rat model for osteoporosis. Journal of bone and mineral metabolism, 41(6), 741-751. [link]

[6] Yu, z., he, s., wang, d., patel, h. K., miller, c. P., brown, j. L., ... & saeh, j. C. (2017). Selective androgen receptor modulator rad140 inhibits the growth of androgen/estrogen receptor–positive breast cancer models with a distinct mechanism of action. Clinical cancer research, 23(24), 7608-7620. [link]

[7] Yu, z., he, s., brown, j., miller, c., saeh, j., & hattersley, g. (2017). Rad140, an orally available selective androgen receptor modulator, inhibits the growth of ar/er positive breast cancer cell line- and patient-derived xenograft models. Cancer research, 77(13_supplement), 3608-3608.[link]

[8] Leung K, Yaramada P, Goyal P, Cai CX, Thung I, Hammami MB. RAD-140 Drug-Induced Liver Injury. Ochsner J. 2022 Winter;22(4):361-365. doi: 10.31486/toj.22.0005. PMID: 36561105; PMCID: PMC9753945.

[9] Yu, z., he, s., wang, d., patel, h. K., miller, c. P., brown, j. L., ... & saeh, j. C. (2017). Selective androgen receptor modulator rad140 inhibits the growth of androgen/estrogen receptor–positive breast cancer models with a distinct mechanism of action. Clinical cancer research, 23(24), 7608-7620. [link]

[10] Burmeister, m. A., fincher, t. K., & graham, w. H (2020). Recreational use of selective androgen receptor modulators. Us pharm, 45(60), 15-8. [link]

[11] Solomon, z. J., mirabal, j. R., mazur, d. J., kohn, t. P., lipshultz, l. I., & pastuszak, a. W. (2019). Selective androgen receptor modulators: current knowledge and clinical applications. Sexual medicine reviews, 7(1), 84-94. [link]

[12] Solomon ZJ, Mirabal JR, Mazur DJ, Kohn TP, Lipshultz LI, Pastuszak AW. Selective androgen receptor modulators: current knowledge and clinical applications. Sex Med Rev. 2019;7(1):84-94. [DOI] [PMC free article] [PubMed] [Google Scholar]

[13] Chong S, Woolnough CA, Koyyalamudi SR, Perera NJ. Reversible Gynecomastia and Hypogonadism Due to Usage of Commercial Performance-Enhancing Supplement Use. JCEM Case Rep. 2024 Aug 14;2(8):luae148. doi: 10.1210/jcemcr/luae148. PMID: 39145153; PMCID: PMC11321837.

[14] Budaya TN, Nurhadi P, Anita KW, Nugroho P, Dhani FK. Effect of selective androgen receptor modulator RAD140 on prostate and testosterone levels in Wistar strain rats with bilateral orchidectomy. Med J Indones [Internet]. 2024Jul.24.

[15] Vignali, J. D., Pak, K. C., Beverley, H. R., DeLuca, J. P., Downs, J. W., Kress, A. T., Sadowski, B. W., & Selig, D. J. (2023). Systematic Review of Safety of Selective Androgen Receptor Modulators in Healthy Adults: Implications for Recreational Users. *Journal of Xenobiotics*, *13*(2), 218-236. https://doi.org/10.3390/jox13020017

[16] Vasireddi, N.; Hahamyan, H.A.; Kumar, Y.; Ng, M.K.; Voos, J.E.; Calcei, J.G. Social media may cause emergent SARMs abuse by athletes: A content quality analysis of the most popular YouTube videos. *Physician Sportsmed.* **2022**, *51*, 175–182. [**Google Scholar**] [**CrossRef**] [**PubMed**]

[17] Christiansen AR, Lipshultz LI, Hotaling JM, Pastuszak AW. Selective androgen receptor modulators: the future of androgen therapy? Transl Androl Urol. 2020 Mar;9(Suppl 2):S135-S148. doi: 10.21037/tau.2019.11.02. PMID: 32257854; PMCID: PMC7108998.

[18] Efimenko IV, Chertman W, Masterson TA, Dubin JM, Ramasamy R. Analysis of the growing public interest in selective androgen receptor modulators. Andrologia. 2021 Dec;53(11):e14238. doi: 10.1111/and.14238. Epub 2021 Sep 12. PMID: 34510504.

Modeling the Count Panel Data for Vehicle Accidents in Iraq

Ban Ghanim Al-Ani [1]

Abstract

Poisson model is one of the most common types of probabilistic models for modeling count data. Therefore, this paper aims to apply Poisson model to panel data of vehicle accidents. This paper studies the extent to which vehicle accidents respond to changes in both the number of registered vehicles and population density in 15 Iraqi Governorates during (2015-2023) by applying three types of Poisson panel data models (pooled, fixed-effects, and random-effects). The Chow and Hausman tests have been conducted to compare the three models; the results show that the fixed effects model is the best among the other models. The results also showed that there is a cross-section dependency among the governorates, and all the variables are stationary in their levels.

According to the best fitted model (fixed effects Poisson regression), the probability of vehicle accidents positively responds significantly and greatly to the number of registered vehicles, and for every 1,000 additional vehicles registered, there will be a 3.5% increase in the expected vehicle accidents number. Also, the probability of vehicle accidents responds positively and significantly to the increase in population density, and for every extra 1,000 people in population density, the number of expected vehicle accidents will increase by 0.9%.

Keywords: *Vehicle Accidents, Panel Count Models, Pooled Poisson Regression Model, Fixed Effects Poisson Regression Model, Random Effects Poisson Regression Model.*

http://dx.doi.org/10.47832/RimarCongress04-3

[1] Department of Statistics and Informatics, College of Computer Science and Mathematics, University of Mosul, Iraq drbanalani@uomosul.edu.iq

Introduction

Several studies have addressed the modelling of vehicle accidents using classical regression models. For example, in a study conducted to investigate factors causing road accidents in India and to reduce the severity of accidents, a dynamic model was developed to show the effect of human factors, roads, vehicles and the environment on road accidents. It was found that 95% of road accidents were caused by human factors [1]. Another study used a linear regression model to investigate the causes of motorcycle accidents in Arusha and Kilimanjaro of Tanzania. It was found that the factors of driver experience, tarmac road condition and driver personal status were strongly correlated with the number of motorcycle accidents [2]. Similarly, a logarithmic linear regression model was used in a study to identify the main factors causing road accidents in Türkiye. The study examined vehicle defects, road defects, driver defects, passenger errors, and pedestrian errors. It was found that road defects had the least impact, while driver defects had the greatest impact on traffic accidents [3]. The development of statistical models of count data has received considerable attention from researchers, and perhaps one of the pioneering works in this area is the work of Hausman, *et. al.* (1984) to derive a variety of models for panel count data, including a fixed-effects and random-effects regression models. This model has been widely used in modelling panel count data for traffic accidents [4]. To identify the important factors contributing to traffic accidents, many researchers have attempted to develop statistical models for this purpose. Several statistical models have been developed for time series data [5], cross-sectional data [6], and panel data [7,8,9]. One such study focused on modelling Malaysian road accidents using a panel data analysis approach. This study aims to identify the factors contributing to the traffic accidents in fourteen Malaysian states over the past 12 years [9].

Due to the non-negative random discrete integer nature of vehicle accident data, using the traditional linear regression procedure will produce unsatisfactory statistical properties, so recent studies have concluded that the counting model is the appropriate methodology for modeling vehicle accidents [10,11]. The Poisson regression model is well suited for cross-sectional count data [12] and the negative binomial regression model is used if the count data is overdispersion (variance is greater than the mean) [13]. The Inter Valued Autoregressive Poisson model is used if the number of accidents is collected over time [14]. In the case of panel count data, the appropriate models are: Pooled Poisson regression (PPR), Fixed-Effects Poisson (FEP), Random-Effects Poisson (REP) model, and these models also can be used the negative binomial distribution instead of the Poisson distribution [15]. Another count model

that has been applied to the field of vehicle accidents is the Generalized Poisson Regression model, which used panel data for the period (1974–1986) on monthly personal road accidents and their severity in eighteen Norwegian countries. This study included a large number of explanatory variables, namely: Traffic density, weather, daylight, road use (exposure), road investment and maintenance expenditure, accident reporting routines, vehicle inspections, seat-belt use, proportion of inexperienced drivers, law enforcement, and alcohol sales. The results showed that the expected number of injuries is positively related to rainfall, while heavy congestion of the road network leads to a decrease in the number of casualties [16]. Variation in panel data analysis is of great importance when developing models to estimate vehicle accidents. In one study, count models were applied to panel data on urban and suburban road crashes in 92 Indiana counties during (1988–1993), both Poisson and Negative Binomial fixed effects models were used to develop the panel model. The results indicated that the increase the crashes number was correlated with increased vehicle miles traveled, population, the percentage of city mileage, and the percentage of urban roads in total vehicle miles traveled [7]. In another study, a Fixed and Random Effects Negative Binomial models derived by Hausman *et al.* (1984) was used to analyze the panel data model, presenting a 20-year of regional bicycle road and pedestrian accidents covering 11 areas in the UK. The results showed that the increase in bicycle and pedestrian road accidents is concentrated in low-income areas, and correlated with the increase in the road network, increased spending on alcohol, and the population in general [17]. One work focused on modeling road accident data using a panel data analysis approach. Fixed-Effects Poisson (FEP) and Negative-Binomial (FENB) models were used to illustrate the dispersion of accident data on a panel of fourteen Malaysian states during (1996-2007). The causal factors of road accidents were studied, namely the number of registered vehicles per month in the state, rainfall amount, number of rainy days, time trend, and seasonality effect. All the proposed models were estimated, and the results showed that road accidents are positively correlated with increasing number of registered vehicles, increasing rainfall amount, time. And seasonality effect indicates that the vehicle accidents is higher in Oct., Nov. and Dec. months [4]. Another type of counting model that can be used to analyze vehicle accidents are Integer Autoregressive (INAR) model, these models were used in a study of annual Nigerian road traffic fatalities between 1950 and 2005. The main objective of the study was to come up with a class of Integer Autoregressive (INAR) models of road-traffic accidents. Different types of count data for time series were considered: aggregated time series data where spatial and temporal units of observation are relatively large and disaggregated time series data where both the spatial and temporal units are relatively small. A comparison of the efficiency of INAR models, Box -Jenkins real value models (such as

ARIMA models), Poisson and Negative Binomial (NB) models was made. The results indicate that the efficiency of ARIMA and INAR Poisson models are quite similar in terms of model fit to vehicle accident data collected in a time series. However, the performance of the INAR Poisson model is found to be much better than that of the ARIMA model for the case of the disaggregated time series traffic accident data where the counts are relatively low [18]. In another study to investigate the main factors of road-accidents in Tanzania and how to reduce them by 2030, the analysis of panel data was used to allow for control of variables that could not be observed over time, and the Pooled Poisson model, Fixed-Effects Poisson model and Random-Effects were applied to evaluate the causes of road accidents. The Fixed-Effects model was the best fitted to the data. The results indicated that all factors were significant but passengers and rail transit were found to be insignificant and were dropped from the final model [19].

Contribution of Current Research

What distinguishes the current research from previous research and studies in the field of panel count data models lies in three main points, which are:

1. As is known when estimating a regression model, regardless of its type, all variables included in it must be stationary, and this requires conducting one of the unit root tests.

2. The use of unit root tests depends on the cross-sectional dependency. When the data is not cross-sectional dependency, a first-generation unit root tests are used, while in the case of cross-sectional dependency, the second-generation unit root tests are used, so it is necessary to conduct a cross-sectional dependency test before estimating the model.

When the researcher reviewed previous studies, he found that they all did not use cross-sectional dependency tests and unit root tests, unlike the current research, which included conducting these tests.

3. This research is the first study in Iraq that deals with panel count data models and their application in an important life sector.

MATERIALS AND METHODS

1. Static Panel Data Models:

1.1. Pooled Regression (PR) Model:

The simplest kind of estimator for panel data is called “pooled (or common) regression model”. This model simply ignores the panel data nature of the data, treating it as if it were cross-sectional data. This model used the ordinary least squares (OLS) method for parameters estimation of the model by combing time series and cross-sectional data as a one set of data [21]. The (PR) model equation is [20]:

$$Y_{it} = \alpha + \boldsymbol{X}_{it}\boldsymbol{\beta} + \varepsilon_{it} \quad ; \quad i=1,2,3,\ldots,N \ , \ t=1,2,3,\ldots,T \qquad (1)$$

where Y_{it} is response (dependent) variable value of the i^{th} observation and t^{th} time, α is the intercept, $\boldsymbol{X_{it}}$ is $(X_{1,it}, X_{2,it}, \ldots, X_{k,it})$, where $\boldsymbol{X}_{\mathrm{j,it}}$ is the value of the j^{th} predictor (independent) variable for the i^{th} observation , $\boldsymbol{\beta}$ is $(\beta_1, \beta_2, \ldots , \beta_k)'$ where β_j is slope or coefficient at the j^{th} independent variable, N is the number of cross-sections, T is the number of time units, and ε_{it} is the error at the i^{th} observation and t^{th} time such that $\varepsilon_{it} \sim N(0, \sigma_{\varepsilon}^2)$.

1.2. Fixed-Effect (FE) Model:

There are several ways to obtain consistent estimators, one of the simplest when there is a correlation between the predictors and the specific individual term is through what is called a “fixed effects estimator” [22]. A fixed-effects model includes estimating the panel regression model parameters by adding dummy variables [23]. This technique is called the Least Square Dummy Variable (LSDV) model. By adding a dummy variable for each individual in the panel, the variance between individuals that cannot be explained by other variables included in the model is explicitly estimated and is therefore allowed to be correlated with the predictors. To avoid complete multicollinearity, one of the individuals or the intercept is excluded from the model. In general, the FE model allows each cross-section unit i to have a distinct intercept regardless all slopes are the same or not. The FE model can be written, as follows:

$$Y_{it} = \alpha_i + \boldsymbol{X}_{it}\boldsymbol{\beta} + \varepsilon_{it} \qquad (2)$$

where α_i is the fixed-effect of the i^{th} observation.

1.3. Random-Effect (RE) Model:

The random-effects model assumes that the distribution of individual effects α_i is independent of the predictors [24]. The RE model estimates panel data using residuals that are not independent across individuals and time. The RE model assumes one constant α for all units, and differences in the intercepts can be included in the error variable, so the error has new assumptions. The rationale base of the random-effects model is that unlike the fixed effects

model, the variance across units is assumed to be random, unlike random-effects assume that the unit error is independent of the predictor [25].

In this model, the estimation of the parameters can be done through the Feasible Generalised Least Squares (FGLS) technique [26]. The (RE) model can be formulated as follows:

$$Y_{it} = \alpha + \boldsymbol{X}_{it}\boldsymbol{\beta} + u_{it} \qquad (3)$$

where $u_{it} = v_i + \varepsilon_{it}$; v_i denotes to the unobservable individual-specific effects, and ε_{it} denotes to the white noise, and $u_i \sim N(0, \sigma_u^2)$.

2. Models of Count Panel Data:

A count random indicates the number of times an event occurs, such as monthly number of vehicle accidents that occurred in a particular geographic area. As with other types of experimental data, count data are also classified into three types: cross-sections, time series, and panel. Panel count data is a set of observations of a count variable that are taken from several sample units at multiple periods. When the response variable takes non-negative integer values, such as the monthly number of vehicle accidents, the daily number of patient visits to the doctor, etc. This means that the response variable is not normally distributed, therefore the commonly used models that fit such data are the Poisson and the Negative Binomial models [8,17,27].

2.1. Pooled Poisson Regression (PPR) Model:

Let (Y_{it}) be a variable distributed as Poisson with a probability mass function:

$$f(y_{it}; \lambda_{it}) = \frac{e^{-\lambda_{it}}(\lambda_{it})^{y_{it}}}{y_{it}!}; i=1,2,3,...,N , t=1,2,3,...,T \qquad (4)$$

λ_{it} is the expected number of y_{it} such that $E(y_{it})=var(y_{it})=\lambda_{it}$.

λ_{it} is positive and represent the location parameter. Define (λ_{it}) as an exponential function of a linear index of the explanatory variables $\lambda_{it}=E(y_{it})=exp(\boldsymbol{x}'_{it}\boldsymbol{\beta})$ [28].

In PPRM, we are modelling a log of the expected counts:

$$ln(E(y_{it})) = \boldsymbol{x}'_{it}\boldsymbol{\beta}$$

The Logarithm of likelihood function is:

$$ln\ L(\boldsymbol{\beta}) = \sum_{i=1}^{N}\sum_{t=1}^{T}(y_{it}\boldsymbol{x}'_{it}\boldsymbol{\beta} - exp(\boldsymbol{x}'_{it}\boldsymbol{\beta}) - lny_{it}!)$$

To maximize $L(\boldsymbol{\beta})$ *we take:*

$$\frac{\partial L(\boldsymbol{\beta})}{\partial \boldsymbol{\beta}} = \mathbf{0}$$

The Poisson maximum likelihood estimator (MLE) solves the first-order conditions:

$$\sum_{i=1}^{N}\sum_{t=1}^{T}(y_{it} - exp(\boldsymbol{x}'_{it}\boldsymbol{\beta}))\,\boldsymbol{x}_{it} = 0 \qquad (5)$$

We can use Newton-Raphson or other optimization algorithms to find the solution (5).

Finally, according to (1), the estimated (PPRM) will be:

$$ln\hat{\lambda}_{it} = \hat{\alpha}_i + \hat{\beta}_1 x_{1,it} + \hat{\beta}_2 x_{2,it} + \ldots + \hat{\beta}_k x_{k,it} \qquad (6)$$

2.2. Fixed Effects Poisson Regression (FEPR) Model:

The conditional probability mass function of the (FEPR) model is:

$$f(y_{it}|\boldsymbol{x}_{it}, \alpha_i, \boldsymbol{\beta}) = \frac{e^{-\alpha_i\lambda_{it}}(\alpha_i\lambda_{it})^{y_{it}}}{y_{it}!};\ i=1,2,3,\ldots,N,\ t=1,2,3,\ldots,T \qquad (7)$$

All characteristics of this model that do not vary with time are expressed by the individual heterogeneity term α_i. Let μ_{it} be the count variable for individual *i* at time *t*, then the expected value of μ_{it} is linked to regressors by:

$$\hat{\mu}_{it} \equiv E[y_{it}|\mathbf{x}_{it}, \alpha_i] = \alpha_i\lambda_{it} = \exp(d_i + \mathbf{x}'_{it}\boldsymbol{\beta})\ ;\ i=1,2,3,\ldots,N\ ,\ t=1,2,3,\ldots,T \qquad (8)$$

where, d_i are cross-section dummy variables, α_i=$exp(d_i)$ **is** the individual effect, the conditional maximum likelihood method is used to estimate the parameters of the model [4]. Since y_{it} follows the Poisson distribution, then the sum $(\sum_{i=1}^{T} y_{it})$ are follow the Poisson distribution with parameters $(\sum_{t=1}^{T}\hat{\mu}_{it} = \alpha_i\sum_{t=1}^{T}\lambda_{it})$.

The estimated Parameters of the model (8) can be obtained by using the Conditional Maximum Likelihood (CML) method which developed by (Hausman *et al.*, 1984), therefore, the Conditional Joint Mass Function (CJMF) of the i^{th} observation is [29]:

$$f\left(y_{i1}, y_{12}, \dots, y_{iT} \left| \sum_{t=1}^{T} y_{it} \right.\right) = \frac{(\sum_{t=1}^{T} y_{it})!}{(\sum_{i=1}^{T} \lambda_{it})^{\Sigma_{t=1}^{T} y_{it}}} \prod_{t=1}^{T} \frac{(\lambda_{it})^{y_{it}}}{y_{it}!}$$

then the conditional log-likelihood can be obtained by taking the log and summing over all individuals:

$$lnL = \sum_{i=1}^{N} \left\{ ln\left(\sum_{t=1}^{T} y_{it}\right)! - \sum_{t=1}^{T} ln(y_{it}!) + \sum_{t=1}^{T} \left[y_{it} \boldsymbol{x}_{it}' \boldsymbol{\beta} - y_{it} ln\left(\sum_{t=1}^{T} exp(\boldsymbol{x}_{it}' \boldsymbol{\beta})\right)\right]\right\}$$

the estimated parameters can be obtained by solving:

$$\sum_{i=1}^{N} \sum_{t=1}^{T} \boldsymbol{x}_{it}' \left(y_{it} - \frac{\sum_{t=1}^{T} y_{it}}{\sum_{i=1}^{T} \lambda_{it}} \lambda_{it} \right) = 0 \qquad (9)$$

2.3. Random Effects Poisson Regression (REPR) Model:

Considering the Poisson conditional probability function as in Eq.(7), alot of studies, like [30,31], assuming that the individual effects α_i have a Gamma distribution with equal parameters (θ, θ) and mean 1 and variance $1/\theta$ [25,27]. The estimators of the REPR model can then be obtained through the maximum likelihood function (MLF) for the i^{th} observation as:

$$f(y_{i1}, y_{12}, \dots, y_{iT} | u_{it}, \boldsymbol{x}_{it}') = \prod_{t=1}^{T} \left(\frac{(\lambda_{it})^{y_{it}}}{y_{it}!} \right) \left[\frac{\theta}{\theta + \sum_{i=1}^{T} \lambda_{it}} \right]^{\theta} \left[\frac{\Gamma(\sum_{i=1}^{T} y_{it} + \theta)}{\Gamma(\theta)} \right] \left[\theta + \sum_{i=1}^{T} \lambda_{it} \right]^{-\Sigma_{i=1}^{T} y_{it}}$$

knowing that this model is includes the intercept merged into $\boldsymbol{x}_{it}'$. The log of the MLF is:

$$lnL = \sum_{i=1}^{N} \left\{ \sum_{t=1}^{T} (y_{it} \boldsymbol{x}_{it}' \boldsymbol{\beta} - ln y_{it}!) + \theta ln\theta - \theta ln \left[\theta + \sum_{t=1}^{T} exp(\boldsymbol{x}_{it}' \boldsymbol{\beta}) \right] + ln\left[\Gamma\left(\sum_{i=1}^{T} y_{it} + \theta \right) \right] - ln[\Gamma(\theta)] - \sum_{t=1}^{T} y_{it} ln\left[\theta + \sum_{t=1}^{T} exp(\boldsymbol{x}_{it}' \boldsymbol{\beta}) \right] \right\}$$

solving:

$$\sum_{i=1}^{N} \sum_{t=1}^{T} \boldsymbol{x}_{it}' \left[y_{it} - \lambda_{it} \left(\frac{\bar{y}_i + \frac{\theta}{T}}{\bar{\lambda}_i + \frac{\theta}{T}} \right) \right] = 0 \qquad (10)$$

to get the estimated parameters, where $\bar{y}_i = T^{-1} \sum_{t=1}^{T} y_{it}$ and $\bar{\lambda}_i = T^{-1} \sum_{t=1}^{T} \lambda_{it}$

3. Cross-Section Dependency and Unit Root Tests:

3.1. Pesaran's (CD) test:

Consider the standard panel data model (1), it is well known that the first-generation unit root tests are performed regardless of the presence of cross-sectional dependency, so their results are inaccurate in this case. To address this problem, second-generation unit root tests are used. Much recent empirical research has found that panel data can be cross-sectionally dependent. One of the cross-sectional dependence tests is the Pesaran (CD) test, which is widely used to test the null hypothesis that errors are not cross-sectionally dependent. The CD test statistic is as follows [32]:

$$CD = \sqrt{\frac{2T}{N(N-1)}} \sum_{i=1}^{N-1} \sum_{j=i+1}^{N} \hat{\rho}_{ij} \qquad (11)$$

where $\hat{\rho}_{ij}$ is the sample estimate of the pairwise correlation of the residuals

$$\hat{\rho}_{ij} = \frac{\sum_{t=1}^{T} u_{it} u_{jt}}{\sqrt{\left(\sum_{t=1}^{T} u_{it}^2\right)\left(\sum_{t=1}^{T} u_{jt}^2\right)}} \qquad (12)$$

and u_{it} is the estimate of e_{it}. Under the null hypothesis of no cross-sectional dependence, Pesaran (2004) concluded that $CD \xrightarrow{d} N(0,1)$. [33]

3.2. Unit Root Test:

When there is cross-sectional dependence, this needs for using one of the second-generation unit root tests. Therefore, we shall employ Cross-sectionally Augmented IPS (CIPS) was proposed by Pesaran (2007). Following the work of Hurlin & Mignon (2007), the below notation to construct the CIPS statistic. In case of no serial correlation, the Cross-sectionally Augmented Dickey-Fuller (CADF) regression for the i^{th} cross-section is defined as follows [34,35]:

$$\Delta y_{i,t} = \alpha_i + \rho_i y_{i,t-1} + c_i \bar{y}_{t-1} + d_i \Delta \bar{y}_t + v_{i,t} \qquad (13)$$

where

$\bar{y}_{t-1}=N^{-1}\sum_{i=1}^{N} y_{i,t-1}$ is the mean of the cross-sectional average at lagged levels, and $\Delta\bar{y}_t=N^{-1}\sum_{i=1}^{N}\Delta y_{i,t}$ is the mean of the first difference for the individual series.

H_0: all individual time series are non − stationary

H_1: at least a fraction $\frac{N_j}{N}$ of individual time series are stationary

i.e

$$H_0: \quad \rho_i = 0 \quad for \qquad i = 1,2,\dots,N$$

$$H_A: \begin{cases} \rho_i < 0 \ for & i=1,2,\dots,N_j \\ \rho_i = 0 \ for & i=N_j+1, N_j+2,\dots,N \end{cases}$$

The CIPS test is given by [9]:

$$CIPS = N^{-1}\sum_{i=1}^{N} CADF_i \qquad (14)$$

where $CADF_i$ is the cross-sectionally augmented Dickey-Fuller statistic for the i-th cross-sectional unit given by the to the t-ratio of ρ_i in Eq.(13). The standard critical values at 10%, 5%, and 1% for different *T* and *N* are tabulated in the appendix of Pesaran (2007) [35].

4. Best Model Selection:

4.1. Chow's Test:

To decide whether the PPR model or FEPR model is more suitable for the panel data analysis, we use Chow test [20]. The two hypotheses are as follows:

$$H_0: \alpha_1 = \alpha_2 = \dots = \alpha_N = 0 \ \ or\ the\ PPR\ model\ is\ the\ best$$

$$H_1: at\ least\ \ one\ \alpha_i \neq 0\ , i = 1,2,\dots,N\ or\ the\ FEPR\ model\ is\ the\ best$$

The test statistic used is:

$$F = \frac{(R^2_{FEM} - R^2_{PRM})/(N-1)}{(1-R^2_{FEM})/(NT-N-k)} \qquad (15)$$

where R^2_{FEM} and R^2_{PRM} are the coefficient of determination for the fixed effects model and pooled regression model respectively. H_0 can be rejected if $F > F(\alpha, N-1, NT-N-k)$, so that the FEPR model is the appropriate model.

4.2. Hausman's Test:

To decide whether the FEPR model or REPR model is suitable for given panel data, we use Huaman test [36]. The hypotheses of this test are as follows:

$$H_0: E(u_{it}|\boldsymbol{x}_{it}) = 0 \;\; or \;\; the\ REM\ model\ is\ the\ best$$

$$H_1: E(u_{it}|\boldsymbol{x}_{it}) \neq 0 \;\; or \;\; the\ FEM\ model\ is\ the\ best$$

The test statistic used is:

$$H = \left(\widehat{\boldsymbol{\beta}}_{FEM} - \widehat{\boldsymbol{\beta}}_{REM}\right)'\left[\boldsymbol{V}(\widehat{\boldsymbol{\beta}}_{FEM}) - V(\widehat{\boldsymbol{\beta}}_{REM})\right]^{-1}\left(\widehat{\boldsymbol{\beta}}_{FEM} - \widehat{\boldsymbol{\beta}}_{REM}\right) \qquad (16)$$

where $\widehat{\boldsymbol{\beta}}_{FEM}$ and $\widehat{\boldsymbol{\beta}}_{REM}$ are estimated slope parameter vector for the FEM and REM models respectively, and $\boldsymbol{V}(.)$ stands for variance-covariance matrix. Since $H \sim \chi^2_{(k)}$ so H_0 is rejected if $H > \chi^2_{(k,\alpha)}$, so the fixed-effects model is the best model.

5. The Data:

The research used secondary data collected by annual statistical reports from the Authority of Statistics and Geographic Information Systems (ASGIS) [37]. The sample contains (15) Iraqi governorates over the period from Jan/2015 to Dec./2023. R-software (plm-package) was used to conduct the statistical analysis.

In our research, the response variable is the number of vehicle accidents. While the explanatory variables, include the registered vehicles in the General Traffic Directorate and population size. A brief description of the selected variables is shown in table 1 .

Table 1. Data description

Variable	Type	Description	Unit
ACC	response	Total vehicle accidents in each governorate per month	number
VEH	explanatory	Total registered vehicles in each governorate per month	number (per 1000)
POP	explanatory	Population size in each governorate per month	number (per 1000)

Results And Discussion

1. Descriptive Analysis of Vehicle Accidents:

Figure 1 shows the annual total number of vehicle accidents during (2015-2023) according to the governorates. Basrah Governorate has the highest number of accidents, while Salah Al-Din Governorate comes last. The clear heterogeneity between the governorates is evident. According to the average annual growth rates of vehicle accidents number, some governorates witnessed a decline in the number of vehicle accidents, namely: Al-Muthanna 0.2%, Al-Najaf 0.4%, Al-Qadisiya 1.2%, Maysan 5.1%, and Dhi Qar 5.4%. Other governorates witnessed a relative stability in the number of vehicle accidents, namely: Babil 1.2%, Kirkuk 3.7%, Baghdad 4.4%, Wasit 7.2%, and Karbala 8.3%. The governorates that witnessed increase in the vehicle accidents number are: Nineveh 21.8%, Diyala 21.2%, Al-Anbar 12.3%, and Salah al-Din 12%.

Table 2 shows the annual averages of the research variables during (2015-2023). In terms of the number of vehicle accidents (ACC), Basrah Governorate has the highest number with an average of 1,371 accidents, followed by Baghdad Governorate with an average of 1,127 accidents, then Najaf Governorate with an average of 1,022 accidents, while Salah al-Din Governorate comes in last place with an average of 232 accidents. In terms of the number of registered vehicles (VEH), Baghdad Governorate came in first place with an average of 2,911,400 vehicles, followed by Nineveh Governorate with an average of 417,2853 vehicles, then Basrah Governorate with an average of 353,124 vehicles, while Muthanna Governorate came in last place with an average of 118,732 vehicles. The total average number of vehicle accidents in all Iraqi governorates included in the study during the period (2015-2023) was 670 accidents.

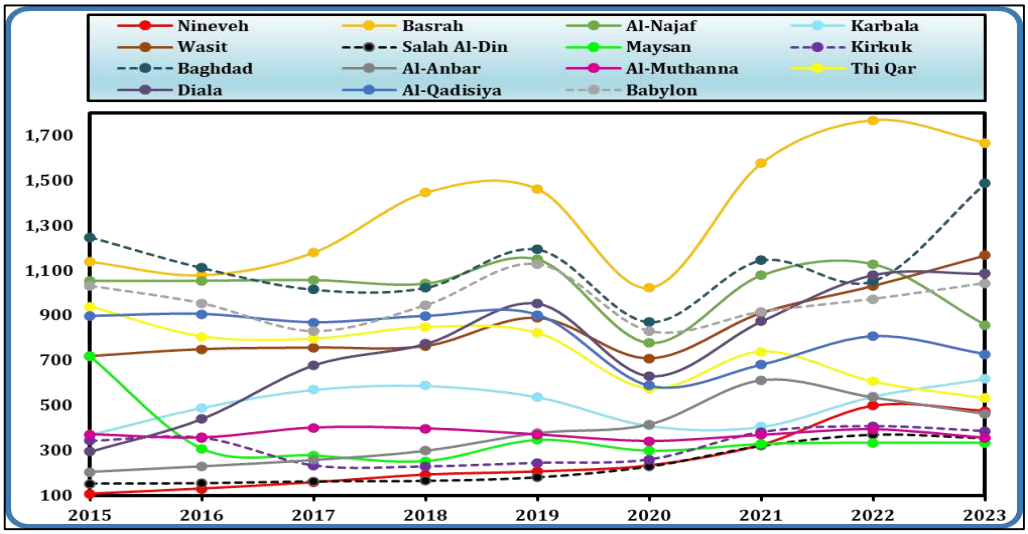

Figure 1. Yearly total number of vehicle accidents (ACC)

For the number of registered vehicles (VEH), Baghdad Governorate came in first with an average of 2,911,400 vehicles, followed by Nineveh Governorate with an average of 417,853 vehicles, then Basra Governorate with an average of 353,124 vehicles, while Muthanna Governorate came in last place with an average of 118,732 vehicles. The total average number of registered vehicles in all Iraqi governorates during the mentioned period was 359,342 vehicles. As for the population (POP), Baghdad Governorate is the most density populated with an average of 8,353,958 people, followed by Nineveh Governorate with an average of 3,734,273 people, then Basrah Governorate with an average of 2,989,808 people, while Muthanna Governorate came in last place with an average of 837,138 vehicles. The total average population in all Iraqi governorates during the mentioned period was 2,248,803 people.

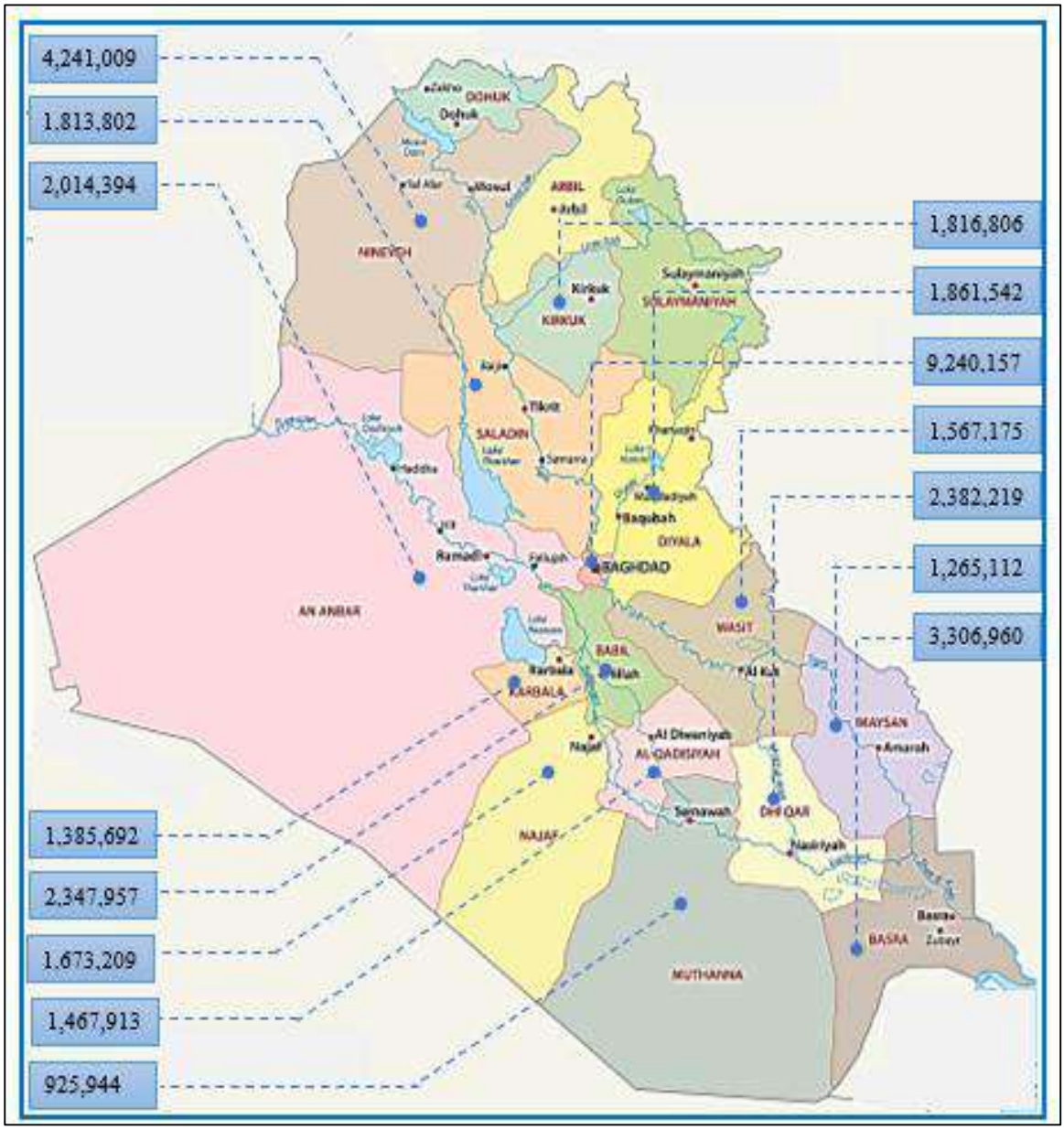

Figure 2. Population projections in Iraqi Governorates for (2023)

The distribution of the yearly number of vehicle accidents by governorates during (2015-2023) is shown in Figure 3 , where the results indicate that Basrah Governorate has a higher vehicle accidents than any governorates with 12,337 accidents, followed by Baghdad Governorate with 10,145 accidents, then Al-Najaf Governorate with 9,195 accidents. While Nineveh Governorate came in the penultimate place in the cumulative vehicle accidents with 257 accidents. Salah Al-Din Governorate is considered to have the lowest number of vehicle accidents with 231 accidents. The total number of vehicle accidents in all Iraqi governorates included in the research during (2015-2023) amounted to 90,466 accidents.

Table 2. The variables' means of the research for (2015-2023)

Government	ACC	VEH	POP
Al-Anbar	376.6667	262.773	1821.198
Al-Muthanna	372.5556	118.732	837.138
Al-Najaf	1021.667	247.099	1512.734
Al-Qadisiya	808.2222	227.119	1327.133
Babylon	960.8889	308.027	2122.850
Baghdad	1127.222	2911.400	8353.958
Basrah	1370.778	353.124	2989.808
Diala	757.0000	253.125	1683.003
Karbala	502.7778	167.657	1252.795
Kirkuk	315.2222	215.633	1642.560
Maysan	354.8889	122.153	1143.781
Nineveh	257.4444	417.853	3834.273
Salah Al-Din	231.5556	252.757	1639.840
Thi Qar	740.0000	179.436	2153.749
Wasit	854.8889	201.528	1417.230
All	670.1185	359.342	2248.803

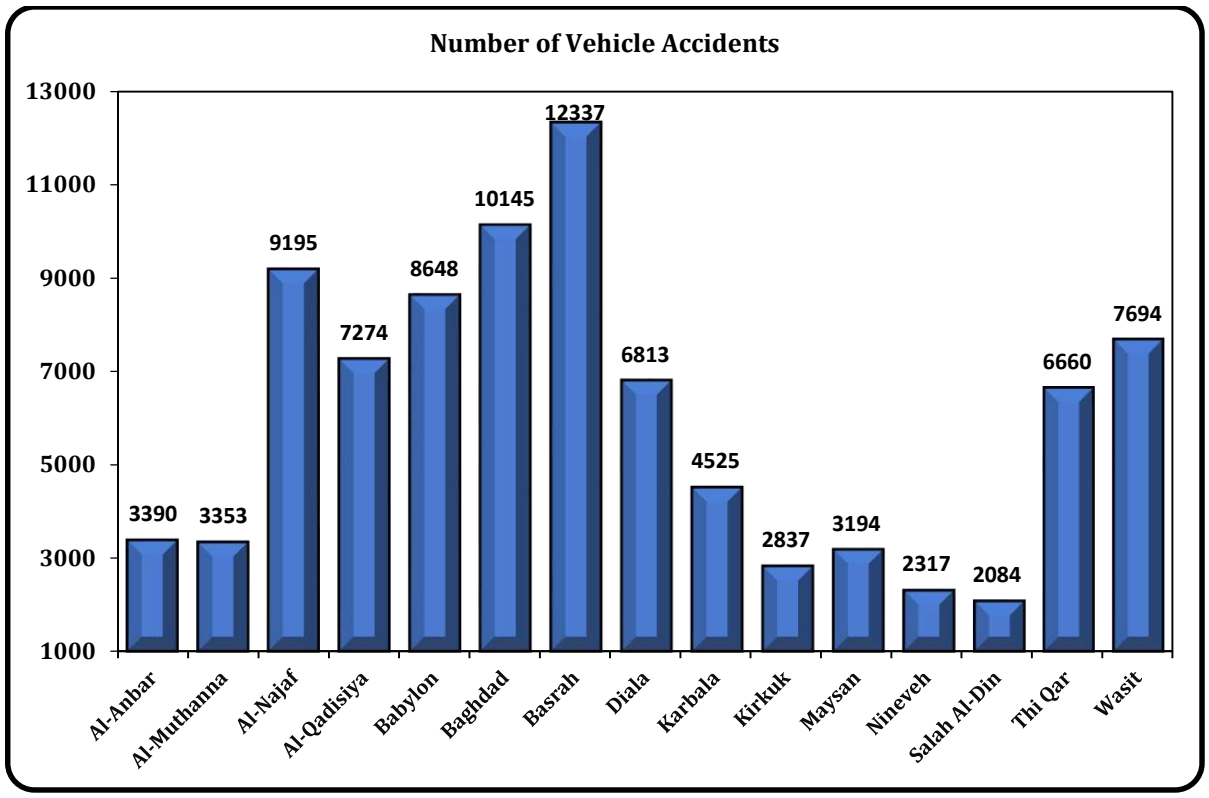

Figure 3. Distribution of cumulative vehicle accidents by governorate from 2015 to 2023

From Table 3, we can note that the ratio of variance-to-mean is close to one for all governorates. So, we believe that the Poisson regression models, in terms of distributional assumptions, might be suitable for the data.

Table 3. Descriptive Statistics for number of vehicle accidents (ACC)

Government	Mean	Max	Min.	Std. Dev.	N
Al-Anbar	376.6667	612	204	20.0422	108
Al-Muthanna	372.5556	401	341	18.6162	108
Al-Najaf	1021.667	1148	778	32.5265	108
Al-Qadisiya	808.2222	906	587	25.9260	108
Babylon	960.8889	1127	830	32.4621	108
Baghdad	1127.222	1486	871	35.2231	108
Basrah	1370.778	1767	1023	40.1084	108
Diala	757.0000	1086	295	25.9124	108

Karbala	502.7778	618	369	23.3445	108
Kirkuk	315.2222	408	228	19.5047	108
Maysan	354.8889	718	252	16.5112	108
Nineveh	257.4444	498	106	21.4655	108
Salah Al-Din	231.5556	370	152	18.1031	108
Thi Qar	740.0000	938	532	24.3618	108
Wasit	854.8889	1168	708	31.4792	108
All	670.1185	1767	106	37.9790	1620

2. Correlations

The correlation between the variables was examined and the findings are given in Table 4. The variables are expected to produce significant correlations within themselves.

Table 4. Correlations between ACC, VEH and POP variable

	ACC	**VEH**	**POP**
ACC	1.000	0.360**	0.369**
VEH		1.000	0.949**
POP			1.000
VIF	---	5.623	7.792
**** indicates significance at the 1% level of testing**			

Table 4 shows that there is a significant correlation at a 1% significance level between the variables, which is in line with the expectations. According to the findings, there is a significant and positive linear relation between the variable ACC and variables VEH and POP and between the variables VEH and POP. These results are consistent with reality, as the population size in the governorates increases, vehicles number will increase, and accordingly, vehicle accidents number will also increase. Also, the results of Table 4 indicate that the data

does not have multicollinearity problem because the values of the variance inflation factor (VIF) are less than 10.

3. Cross-Section Dependency and Unit Root Tests:

The results of cross-section dependency reported in Table 5 suggest that the null hypothesis can be rejected at 1% significant level for each variable, i.e. ACC, VEH and POP have cross-sectional dependence in all governorates**.** In practice, the accepting of the alternative hypothesis implies that the significant changes in a certain variable in any governorate will generate significant changes in the same variable in the other governorates.

Table 5. Pesaran (CD) Cross-Sectional Dependence test results

Variable	Pesaran CD	p-value
ACC	5.9499**	< 0.01
VEH	26. 7201**	< 0.01
POP	30.7408**	< 0.01
**** indicates significance at the 1% level of testing**		

According to the results of table 6, second-generation unit root tests that considering cross-sections dependency will be applied to all variable series, the results are reported in Table 6

Table 6. CIPS second-generation unit root test results

Variables	CIPS	p-value	Remark
ACC	-6.0447**	< 0.01	I(0)
VEH	-11.3387**	< 0.01	I(0)
POP	-7.2794**	< 0.10	I(0)
**** indicates significance at the 1% level of testing**			

According to CIPS unit root test results, the variables ACC, VEH and POP do not have unit roots at 0.01 significant level, meaning that variables are stationary at their levels, i.e., the time series of the three variables have an order of integration I(0).

4. Estimation of Poisson Regression Models:

Table 7. explains the results of PRP, FEPR and REPR models. The parameters of the PPR and FEPR models are estimated by CML method, while parameters of the REPR model are estimated using the MLE method.

Table 7. Parameter estimation of Poisson regression models

Variable	PPR Model	FEP Model	REP Model
Intercept	6.2841**	3.78246	-0.35102
VEH	-0.13814	0.45004*	0.24663*
POP	0.12728**	-141.8297**	241.7705
Root MSE	340.2587	133.7434	143.4938
R^2	0.4268	0.9054	0.089649
F-statistic	49.1487	70.5590	24.1352
Prob.(F-statistic)	0.0000	0.0000	0.0000
Wald statistics (χ^2)	16.5911	44.3925	13.33530
Prob.(χ^2)	0.0000	0.0000	0.0010
Chow Test (F)	69.50329		
Prob.(F)	0.0000		
Hausman Test (χ^2)		7.8343	
Prob.(χ^2)		0.0000	
**** & * indicate significance at the 1% and 5% levels of testing respectively**			

Table 8 explain that the three models are statistically significant based on the p-value of the Wald test that less than 1%. This means that it reflects the substantial influence of both the number of registered vehicles and the population size on the expected number of vehicle accident.

When we compare the PPR and FEP models based on Chow's test, we find that the p-

value of F is less than 1%, which means rejecting the null hypothesis, and therefore the FEP model fits the data better than the PRP model. On the other hand, depending on the Hausman test results, if p-value is less than 1%, then we accept that the FEPR model is more suitable than the REPR model.

As for the interpretation of the estimators of the FEP model, we note that by assuming that the population is fixed, the number of registered vehicles will have a significant and positive effect on the likelihood of vehicle accidents occurrence, when the number of registered vehicles increases by one unit (1000 vehicles) this implies that the expected number of vehicle accidents will be increased by (0.0342). This can be said in other words, according to the odd ratio ($exp(\hat{\beta}_1) = 1.035$), there is a 3.5% increase in the expected number of vehicle accidents for each extra 1000 registered vehicles. This implies that the vehicle accidents number is expected to increase with an increase in the number of registered vehicles in the governorates. This positive effect is consistent with the results on the vehicle accidents studies [4,22,38].

On the other side, by assuming the number of registered vehicles is fixed, the population parameter estimator has a significant and positive effect on the likelihood of vehicle accidents occurrence, when the population size increases by one unit (1000 persons) this implies that the expected number of vehicle accidents will be increased by (0.009), and the odd ratio ($exp(\hat{\beta}_2) = 1.009$), indicates a 0.9% increase in the expected number of vehicle accidents for each extra 1000 persons. This implies that the vehicle accidents number is expected to increase with increasing population in the governorates. This finding is consistent with many previous studies [39,40,41,42].

Conclusions

This research examined the effect of registered vehicles and population density on the likelihood of vehicle accidents occurrence in 15 Iraqi Governorates during (2015-2023) by applying three types of Poisson panel data models (pooled, fixed-effects, and random-effects). The Chow and Hausman tests have been conducted to compare among the three models; lastly, the Hausman test result indicates that the FEP model is better than other models. The data analysis and hypothesis testing, results explained that there is a cross-sectionally dependency among the governorates, which means any significant changes in a certain variable in any governorate will produce changes in the same variable in the other governorates. Another result is that all the research variables are stationary in their levels.

According to the best-fitted model (FEPR), the registered vehicles number have a positive

and significant effect on the likelihood of vehicle accidents occurrence, and there is a 3.5% increase in the expected number of vehicle accidents for each extra 1000 registered vehicles. Also, the population density has a positive and significant effect on the likelihood of vehicle accidents occurrence, and there is a 0.9% increase in the expected number of vehicle accidents for each extra 1000 population density size.

Although the current research showed the clear effect of explanatory variables on vehicle accidents, these variables cannot be considered direct factors for the increase in vehicle accidents. Many cities in the world witness large populations and vehicles, but they are less in the number of accidents. The current research focused on the theoretical aspect and how to use counting models in studying some real phenomena. Therefore, the research recommends a more in-depth study of the factors affecting the increase in vehicle accidents with the possibility of addressing dynamic panel Poisson models as they produce short- and long-term relationships.

Acknowledgments

The author would like to express his appreciation to the academic staff of the Department of Statistics and Informatics, College of Computer Science and Mathematics, University of Mosul. The author also wishes to thank the Authority of Statistics and Geographic Information Systems (ASGIS) for providing the data.

References:

[1] Kumar, S.N. & Umadevi, G. (2011). Application of system dynamic simulation modelling in road safety. 3rd International Conference on Road Safety and Simulation Purdue University Transportation Research Board, Indianapolis: 14-16.

[2] Nyakyi, V.P., Kuznetsov, D. & Nkansah-Gyekye, Y. (2014). Validating regression models to assess factors for motorcycle accidents in Tanzania. Science Journal of Applied Mathematics and Statistics, 2: 97-101.

[3] Tortum, A., Çodur, M.Y., & Kilinç, B. (2012). Modelling traffic accidents in Turkey using regression analysis. Journal of the Institute of Science and Technology, 2: 69-78.

[4] Yaacob, W.F., Lazim, M.A. & Wah, Y.B. (2011). Applying fixed effects panel count model to examine road accident occurrence. Journal of Applied Sciences, 11(7): 1185-1191.

[5] Quddus, M.A. (2008). Time series data models application to traffic accidents. Acci. Anal. Prev., 40: 1732-1741.

[6] Loeb, P.D. (1985). The efficacy and cost-effectiveness of motor vehicle inspection using cross-sectional data: an econometric analysis. South Econ. J., 52: 500-509.

[7] Karlaftis, M.G. & Tarko, A.P. (1998). Heterogeneity considerations in accidents modeling. Acci. Anal. Prev., 30: 425-433.

[8] Kumara, S.S. & Chin, H.C. (2004). Study of fata traffic accidents in Asia Pacific countries. Transport. Res. Record, 1987: 43-47.

[9] Nhan, T.T. (2007). Evaluating an intervention to prevent motorcycle injuries in Malaysia: process, performance and policy. Ph.D. Thesis, John Hopkins University, USA.

[10] Kweon, Y.J. & Kockelman, K.M. (2004). Spatially disaggregate panel models of crash and injury counts: The effect of speed limits and design. Proceedings of the 83rd TRB Annual Meeting, Washington DC.

[11] Miaou, S.P., Patricia, S.H., Wright, T., Rathi, A.K. & Davis, S.C. (1992). Relationship between truck accidents and highway geometric design: A Poisson regression approach. Transport. Res. Record., 1407: 35-41.

[12] Miaou, S.P. & Lum, H. (1993). Modeling vehicle accidents and highway geometric design relationships. Acci. Anal. Prev., 25: 689-709.

[13] Lord, D. (2006). Modelling motor vehicle crashes using Poisson-Gamma models: Examining the effects of low sample mean values and small size on the estimation of the fixed dispersion parameter. Acci. Anal. Prev., 38: 751-766.

[14] Quddus, M.A. (2008). Time series count data models: An empirical application to traffic accidents. Acci. Anal. Prev., 40: 1732-1741.

[15] Chin, H.C. & Quddus, M.A. (2003). Applying the random effect negative binomial model to examine traffic accident occurrence at signalized intersections. Acci. Anal. Prev., 35: 363-259.

[16] Fridstrom, L. & Ingebrigsten, S. (1991). An aggregate accident model based on pooled, regional time series data. Acci. Anal. Prev., 23: 363-378.

[17] Noland, R.B. & Quddus, M.A. (2004). Analysis of pedestrian and bicycle casualties with regional panel data. Transport. Res. Record, 1897: 28-33.

[18] Ahmed, M.M., Mohammad, M. & Rashad, A.M. (2019). Time series analysis of road traffic accidents in Nigeria. Global Scientific Journals, 7(12): 1450-1461.

[19] Hausman, J.A., Hall, B.H. & Griliches, Z. (1984). Econometric models for count data with an application to the patents-R & D relationship. Econometrica, 52(4): 909-938.

[20] Ratnasari, V., Audha, S.H., & Dani, A.T.R. (2023). Statistical modelling to analyze factors affecting the middle-income trap in Indonesia using panel data regression. Methods X, 11, 102379.

[21] Biørn, E. (2016). Econometrics of panel data: methods and applications. Oxford University Press.

[22] Baltagi, B.H. (2011). Econometrics. 5th edition, Springer, Berlin.

[23] Wardhana, F.A., & Indawati, R. (2021). Panel data regression analysis for factors affecting infant mortality rate in East Java 2013-2017. Indonesian Journal of Public Health, 16(3): 437–448.

[24] Baltagi, B.H., Cameron, A.C. & Trivedi, P.K. (2015). Count panel data. In Baltagi, B.H. editor, The Oxford Handbook of Panel Data. Oxford University Press.

[25] Hsiao, C. (2003). Analysis of panel data. 2nd edition, Cambridge University Press, Cambridge.

[26] Wooldridge, J.M. (2013). Introduction to econometrics: EMEA Edition, 1st edition, Cengage Learning EMEA, London.

[27] Angers, J.F., Desjardins, D., Dionne, G., & Guertin, F. (2018). Modelling and estimating individual and firm effects with count panel data. ASTIN Bulletin: The Journal of the IAA., 48(3): 1049-1078.

[28] Boucher, J.P. & Denuit, M. (2006). Fixed versus random effects in Poisson regression models for claim counts: A case study with motor insurance. ASTIN Bulletin: The Journal of the IAA, 36(1): 285-301.

[29] Vitalis, N., Runyoro, A.K., & Selemani, M. (2022). Assessing factors for occurrence of road accidents in Tanzania using panel data analysis: Road Safety Perspective, 12: 123-136.

[30] Cameron, A.C. & Trivedi, P.K. (2013). Regression analysis of count data. Cambridge University Press, Cambridge.

[31] Winkelmann, R. (2008). Econometric analysis of count data. 5th edition, Springer-Verlag, Berlin.

[32] Hoyos, R.E. & Sarafidis, V. (2006). Testing for cross-sectional dependence in panel-data models. The Stata Journal, 6(4): 482–496.

[33] Pesaran, M.H. (2004). General diagnostic tests for cross section dependence in panels. University of Cambridge, Faculty of Economics, Cambridge Working Papers in Economics No. 0435.

[34] Hurlin, C. & Mignon, V. (2007). Second generation panel unit root tests. Working Papers, HAL.

[35] Pesaran, M.H. (2007). A simple panel unit root test in the presence of cross-section dependence. Journal of Applied Econometrics, 22(2): 265–312.

[36] Pratiwi, K.D. (2022). E-Commerce and economic growth in Indonesia: Analysis of panel data regression. Gema Publica, 7(1): 171–186.

[37] Authority of Statistics and Geographic Information Systems (ASGIS), Annual reports for years from 2015 to 2023. Iraq.

[38] Jessiw, W.S. & Yuan, W. (1998). The efficacy of safety policies on traffic fatalities in Singapore. Acci. Anal. Prev., 30: 745-754.

[39] Blatt, J. & Furman, S.M. (1998). Residence location of drivers involved in fatal crashes. Accident Analysis and Prevention, 30(6): 705–711.

[40] Cespedes, L., Ayuso, M. & Santolino, M. (2024). Effect of population density in aging societies and severity of motor vehicle crash injuries: the case of Spain. Eur. Transp. Res. Rev. 16(48): 1-15.

[41] Li, Z., Wang, W., Liu, P., Bigham, J.M., & Ragland, D.R. (2013). Using geographically weighted Poisson regression for county-level crash modeling in California. Safety Science, 58: 89–97.

[42] Zwerling, C., Peek-Asa, C., Whitten, P.S., Choi, S.W., Sprince, N.L., & Jones, M.P. (2005). Fatal motor vehicle crashes in rural and urban areas: Decomposing rates into contributing factors. Inj. Pre., 11(1): 24–28.

Study and Estimation of the Hormone Visfatin and its Relationship to Diabetes Mellitus and Obesity

Omar M. Hameed [1]

Othman K. Abdulhameed [2]

Thana Y. Yousif [3]

Abstract

Visfatin is a recently identified hormone of adipocytes, it is a multifunctional peptide that is endocrine, autocrine, and paracrine. Recent studies have highlighted the potential influence of the hormone visfatin on the progression of many diseases. The research involves estimation of the visfatin hormone levels in the serum of individuals with type 2 diabetes mellitus (T2DM) and obesity, in comparison to a control group. Furthermore, the lipid profile was determined by assessing six specific parameters, which are: Total Cholesterol, high-density lipoprotein cholesterol (HDL-C), triglycerides (TGs), low-density lipoprotein-cholesterol (LDL-C), very low density lipoprotein cholesterol (VLDL-C) and atherogenic index (AI).

This study has been conducted on (90) sample ranging from (38-85) years: (60) of them are T2DM with obesity patients and (30) samples as control group, where the study was divided into three main parts as follows: Assessment of the levels of visfatin hormone and lipid profile in T2DM with obesity patients and the comparison between the levels of biochemical parameters in the blood serum of male T2DM with obesity patients and the female T2DM with obesity patients, beside of, the comparison between body mass index(BMI) groups for patients.

The patients had a significant increase in visfatin levels compared to the control group. According to the findings, BMI is directly correlated with an increase in visfatin levels. Clinical data indicated a notable difference in visfatin levels between female and male patients. The evidence suggests that visfatin hormone is a reliable indicator for the diagnosis of diabetes in individuals with obesity.

Keywords: *Visfatin, Diabetes, Obesity, Lipid, BMI.*

http://dx.doi.org/10.47832/RimarCongress04-4

[1] College of Science, University of Mosul, Iraq omar.mohammad@uomosul.edu.iq

[2] College of Pharmacy, Alnoor University, Iraq othman.qusay@alnoor.edu.iq

[3] College of Science, University of Mosul, Iraq thana.y.yousif@uomosul.edu.iq

1.Introduction

Diabetic complications arise from persistently elevated blood sugar (glucose) levels. It develops when insulin isn't properly absorbed by the body or when the pancreas doesn't make any insulin at all. Diabetic complications can strike at any age. Although most forms of diabetes are chronic (long-term), they are all manageable with medication and changes to one's lifestyle [1,2].

Carbohydrates in food and drink are the principal sources of glucose, sometimes known as sugar. Your body uses it as its principal energy source. Glucose is carried throughout your body by the blood and used as fuel by every cell [2].

Once glucose enters your bloodstream, it requires a key to travel to its proper destination. The most important hormone is insulin. Hyperglycemia, often known as high blood sugar in which glucose accumulation in the bloodstream occurs either as a result of inadequate insulin synthesis or incorrect insulin usage [3,4].

1.1. Type 2 diabetes mellitus:

A malfunction in sugar metabolism regulation results in type 2 diabetes, which is characterized by high blood sugar levels. This results from insufficient insulin production and reduced cellular response to insulin, affecting the immune, neurological, and cardiovascular systems [5-6].

Type 2 diabetes is primarily caused by insulin resistance in adipose tissue, skeletal muscle, and the liver, along with insufficient insulin production by the pancreas, with excess weight and a sedentary lifestyle being major risk factors [7,8,9].

1.2. Obesity:

Obesity is defined as an excessive or unhealthy accumulation of fat to dangerous levels [10]. The primary cause is excessive calorie intake, with obesity characterized by a Body Mass Index (BMI) ≥ 30 kg/m² and excess adipose tissue [11]. Recognized as a major health concern, obesity raises the risk of diabetes, high blood pressure, heart disease, sleep apnoea, and certain cancers [12,13]. It typically stems from excessive calorie intake and insufficient physical activity but can also be influenced by genetics, endocrine disorders, medications, and psychological factors [11,13].

Although the origin of insulin resistance remains unknown, it is well-documented that being overweight and lack of physical activity worsen the condition. Insulin resistance plays a significant role in the progression of type 2 diabetes, and the fact that reducing body fat can help manage or even reverse the disease highlights this connection.[14].

1.3. Visfatin hormone and its Relationship to Type 2 Diabetes Mellitus with obesity:

Visfatin is a recently identified hormone of adipocytes and type 2 diabetes mellitus is directly correlated with plasma visfatin levels. visfatin produces hypoglycemia by attaching the insulin receptor at an alternative spot differ in the location where insulin binds. Insulin, somatostatin, and statins downregulate visfatin, while hypoxia, inflammation, and hyperglycemia upregulate it [15].

This hormone has been detected in the kidney, spleen, brain, testis and lung, among other tissues and organs. It is present in both the cytoplasm and the nucleus of cells, and it is predominantly found in visceral adipose tissue. It has additionally been demonstrated that it is increased in certain animal models of obesity [16].

Several recent studies indicate that the onset and progression of type 2 diabetes mellitus may hinge on the role played by visfatin hormone. Research suggests that individuals with type 2 diabetes and obesity may exhibit raised concentration of visfatin hormone. It is believed that disruptions in visfatin hormone secretion could be a contributor to insulin resistance and diabetes development [17,18]. There are multiple mechanisms that support the link between visfatin and the development and exacerbation of type2 diabetes associated with obesity [19,20].

Obese individuals, especially with central obesity (fat buildup in the abdomen region) have an increase in visceral adipose tissue. These tissues secrete are larger amounts of visfatin than subcutaneous adipose tissue [20]. Visfatin levels in the bloodstream are elevated by excess visceral adipose tissue, which is connected to insulin resistance and a greater chance of evolving type 2 diabetes. An excess of visfatin can stimulate an inflammatory response in the body, which increases insulin resistance and hinders the regulation of the level of blood glucose [20,21].

2. Materials and Methods

60 patients were enrolled in this study who were diagnosed with type 2 diabetes and obesity. The diagnoses were made by specialists at the Care Unit and Center for Diabetes and

Obesity Treatment. Serum samples were collected between January 2024 and March 2024 from patients at Ibn Sina Teaching Hospital, Al-Salam Teaching Hospital in Mosul, and private laboratories. Clinical diagnoses for all cases were conducted by diabetes specialists. The patients, ranging in age from 38 to 85, were identified as having both diabetes and obesity. The control group comprised 30 healthy individuals who tested negative for both diabetes and obesity. These participants were matched in age with the patient group and had no prior history of any illnesses.

A venous blood sample of 10 milliliters was obtained from each patient. The samples were left to clot at 25°c for 10–20 minutes, followed by the separation process for obtaining serum through centrifugation at 3500 xg for ten minutes. Three portions of the serum were separated and kept at -20°C for later examination.

Serum human visfatin was quantified using Bioassay Laboratory Technology ELISA kit (Cat. No. E0025Hu, China) according to the protocol established by the manufacturer.

Biolabo (france) assay Kit were used to determination of HDL, cholesterol and triglyceride in the serum. An enzyme-driven reaction is utilized in the total cholesterol assay to measure both cholesterol esters and free cholesterol. While the enzymatic hydrolysis of serum triglycerides by lipase during triglyceride estimation results in the generation of free fatty acids and glycerol.. For this two parameters, hydrogen peroxide is created during the process, and it is then identified using a highly specific colorimetric spectrophotometer. The determination of HDL-C involved the precipitation of VLDL, LDL and chylomicron phosphotungstic acid (PTA) and Magnesium chloride then the supernatant was used to the estimation.

Data analysis utilized SPSS version 26, presenting results as mean ± standard error (SE). A t-test assessed differences between groups, with $p \leq 0.05$ regarded as significant. To evaluate significant correlations, Pearson's correlation coefficient was utilized, and one-way ANOVA was used for comparisons involving multiple variables [21].

3. Results

As presented in **Table 1**, the results reveal a significant increase in the concentration of visfatin in the patient group compared to the control group. Furthermore, the patients exhibited considerably higher levels of HDL, LDL, VLDL, triglycerides, cholesterol and the AI.

The data as shown in **Table 2** referred that in obese diabetes patients, females tend to have higher visfatin levels than males., and lipid profile levels indicate a highly significant

increase in male diabetes with obesity patients compared to female diabetes with obesity patients.

The clinical results demonstrated a significant difference in BMI, visfatin, LDL, and the atherogenic index across the three BMI groups in the patient population. These results are outlined in **Table 3**.

Table 1. Levels of the parameters measured in blood serum of diabetes with obesity patients and their comparison with the control group.

Measured Parameters	Control group N=30		Diabetes with obesity patients N=60		(P) value
	Mean	SD	mean	SD	
Age (years)	60.41	10.90	57.42	9.75	0.161
BMI	34.40	4.16	37.32	5.62	0.126
Cholesterol (mg/dl)	198.50	22.58	369.45	35.68	0.003**
Triglycerides (mg/dl)	147.17	21.96	333.47	37.84	0.002**
HDL (mg/dl)	50.37	13.13	30.33	6.62	0.0001***
LDL (mg/dl)	117.64	16.61	305.11	27.41	0.001**
VLDL (mg/dl)	29.32	8.13	72.55	14.65	0.001**
AI	4.13	0.77	12.34	1.54	0.0001***
Visfatin (ng/mL)	21.90	4.09	27.24	2.76	0.043*

*** Significant difference from the control group at P≤0.05**

Table 2. Levels of some parameters measured in blood serum of patients female and their comparison with the patients male.

Measured Parameters	Patients female N=29		Patients male N=31		(P) value
	Mean	SD	Mean	SD	
Age (years)	57.72	9.17	56.00	9.91	0.24
BMI	36.92	7.89	37.34	7.32	0.838
Cholesterol (mg/dl)	377.56	36.42	376.67	22.77	0.989
Triglycerides (mg/dl)	236.48	32.22	292.51	27.42	0.031*

HDL (mg/dl)	37.78	8.57	32.75	8.47	0.043*
LDL (mg/dl)	283.17	21.55	313.56	20.52	0.042*
VLDL (mg/dl)	48.67	6.95	63.81	5.74	0.048*
AI	9.81	6.69	11.80	7.07	0.335
Visfatin (ng/mL)	25.13	11.12	21.98	2.77	0.042*

*** Significant difference from the control group at P≤0.05**

Table 3. Comparison between BMI groups for patients.

Biochemical Parameters	**Stages (mean ± SD)**			
	Stage I **Patients BMI 30-34.9** **N=32**	**Stage II** **Patients BMI 35-39.9** **N=14**	**Stage III** **Patients BMI 40 and over** **N=14**	
BMI	32.03 ± 1.76	37.05 ± 1.52	48.54 ± 6.14	0.0001***
Cholesterol (mg/dl)	316.31 ± 88.39	325.53 ± 24.12	480.71 ± 27.20	0.069
Triglycerides (mg/dl)	258.64 ± 53.79	321.30 ± 39.33	323.30 ± 47.16	0.613
HDL (mg/dl)	36.41 ± 9.51	31.46 ± 9.22	30.57 ± 6.76	0.245
LDL (mg/dl)	245.61 ± 42.03	297.50 ± 24.59	423.11 ± 45.27	0.037*
VLDL (mg/dl)	51.72 ± 20.75	64.26 ± 21.86	65.97 ± 22.51	0.492
AI	8.42 ± 1.78	12.76 ± 2.89	14.25 ± 3.96	0.012**
Visfatin (ng/mL)	22.89 ± 4.94	27.11 ± 4.62	28.60 ± 5.88	0.045*

*** Significant difference from the control group at P≤0.05**

4. Discussion

Visfatin, secreted in significant amounts by the visceral adipose tissue that is more active in metabolism compared to subcutaneous fat, tends to be elevated When individuals have excess visceral fat. Research suggests that visfatin may impact insulin sensitivity, a crucial factor often reduced in type 2 diabetes. Additionally, researchers suggest that people with type 2 diabetes

frequently exhibit higher visfatin levels, emphasizing its potential character in the development of the disease, as illustrated in **Table 1**.

The findings demonstrated a highly significant elevation in lipid profile levels in diabetic patients with obesity. The lipid profile, a key clinical parameter is frequently elevated in individuals with both diabetes and obesity due to several interconnected factors [22,23]:

Insulin resistance is a common condition in individuals with obesity and type 2 diabetes, where the body's cells exhibit a diminished response to insulin. As a result, insulin levels in the blood rise, disrupting fat metabolism and promoting fat accumulation in the liver. This process contributes to elevated triglyceride levels and an increase in cholesterol and LDL [23].

Chronic inflammation associated with obesity leads to a persistent inflammatory state in adipose tissue. This condition stimulates the release of inflammatory cytokines, which interfere with normal fat metabolism and contribute to elevated lipid levels in the bloodstream [24].

Visceral fat, which surrounds internal organs, is more active than subcutaneous fat in releasing free fatty acids into the bloodstream. Elevatated concentration of fatty acids subsequently lead to an increased production of triglycerides in the liver [25].

Elevated Visfatin Levels: excessive secretion of visfatin can disrupt normal fat distribution and contribute to metabolic dysregulation.

Hormonal Dysregulation: Obesity and diabetes are linked to changes in the concentration of hormones like leptin and adiponectin, which are crucial for maintaining appetite and regulating fat metabolism. These hormonal disturbances can result in higher lipid level in the blood [26].

As shown in Table 2, women exhibited a significant difference in visfatin and lipid profile. Research suggests that visfatin, may be influenced by hormonal and genetic differences between sexes. Consequently, women with obesity and diabetes often exhibit higher visfatin levels than men with the same condition [27,28].

The elevated visfatin levels in females compared to males in these patients can be explained by a combination of overlapping factors, including hormonal fluctuations and gender-specific metabolic characteristics [29]:

Sex Hormones: Estrogen and progesterone, the primary sex hormones in women, play a role in regulating visfatin production and secretion. These hormones promote fat storage and enhance visfatin expression in adipose tissue, contributing to its higher levels in women [30] .

Fat Distribution: Women have a tendency to store lipid in the thighs and buttocks, men tend to accrue more abdominal fat. These differences influence visfatin levels, as subcutaneous and visceral fat contribute differently to its production [31].

Genetic Factors: Variations in gene expression between men and women can affect visfatin production, as genes involved in its regulation may function differently in each sex [32].

4.1. The comparison between BMI groups for the patients:

The patient group was divided into three stages (I, II, and III) based on their body mass index (BMI) for comparison.

As body mass index (BMI) increases, visfatin levels also tend to rise. This is attributed to the higher amount of adipose tissue, which BMI estimates based on an individual's weight and height, leading to elevated visfatin concentrations [33]. With an increase in BMI, there is a corresponding rise in adipose tissue, which serves as the primary source of visfatin secretion. Individuals with a higher BMI typically have more visceral fat, leading to elevated visfatin levels in the bloodstream [34]. BMI and visfatin levels have consistently been found to have a positive correlation in clinical studies, suggesting that obese individuals tend to have higher visfatin levels compared to those with a normal weight [35].

Additionally, this study has revealed an increase in LDL levels and a direct correlation between LDL and atherogenic index (AI) as BMI rises. LDL levels tend to increase due to factors such as increased adipose tissue, insulin resistance, chronic inflammation, poor dietary habits, and hormonal imbalances. This emphasizes the importance of managing weight to maintain healthy cholesterol levels [36, 37].

In conclusion, the study focus on the role of visfatin hormone as a diagnostic marker for diabetes in obese patients, the relationship between lipid profiles and different types of diabetes, the connection between visfatin and other diseases. These investigations aim to provide deeper insights into the pathophysiology of diabetes and obesity and improve diagnostic for these conditions.

5. Conclusion:

BMI is directly correlated with an increase in visfatin levels. The evidence too suggests that visfatin hormone is a reliable indicator for the diagnosis of diabetes in individuals with obesity.

6. References:

[1] Kaul, K., Tarr, J. M., Ahmad, S. I., Kohner, E. M., & Chibber, R. (2013). Introduction to diabetes mellitus. Diabetes: an old disease, a new insight, 1-11.

[2] Alam, U., Asghar, O., Azmi, S., & Malik, R. A. (2014). General aspects of diabetes mellitus. Handbook of clinical neurology, 126, 211-222.

[3] Blair, M. (2016). Diabetes mellitus review. Urologic nursing, 36(1).

[4] Bastaki, S. (2005). Diabetes mellitus and its treatment. International journal of Diabetes and Metabolism, 13(3), 111-134.

[5] DeFronzo, R. A., Ferrannini, E., Groop, L., Henry, R. R., Herman, W. H., Holst, J. J., ... & Weiss, R. (2015). Type 2 diabetes mellitus. Nature reviews Disease primers, 1(1), 1-22.

[6] Hameed, O. M., & Al-Helaly, L. A. (2021). Evaluation the level of Total Fucose and Some Enzymes in the Blood of Patients with Neurological Diseases. Egyptian Journal of Chemistry, 64(10), 5613-5618.

[7] Grootenhuis, P. A., Snoek, F. J., Heine, R. J., & Bouter, L. M. (1994). Development of a type 2 diabetes symptom checklist: a measure of symptom severity. Diabetic Medicine, 11(3), 253-261.

[8] Langenberg, C., & Lotta, L. A. (2018). Genomic insights into the causes of type 2 diabetes. The Lancet, 391(10138), 2463-2474.

[9] Hameed, O. M. (2023). Estimation of some Trace Elements in the Sera of People with Myocardial Infarction Disease. In E3S Web of Conferences (Vol. 391, p. 01124). EDP Sciences

[10] Verma, S., & Hussain, M. E. (2017). Obesity and diabetes: an update. Diabetes & Metabolic Syndrome: Clinical Research & Reviews, 11(1), 73-79.

[11] Kopelman, P. G. (2000). Obesity as a medical problem. Nature, 404(6778), 635-643.

[12] Hameed, O. M., Rashed, S. H., & Al-Helaly, L. A. (2023). Changes in the level of zinc and copper and some biochemical parameters in patients with chronic kidney failure. Biomedical and Biotechnology Research Journal (BBRJ), 7(1), 118-122

[13] Segula, D. (2014). Complications of obesity in adults: a short review of the literature. Malawi Medical Journal, 26(1), 20-24.

[14] Schuster, D. P. (2010). Obesity and the development of type 2 diabetes: the effects of fatty tissue inflammation. Diabetes, metabolic syndrome and obesity: targets and therapy, 253-262.

[15] Adeghate, E. (2008). Visfatin: structure, function and relation to diabetes mellitus and other dysfunctions. Current medicinal chemistry, 15(18), 1851-1862.

[16] Alkanaani, M. I., Rajab, E. R., Abdulwahed, A. M., Dabos, T., Alshammiri, B., Abdullah, S. N., & Al-Samarraie, M. Q. (2020). Visfatin hormone level and lipid profile in some hyperlipidemia patients in samarra city. Biochem. Cell. Arch, 20(1), 1191-3.

[17] Hug, C., & Lodish, H. F. (2005). Visfatin: a new adipokine. Science, 307(5708), 366-367.

[18] Li, Z. P., Zhang, M., Gao, J., Zhou, G. Y., Li, S. Q., & An, Z. M. (2014). Study of the correlation between growth hormone deficiency and serum leptin, adiponectin, and visfatin levels in adults. Genet Mol Res, 13(2), 4050-6.

[19] Li, L., Yang, G., Li, Q., Tang, Y., Yang, M., Yang, H., & Li, K. (2006). Changes and relations of circulating visfatin, apelin, and resistin levels in normal, impaired glucose tolerance, and type 2 diabetic subjects. Experimental and clinical endocrinology & diabetes, 114(10), 544-548.

[20] El-Shafey, E. M., El-Naggar, G. F., Al-Bedewy, M. M., & El-Sorogy, H. (2012). Is there a relationship between visfatin level and type 2 diabetes mellitus in obese and non-obese patients. J Diabetes Metab S, 11(2).

[21] Esteghamati, A., Alamdari, A., Zandieh, A., Elahi, S., Khalilzadeh, O., Nakhjavani, M., & Meysamie, A. (2011). Serum visfatin is associated with type 2 diabetes mellitus independent of insulin resistance and obesity. Diabetes research and clinical practice, 91(2), 154-158.

[22] Hajianfar, H., Bahonar, A., Entezari, M. H., Askari, G., & Yazdani, M. (2012). Lipid profiles and serum visfatin concentrations in patients with type II diabetes in comparison with healthy controls. International Journal of Preventive Medicine, 3(5), 326.

[23] Gligor, R., Zdremţan, D., Pilat, L., Matei, I., Ionescu-Tîrgovişte, C., & Crisnic, I. (2012). Correlations of visfatin with the lipidic metabolism in diabetic and obese patients. Age (years), 60(11.55), 42-3.

[24] Engin, A. (2017). The pathogenesis of obesity-associated adipose tissue inflammation. Obesity and lipotoxicity, 221-245.

[25] Alves-Bezerra, M., & Cohen, D. E. (2017). Triglyceride metabolism in the liver. Comprehensive physiology, 8(1), 1.

[26] Dilworth, L., Facey, A., & Omoruyi, F. (2021). Diabetes mellitus and its metabolic complications: the role of adipose tissues. International journal of molecular sciences, 22(14), 7644.

[27] Chang, Y. H., Chang, D. M., Lin, K. C., Shin, S. J., & Lee, Y. J. (2011). Visfatin in overweight/obesity, type 2 diabetes mellitus, insulin resistance, metabolic syndrome and cardiovascular diseases: a meta-analysis and systemic review. Diabetes/metabolism research and reviews, 27(6), 515-527.

[28] Mehdizadeh, A., Hamzezadeh, S., & Tofighi, A. (2016). Investigation of plasma visfatin changes in women with type 2 diabetes followed by endurance, resistance and combined exercise: the role of lipid profile, glycemic indices and insulin resistance. J. Diabetes Metab., 7, 703.

[29] De Luis, D. A., Aller, R., Gonzalez Sagrado, M., Conde, R., Izaola, O., & De la Fuente, B. (2013). Serum visfatin levels and metabolic syndrome criteria in obese female subjects. Diabetes/Metabolism Research and Reviews, 29(7), 576-581.

[30] Annie, L., Gurusubramanian, G., & Roy, V. K. (2019). Estrogen and progesterone dependent expression of visfatin/NAMPT regulates proliferation and apoptosis in mice uterus during estrous cycle. The Journal of steroid biochemistry and molecular biology, 185, 225-236.

[31] Nelder, M. (2020). The role of an addictive tendency towards food and patterns of body fat distribution in obesity and metabolic health (Doctoral dissertation, Memorial University of Newfoundland).

[32] Dutta, S., Sengupta, P., Jegasothy, R., & Akhigbe, R. (2021). Resistin and visfatin: â€˜ connecting threadsâ€™ of immunity, energy modulations and male reproduction. Chemical Biology Letters, 8(4), 192-201.

[33] Kamińska, A., Kopczyńska, E., Bronisz, A., Żmudzińska, M., Bieliński, M., Borkowska, A., ... & Junik, R. (2010). An evaluation of visfatin levels in obese subjects. Endokrynologia Polska, 61(2), 169-173.

[34] Abdulmuttaleb, N. A., Mohammed, M. Q., & Mohsein, O. A. (2024). The impact of adipocytokines on thyroid function and obesity: A narrative review. development, 8, 9.

[35] Samara, A., Pfister, M., Marie, B., & Visvikis-Siest, S. (2008). Visfatin, low-grade inflammation and body mass index (BMI). Clinical endocrinology, 69(4), 568-574.

[36] Kelly, A. S., Jacobs Jr, D. R., Sinaiko, A. R., Moran, A., Steffen, L. M., & Steinberger, J. (2010). Relation of circulating oxidized LDL to obesity and insulin resistance in children. Pediatric diabetes, 11(8), 552-555.

[37] Njajou, O. T., Kanaya, A. M., Holvoet, P., Connelly, S., Strotmeyer, E. S., Harris, T. B., ... & Hsueh, W. C. (2009). Association between oxidized LDL, obesity and type 2 diabetes in a population-based cohort, the Health, Aging and Body Composition Study. Diabetes/metabolism research and reviews, 25(8), 733-739.

A New Intrusion Detection Approach Based on RNA Encoding and K-Means Clustering Algorithm Using KDD-Cup99 Dataset

Omar Fitian Rashid [1]

Safa Ahmed Abdulsahib [2]

Imad J. Mohammed [3]

Abstract

Intrusion detection systems (IDS) are useful tools that help security administrators in the developing task to secure the network and alert in any possible harmful event. IDS can be classified either as misuse or anomaly, depending on the detection methodology. Where Misuse IDS can recognize the known attack based on their signatures, the main disadvantage of these systems is that they cannot detect new attacks. At the same time, the anomaly IDS depends on normal behaviour, where the main advantage of this system is its ability to discover new attacks. On the other hand, the main drawback of anomaly IDS is high false alarm rate results. Therefore, a hybrid IDS is a combination of misuse and anomaly and acts as a solution to overcome the disadvantages of these two methods. In this paper, a new hybrid IDS is proposed based on the RNA encoding idea and applying the K-means clustering algorithm. Firstly, choosing random records for both training and testing. Secondly, propose RNA encoding by calculating all possible record values within dataset and generating RNA characters for each value, then dividing it into blocks. The third step is done by searching and extracting normal keys based on the most repeated blocks, and the same procedure is applied to extract the attack keys. Finally, the K-means clustering method is used to classify the testing records based on extracted keys. The proposed method is evaluated by calculating the detection rate (DR), false alarm rate (FAR), and accuracy, where the achieved DR, FAR, and accuracy are equal to 91.13%, 0.46%, and 92.02% respectively. Based on the achieved results, it can be said that the proposed hybrid IDS has high DR and accuracy results, can detect new attacks, and can solve the problem of anomaly IDS by getting a low false alarm rate result.

Keywords: *Intrusion Detection, Hybrid, Misuse, Anomaly, Clustering.*

http://dx.doi.org/10.47832/RimarCongress04-5

[1] College of Science, University of Baghdad, Iraq Omar.f@sc.uobaghdad.edu.iq

[2] College of Science, University of Baghdad, Iraq safa.a@sc.uobaghdad.edu.iq

[3] College of Science, University of Baghdad, Iraq emad.j@sc.uobaghdad.edu.iq

1. Introduction

With the fast evaluation of the Internet, today's community highly uses networked systems, where this integration involves different types of data and information within networked systems. On the other hand, various cyber security threats happen in the network. Cybersecurity is an important zone of investigation due to its importance in securing data and information [1]. Network security technology refers to techniques that protect programmers, networks, computers, and data from being damaged, attacked, or accessed by unauthorized persons [2]. An intrusion detection system (IDS) method is a part of a network security technique that is used to check a network or computer for malicious activity or policy violations [3]. These systems are used to monitor malicious transactions over network traffic and then send alerts or take proactive, reactive measures as soon as they are observed. The real-time monitoring method provides real-time monitoring of network traffic and computer activity to detect abnormal or suspicious behavior in a timely manner. However, with the increasing complexity of network attacks, traditional IDS methods fail to meet the growing demand for network security detection [4].

Various IDS methods are proposed in different publications research that are used to detect threats over the internet. Li et al. [5] presented a Hybrid DoS Attack IDS that used signature and anomaly detection and could recognize known and unknown DoS attacks. A new IDS frame is proposed by [6] for the next generation of the Internet of Things, where the Minmax method is applied for collecting and pre-processing information. The Marine Predator method is used for feature selection, and these features are used by the neural network method. A novel IDS technique is proposed by [7] by using parallel long-short-term memory, which used the parallelism power that led to achieving efficient and accurate results. Two DNA encoding methods are applied for IDS by [8]; these methods have different DNA lengths, where these methods are used for encoding the dataset records, then extracting the keys and their positions, and finally, a matching algorithm is used.

A cyber-IDS method is proposed by changing the superimposed component slope for the ends of the line segment [9], where the suggested method can identify cyber-attacks from internal faults. An efficient IDS is proposed by using a stream classification method with the use of stream-based learning with limited labels [10]. Zarzoor et al. [11] suggested a new IDS method by using a spike neural network and decision tree, and the decision tree is used to extract samples, then used these samples for the spike neural network method. A new idea for IDS by using deep learning is presented [12]; this method can detect targeting metaverse-IoT

communications attacks by applying the kernel principal component analysis that is used for feature selection and applying the convolutional neural networks method that is used to identify and classify the attacks. Örs and Levi [13] presented a machine learning-based multi-class classifier where the proposed method can detect 6 attack types and find the attackers' network addresses. An IDS for large-scale IoT networks is suggested by [14], where this system uses a machine learning method to find relevant features. The extracted features are trained with different machine learning methods, such as the random forest algorithm and the extra trees method. A new IDS for IoT is presented by [15], where the suggested system starts by categorizing network traffic values into four groups and then applying majority voting to select the classification results. Finally, used an unsupervised elliptic envelope method for classification. A new IDS technique is suggested based on DNA encoding [16]; the first step is done by representing each record value with four DNA characters, then extracting the classification keys, and the last step is applying the Brute-force algorithm for matching based on the extraction keys. Sharma et al. [17] presented a novel IDS for IoT based on a deep learning method, where a deep neural network method was used to extract the features. Then, they tuned the proposed method by using different parameters. Analyzed the main limitations of hybrid IDS methods and then suggested a novel hybrid IDS method by using the Firefly algorithm and Fast Learning Network, which led to overcoming most of the limitations of the previous works [18]. A novel IDS technique is presented for IoT networks [19] based on machine learning, where the proposed method can detect cyber-attacks effectively and select the important features that lead to less training time.

2. Materials and methods

The proposed hybrid intrusion detection system method aims to identify unauthorized use, misuse, and abuse of computer systems or networks. The proposed IDS method is hybrid, which means it combines the two approaches (misuse and anomaly) in one system. The suggested system consists of five steps, as shown in Figure 1. These steps are selecting the dataset, RNA encoding, normal keys extraction, attack keys extraction, and applying the clustering algorithm.

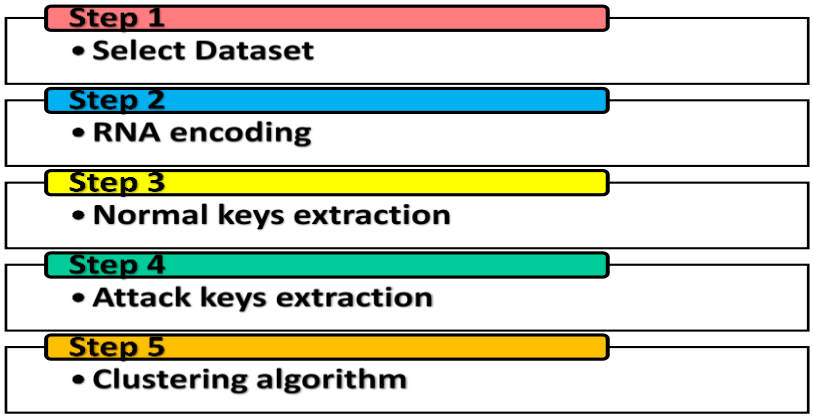

Figure 1. Proposed hybrid intrusion detection system steps

The first step is done by selecting the dataset that is used for both training and testing. The KDD-Cup99 dataset is used for this purpose because it is a public repository to promote research works, and it consists of thousands of records and has 38 attack types. After choosing the dataset, 3000 random records are used for the training phase, while 9000 random records are used for testing. The next step is building an RNA encoding table that is used to convert all record values into RNA characters; this method is done by calculating all possible record values in the KDD-Cup99 dataset, and these values are equal to 96 different values in the encoding process each value are represented by four random RNA characters which can handle and represent all possible value without repletion. Table 1 shows the proposed RNA encoding table for all 96 record values.

Table 1. Proposed RNA encoding method

Record value	RNA characters	Record value	RNA characters
SF	CCGC	S3	AUAC
OTH	GAAG	RSTOSO	CGGA
RSTO	ACUC	S0	UCCU
REJ	CCAC	RSTR	GGCA
S1	AGUC	SH	GGUU
S2	CCCA	0	CUAU
1	CUUC	6	GUAG
2	UAUC	7	AUGA
3	GGGC	8	CAAG
4	CACC	9	GAAU
5	UGAC	.	UUCU
HTTP	UGGC	HOSTNAMES	GCCC
HTTP 443	AUCU	CSNET NS	UAGC
DOMAIN U	GUAA	POP 2	AAAC
ECR I	AACA	SUNRPC	UGCU
SMTP	AGGG	LDAP	GAGU
ECO I	UAAG	DISCARD	GUGC
TELNET	CCAG	NAME	GAUG
NTP U	UGAU	KLOGIN	UAGU

URP I	CAGA	IRC	UCUU
Z39 50	UACC	X11	GUUC
FTP	UUCG	NNSP	AUUG
SSH	CAAC	NNTP	CAAA
WHOIS	UCAC	IMAP4	GCAC
CTF	AUGU	SQL NET	GUCA
LINK	UCGA	LOGIN	ACAU
SUPDUP	GCUA	SHELL	GCCU
ISO TSAP	UGCA	PRINTER	CAGU
UUCP PATH	CAUA	EFS	CGCU
FINGER	ACGU	DAYTIME	AGUA
EXEC	GCUU	SYSTAT	UAUG
NETBIOS DGM	GGUC	NETSTAT	GUGA
COURIER	CCGA	TIME	UACU
PM DUMP	CGUG	ECO	ACCG
TFTP U	CGAG	ICMP	CGAA
RED I	CGUC	MTP	AUUC
FTP DATA	AGCU	NETBIOS NS	ACCA
POP 3	CAGG	UUCP	GAUC
AUTH	GUAU	AOL	ACCU
OTHER	AUAA	HTTP 8001	UUAA
PRIVATE	UCCA	NETBIOS SSN	UUGG
VMNET	AAAG	KSHELL	UUCC
BGP	GGAC	HTTP 2784	ACGC
DOMAIN	GUCU	URH I	GCGA
GOPHER	GAGG	TIM I	GAUU
REMOTE JOB	ACCC	HARVEST	UCAG
RJE	UUGC	TCP	CCUU
UDP	GUUA	ICMP	CCGG

For more explanation about the RNA encoding process, the following example shows the RNA encoding for the following record, and the RNA encoding in details are illustrated in Figure 2.

"0,tcp,http,SF,223,185,0,0,0,0,0,1,0,0,0,0,0,0,0,0,0,0,4,4,0.00,0.00,0.00,0.00,1.00,0.00,0.00,71,255,1.00,0.00,0.01,0.01,0.00,0.00,0.00,0.00"

CUAUCCUUUGGCCCGCUAUCUAUCGGGCCUUCCAAGUGACCUAUCUAUCUAUCUAUCUAUCUUCCUAUCUAUCUAUCUAUCUAUCUAUCUAUCUAUCUAUCUAUCACCCACCCUAUUUCUCUAUCUAUCUAUUUCUCUAUCUAUCUAUUUCUCUAUCUAUCUAUCUAUUUCUCUAUCUAUCUUCUUCUCUAUCUAUCUAUUUCUCUAUCUAUCUAUGACUUCUAUCUGACUGACCUUCUUCUCUAUCUAUCUAUUUCUCUAUCUAUCUAUUUCUCUAUCUUCCUAUUUCUCUAUCUUCCUAUUUCUCUAUCUAUCUAUUUCUCUAUCUAUCUAUUUCUCUAUCUAUCUAUUUCUCUAUCUAU

0	**tcp**	**http**	**sf**
CUAU	CCUU	UGGC	CCGC
223	**185**	**0**	**0**
UAUCUAUCGGGC	CUUCCAAGUGAC	CUAU	CUAU
0	**0**	**0**	**1**
CUAU	CUAU	CUAU	CUUC
0	**0**	**0**	**0**
CUAU	CUAU	CUAU	CUAU
0	**0**	**0**	**0**
CUAU	CUAU	CUAU	CUAU
0	**0**	**4**	**4**
CUAU	CUAU	CACC	CACC
0.00	**0.00**	**0.00**	**0.00**
CUAUUUCUCUAUCUAU	CUAUUUCUCUAUCUAU	CUAUUUCUCUAUCUAU	CUAUUUCUCUAUCUAU
1.00	**0.00**	**0.00**	**71**
CUUCUUCUCUAUCUAU	CUAUUUCUCUAUCUAU	CUAUUUCUCUAUCUAU	AUGACUUC
255	**1.00**	**0.00**	**0.01**

UAUCUFACUGAC	CUUCUUCUCUAUC UAU	CUAUUUCUCUAUC UAU	CUAUUUCUCUAUC UUC
0.01	**0.00**	**0.00**	**0.00**
CUAUUUCUCUAUC UUC	CUAUUUCUCUAUC UAU	CUAUUUCUCUAUC UAU	CUAUUUCUCUAUC UAU
0.00			
CUAUUUCUCUAUC UAU			

Figure 2. RNA encoding in details

The third step of the proposed system is normal key extraction, and this step is done based on the following steps:

- Segmenting records: segment normal and attacks records into blocks with different sizes which include three, four, five, and six-character blocks.

- Removing shared blocks: remove all blocks from normal records that found in the attack record blocks.

- Finding frequent blocks: calculate the block frequency then identifies normal keys by counting their frequency since these blocks occur most frequently in legitimate network traffic.

- Selection of normal keys: The most repeated blocks are chosen as normal keys, where the extracted normal keys are listed in Table 2. Where these keys is used to determine if new records belong to the normal or anomalous category.

- Each normal key was selected as five characters long to strike the right balance between record uniqueness and data applicability. The system's ability to differentiate between records is diminished because two-to-three-character keys are too frequently used in normal and attack records. Long keys which exceed seven characters tend to perform poorly because they identify rare patterns that cannot be applied to normal records in a generalized manner.

Table 2. The extracted normal keys

No.	Key
1	AUGUU
2	UGUUA
3	CGCUA
4	GGCUA

After extracting the normal keys, the same process is done to extract attack keys; and this step is done based on the following steps:

- Segmenting records: segment attack and normal records into blocks with different sizes which include three, four, five, and six-character blocks.

- Removing shared blocks: remove all blocks from attack records that found in the normal record blocks.

- Finding frequent blocks: calculate the block frequency then identifies attack keys by counting their frequency since these blocks occur most frequently in legitimate network traffic.

- Selection of attack keys: The most repeated blocks are chosen as attack keys, where the extracted attack keys are displayed in Table 3. These keys are used to determine if new records belong to the normal or anomalous category.

Table 3. The extracted attack keys

No.	Key
1	UUGAG
2	UCCUC
3	CGCUG
4	CUUUG

The last step of the proposed method is applying a clustering algorithm to cluster the testing records, either normal or attack, based on extracted normal and attack keys. The dataset records need to be pre-processed before applying the clustering algorithm, and these records need to be converted to RNA characters based on the building RNA encoding that was mentioned previously, followed by the K-Means clustering algorithm for this purpose. Figure 3 shows the idea of the K-Means clustering algorithm and classifies the testing records into normal or attack clusters. The steps of the application K-Means algorithm are as follows:

Step 1: specify the number of clusters “k”, which is equal to two clusters (normal cluster and attack cluster).

Step 2: initialize the cluster canters (centroids) based on the extracted normal and attack keys.

Step 3: assign each data point to the cluster based on the similarity between the cluster center and record block.

Step 4: Repeat step 3 for all testing dataset records.

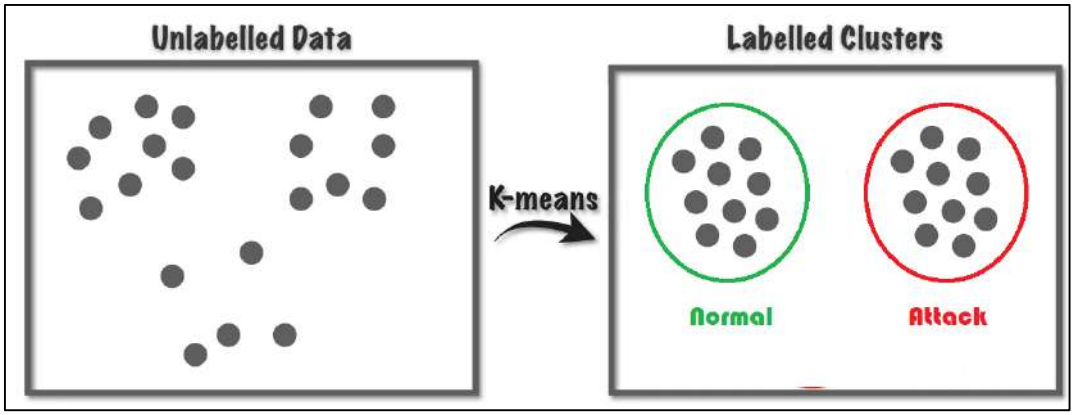

Figure 3. K-Means clustering algorithm

3. Results and discussions

Different aspects, such as the detection rate (DR), false alarm rate (FAR), and accuracy, can measure the performance of the proposed hybrid intrusion detection system where DR represents the ratio of the number of correctly detected attacks to the total number of attacks. At the same time, FAR is the ratio of the number of normal connections that are incorrectly misclassified as attacks to the total number of normal connections, and accuracy is measuring the ratio of the number of truly classified connections to the total number of connections. The DR, FAR, and accuracy results obtained using the proposed method based on extracted normal keys only and based on attack keys only are represented in Table 4 and Figure 4.

Table 4. The achieved results used normal keys only and attack keys only

	Based on normal keys	**Based on attack keys**
DR	90.95%	88.26%
FAR	7.14%	11.74%
Accuracy	91.42%	91.07%

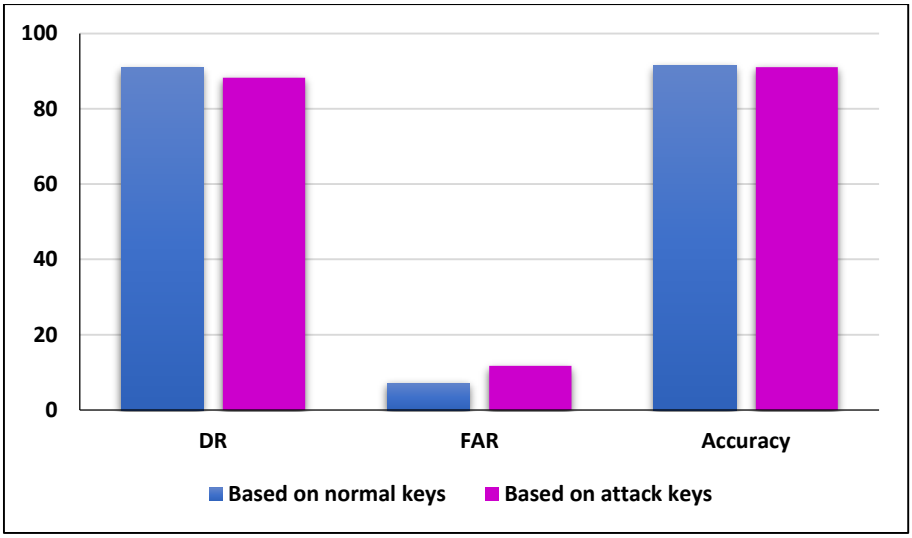

Figure 4. The achieved results used normal keys only and attack keys only

As mentioned in Table 4 and Figure 4, the DR, FAR, and accuracy results obtained by using normal keys are equal to 90.95%, 7.14%, and 91.42%respectively. The achieved DR, FAR, and accuracy results by using attack keys are equal to 88.26%, 11.74%, and 91.07% respectively.

The DR, FAR, and accuracy results achieved based on the proposed hybrid IDS method are stated in Table 5 and Figure 5.

Table 5. The achieved results of the proposed hybrid IDS

	Proposed hybrid IDS
DR	91.13%
FAR	0.466%
Accuracy	92.022%

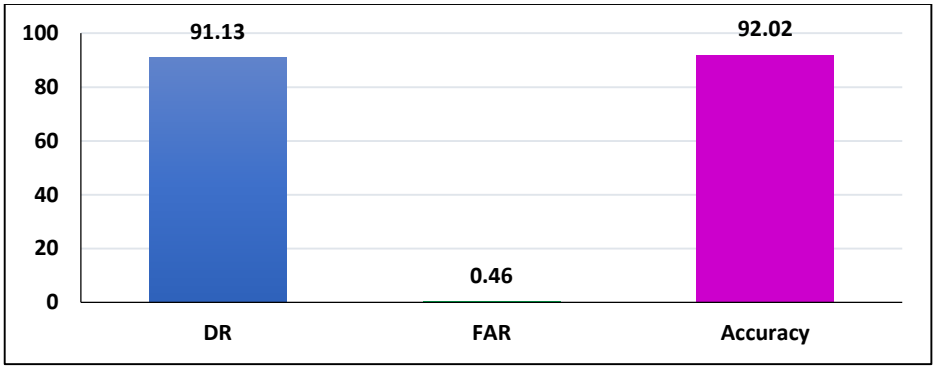

Figure 5. The achieved results of the proposed hybrid IDS

Table 5 and Figure 5 showed that the achieved DR, FAR, and accuracy by the proposed hybrid IDS are equal to 91.13%, 0.466%, and 92.022% respectively. Compared with results obtained by using normal keys only or attack keys only, the proposed IDS method has the highest DR and accuracy results and the lowest FAR results.

4. Conclusion

This study proposed a hybrid intrusion detection system by combining the idea of both anomaly and misuse of IDS to try to overcome their disadvantages. The proposed method has five steps: starting by selecting random records for both training and testing, then proposing an RNA encoding method to convert these records into RNA characters, extracting the normal keys based on the repetition of blocks, then by the same idea extracted the attack keys, and finally applied K-means clustering algorithm to classify the testing records as normal or attacks based on the extracted keys. The results showed that the proposed system provides low FAR and, at the same time, achieves high DR and accuracy.

References:

[1] A. F. Jahwar and S. Y. Ameen, "A review on cybersecurity based on machine learning and deep learning algorithms," *Journal of Soft Computing and Data Mining*, vol. 2, no. 2, pp. 14-25, 2021.

[2] Q. Liu and T. Zhang, "Deep learning technology of computer network security detection based on artificial intelligence," *Computers and Electrical Engineering*, vol. 110, p. 108813, 2023.

[3] M. Usama, M. Asim, S. Latif, and J. Qadir, "Generative adversarial networks for launching and thwarting adversarial attacks on network intrusion detection systems," in *2019 15th international wireless communications & mobile computing conference (IWCMC)*, 2019: IEEE, pp. 78-83.

[4] D. Gümüşbaş, T. Yıldırım, A. Genovese, and F. Scotti, "A comprehensive survey of databases and deep learning methods for cybersecurity and intrusion detection systems," *IEEE Systems Journal*, vol. 15, no. 2, pp. 1717-1731, 2020.

[5] S. Li, Y. Cao, S. Liu, Y. Lai, Y. Zhu, and N. Ahmad, "Hda-ids: A hybrid dos attacks intrusion detection system for iot by using semi-supervised cl-gan," *Expert Systems with Applications*, vol. 238, p. 122198, 2024.

[6] Y. Djenouri, A. Belhadi, G. Srivastava, J. C.-W. Lin, and A. Yazidi, "Interpretable intrusion detection for next generation of Internet of Things," *Computer Communications*, vol. 203, pp. 192-198, 2023.

[7] M. Sudha, V. M. K. Reddy, W. D. Priya, S. M. Rafi, S. Subudhi, and S. Jayachitra, "Optimizing intrusion detection systems using parallel metric learning," *Computers and Electrical Engineering*, vol. 110, p. 108869, 2023.

[8] O. F. Rashid, Z. A. Othman, S. Zainudin, and N. A. Samsudin, "DNA encoding and STR extraction for anomaly intrusion detection systems," *IEEE Access*, vol. 9, pp. 31892-31907, 2021.

[9] K. Gupta, R. Mohanty, S. Sahoo, and B. K. Panigrahi, "Cyber intrusion detection for line current differential relays in DC distribution system," *Sustainable Energy, Grids and Networks*, vol. 34, p. 101065, 2023.

[10] A. A. Abdulrahman and M. K. Ibrahem, "Intrusion detection system using data stream classification," *Iraqi Journal of Science*, vol. 62, no. 1, pp. 319-328, 2021.

[11] A. R. Zarzoor, N. A. S. Al-Jamali, and D. A. A. Qader, "Intrusion detection method for internet of things based on the spiking neural network and decision tree method," *International Journal of Electrical and Computer Engineering*, vol. 13, no. 2, p. 2278, 2023.

[12] [T. Gaber, J. B. Awotunde, M. Torky, S. A. Ajagbe, M. Hammoudeh, and W. Li, "Metaverse-IDS: Deep learning-based intrusion detection system for Metaverse-IoT networks," *Internet of Things*, vol. 24, p. 100977, 2023.

[13] F. K. Örs and A. Levi, "Data driven intrusion detection for 6LoWPAN based IoT systems," *Ad Hoc Networks*, vol. 143, p. 103120, 2023.

[14] S. Fraihat, S. Makhadmeh, M. Awad, M. A. Al-Betar, and A. Al-Redhaei, "Intrusion detection system for large-scale IoT NetFlow networks using machine learning with modified Arithmetic Optimization Algorithm," *Internet of Things*, vol. 22, p. 100819, 2023.

[15] M. Vishwakarma and N. Kesswani, "A new two-phase intrusion detection system with Naïve Bayes machine learning for data classification and elliptic envelop method for anomaly detection," *Decision Analytics Journal*, vol. 7, p. 100233, 2023.

[16] O. F. Rashid, Z. A. Othman, and S. Zainudin, "Four char DNA encoding for anomaly intrusion detection system," in *Proceedings of the 2019 5th International Conference on Computer and Technology Applications*, 2019, pp. 86-92.

[17] B. Sharma, L. Sharma, C. Lal, and S. Roy, "Anomaly based network intrusion detection for IoT attacks using deep learning technique," *Computers and Electrical Engineering*, vol. 107, p. 108626, 2023.

[18] M. Q. Alsudani, S. H. A. Reflish, K. Moorthy, and M. M. Adnan, "A new hybrid teaching learning based Optimization-Extreme learning Machine model based Intrusion-Detection system," *Materials Today: Proceedings*, vol. 80, pp. 2701-2705, 2023.

[19] S. Roy, J. Li, B.-J. Choi, and Y. Bai, "A lightweight supervised intrusion detection mechanism for IoT networks," *Future Generation Computer Systems*, vol. 127, pp. 276-285, 2022.

Novel method for the Synthesis of magnetic Copper-Iron Oxide Nanocomposite and Its Anti-Corrosion Activity on Carbon steel

Mohanad Kadhem Alshujery [1]

Marowah H. Jehad [2]

Omar T. Hussein [3]

Abstract

A Novel binary $Cu_2Fe_2O_6$ nanocomposite was synthesized via photo-irradiation using copper and iron salts, with water as the solvent. The synthesis was conducted under 130-watt power and 25 minutes of irradiation, the resulting $Cu_2Fe_2O_6$ nanoparticles were characterized be Scanning Electron Microscopy (SEM), Atomic Force Microscopy (AFM), and X-ray Diffraction (XRD) to determine their morphology and crystal structure. X-ray mapping was used to determine the elemental composition of the sample. The optical band gap of the nanocomposite was calculated as 1.66 eV using photoluminescence spectroscopy (PL). The average size of the $Cu_2Fe_2O_6$ nanoparticles was found to be approximately 40 nm, and the XRD data confirmed a cubic crystalline structure with an average crystal size of around 29 nm. The synthesized nanoparticles were applied as a protective coating for corrosion prevention on carbon steel, demonstrating a protection efficiency of 76% at 308K. These finding indicate that $Cu_2Fe_2O_6$ nanoparticles are highly effective in protecting carbon steel from corrosion.

Keywords: *$Cu_2Fe_2O_6$ Nanoparticles, Corrosion Protection, Carbon Steel, Sea Water, Photo-Irradiation.*

http://dx.doi.org/10.47832/RimarCongress04-6

[1] Ministry of Education, Baghdad General Directorate of Education, Iraq mohanndkadhem@gmail.com

[2] College of Science for Women, University of Baghdad, Iraq marowah.h@csw.uobaghdad.edu.iq

[3] College of Science, Al- Nahrain University, Iraq omar.taha@nahrainuniv.edu.iq

1- Introduction

Metal oxides, particularly nanostructured metal oxides, have gained significant attention due to their wide range of technological applications, including corrosion inhibitors, catalysts, sensor, microelectronic circuits, fuel cells, and piezoelectric devices. A major focus in nanotechnology is the development of nanostructures with unique properties that differ from their bulk counterparts[1].

Oxidized nanoparticles exhibit distinctive chemical and physical behaviors due to their small size and high surface area, which influence their electronic, magnetic, and optical properties[2]. Nanocomposites, which combine different phases at the nanoscale ($\leq$ 100 nm), are designed to enhance material properties, the composite leverage nanoscale building blocks to achieve improved physical and chemical Characteristics[3, 4]. Copper-iron oxide nanocomposite are particularly beneficial in electrical and microwaves devices due to their high electrical resistivity, low core loss, and strong mechanical properties [5]. Additionally, these nanocomposites exhibit a high saturation magnetization and a large snoek's limit, making them ideal for high frequency application [6, 7]. The primary objective of this study is to investigate the corrosion protection performance of $Cu_2Fe_2O_6$ nanoparticles when applied to carbon steel substrates using the Electrophoretic deposition (EPD) technique, which is a simple method used to coat materials with nanocomposite. It involves the application of a stable nanoparticle solution under a direct current (DC) field, leading to the deposition pf nanoparticles onto a substrate, such as carbon steel surfaces[8]. The research aims to enhance the durability and efficiency of corrosion- resistant coating through an optimized nanocomposite synthesis and application process [9, 10].

2- Experımental Methods

2.1 Materials:

All chemicals were purchased from BDH, Merck, and sigma-Aldrich. The photo-irradiation system, as depicted in Figure 1, was used to synthesize $Cu_2F_2O_6$ nanoparticles, the irradiation source was 130-watt mercury medium-pressure lamp with a peak intensity at 365 nm, and the reaction was carried out in a quartz tube immersed in a nanoparticle solution inside a Pyrex reactor. Temperature control was maintained using an ice bath.

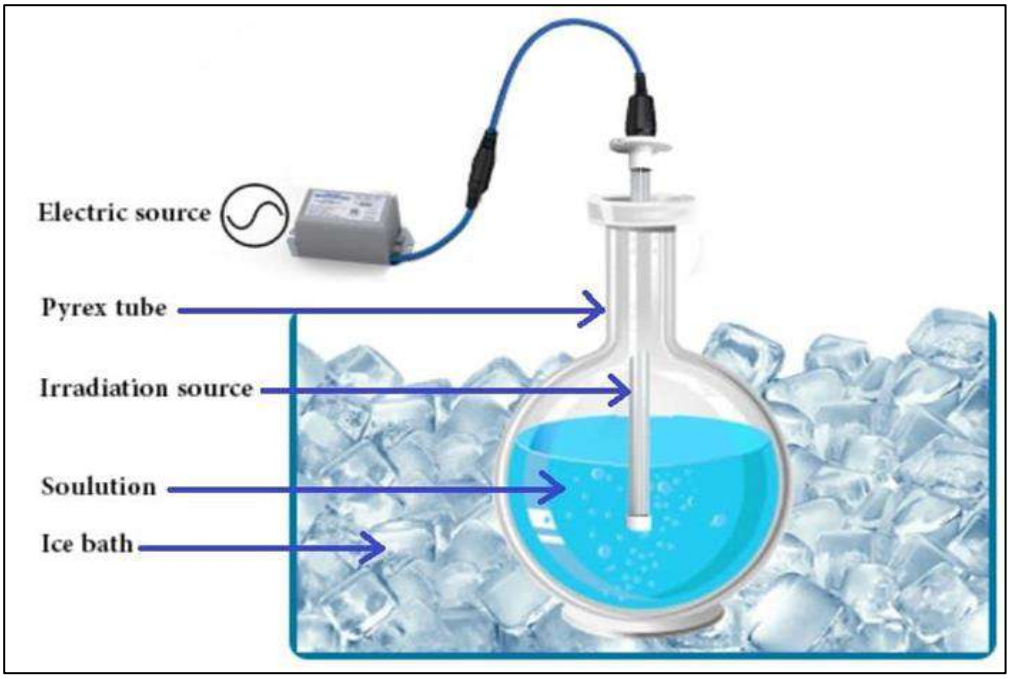

Figure 1. Photo Irradiation Cell

2.2 Synthesis of $Cu_2Fe_2O_6$ Nanoparticles:

A solution of copper sulfate pentahydrate ($CuSO_4.5H_2O$) and iron oxalate hydrate ($FeC_2O_4.H_2O$) was prepared, each at concentration of 0.01 Mol/L, in a 1:1 molar ratio. Urea (0.01 mol/L) was added to the solution, followed by UV irradiation for 25 minutes. The solution was then cooled to 5°C. after irradiation, 0.1N NaOH was added to precipitate the nanoparticles, which were subsequently dried at 100°C and calcined at 300°C for 3 Hours C [11-14].

2.3 Preparation of $Cu_2Fe_2O_6$ Nanocomposite solution:

To prepare an emulsion, 1.5 g of $Cu_2F_2O_6$ nanoparticle powder was mixed with 150 ml of ethanol (1% wt.). This solution was then used for the electrophoretic deposition of $Cu_2F_2O_6$ nanocomposite onto a CS substrate [15, 16].

2.4 Electrophoretic Deposition (EPD):

The deposition of $Cu_2F_2O_6$ nanoparticles was performed in a deposition cell, where CS specimens were used as the working electrode, the electrodes were immersed in the emulsion solution, and a DC potential of 15 V was applied for 30 minutes, after deposition, the coated specimens were washed with distilled water and dried using a hair dryer[17].

2.5 Electrochemical Measurements:

Electrochemical corrosion testing was conducted using a potentiostat (Mlab, Germany). With a three-electrode system: a CS working electrode, a platinum counter electrode, and a

silver-silver chloride reference electrode. The open circuit potential (OCP) was measured for 15 Minutes, followed by polarization tests at temperature ranging from 298 to 328 K[18].

3- Results And Discussion

3.1 XRD Analysis:

The XRD patterns of $Cu_2F_2O_6$ nanoparticles (Figure 2) reveal broad peaks, characteristic of nanomaterials, with diffraction peaks at 17.6°, 30.69°, 35.0°,43.7° 53.8°, and 62.5° correspond to Cu_2O_3 and γ-Fe_2O_3 phases. the crystallite size was determined using the sheerer equation, yielding an average size of 28 nm[19].

$$D = \frac{k\lambda}{\beta \cos\theta} \qquad (1)$$

Where k =0.9 is the Scherrer constant, λ is the Cu-K radiation wavelength, β is full width at half maximum, and θ is the Bragg angle, computed from 2θ values matching to maximum intensity peak in XRD pattern [20]. Prepared by assigned to cubic crystal phase according to the standard XRD patterns

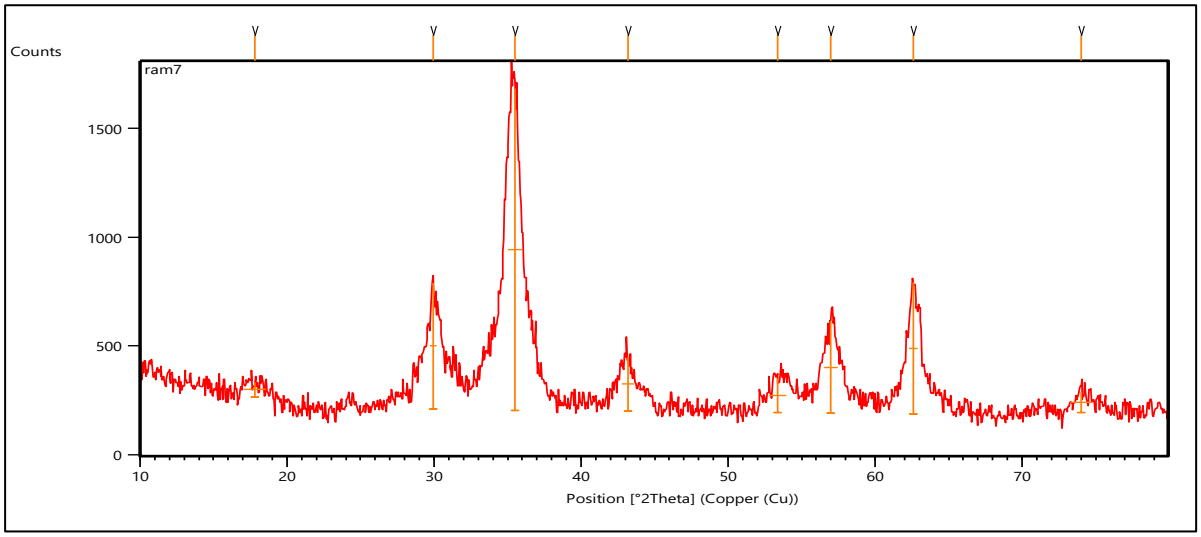

Figure 2. Shows the XRD patterns of the samples of Cu2Fe2O6 nanoparticles

3.2 AFM and SEM Analysis:

AFM image (Figures 3 and 4) showed that the average particle size was 53.72 nm, with a distribution ranging from 30 nm to 75 nm as shown in table 1. SEM images (Figure 5) confirmed that the $Cu_2F_2O_6$ nanoparticles had smooth surfaces and high crystallinity, with an estimated average particle size of 69 nm.

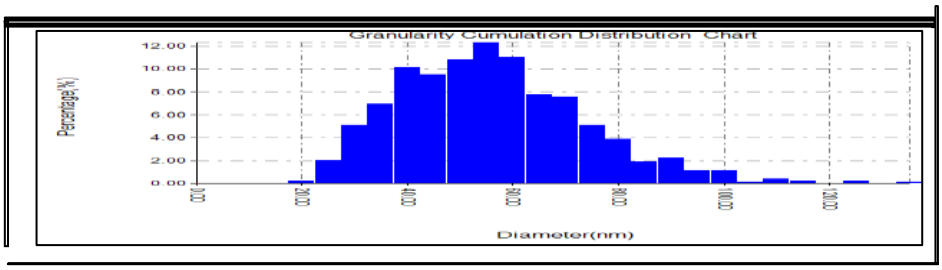

Figure 3. Percentage of Diameters Cu2Fe2O6NPs

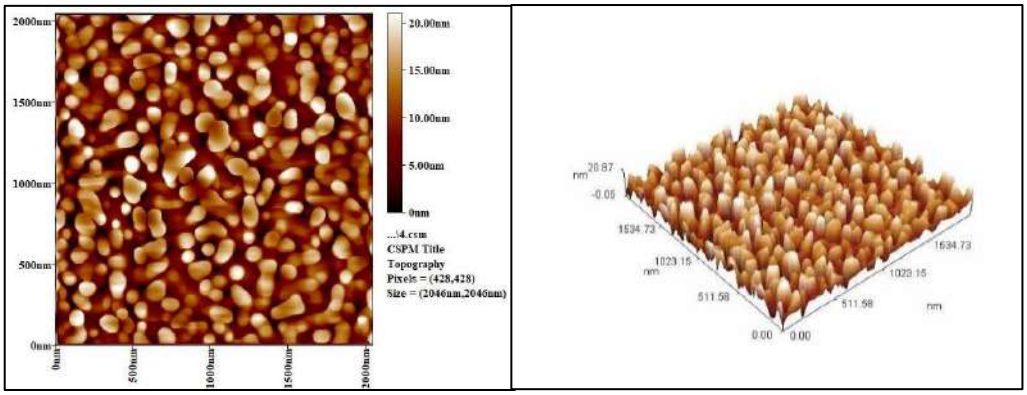

Figure 4. AFM image of Cu2Fe2O6NP

Table 1. the average diameter of Cu2Fe2O6NPs

Avg. Diameter:53.72 nm	**<=10% Diameter:30 nm**
50% Diameter:50 nm	**<=90% Diameter:75 nm**

diameter (nm)<	Volume (%)	Cumulation (%)	Diameter (nm)<	Volume (%)	Cumulation (%)	Diameter (nm)<	Volume (%)	Cumulation (%)
20.00	0.26	0.26	60.00	11.01	67.99			
25.00	2.05	2.30	65.00	7.81	75.80	100.00	1.15	98.85
30.00	5.12	7.43	70.00	7.55	83.35	105.00	0.13	98.98
35.00	6.91	14.34	75.00	5.12	88.48	110.00	0.38	99.36
40.00	10.12	24.46	80.00	3.84	92.32	115.00	0.26	99.62
45.00	9.48	33.93	85.00	1.92	94.24	125.00	0.26	99.87
50.00	10.76	44.69	90.00	2.30	96.54	135.00	0.13	100.00
55.00	12.29	56.98	95.00	1.15	97.70			

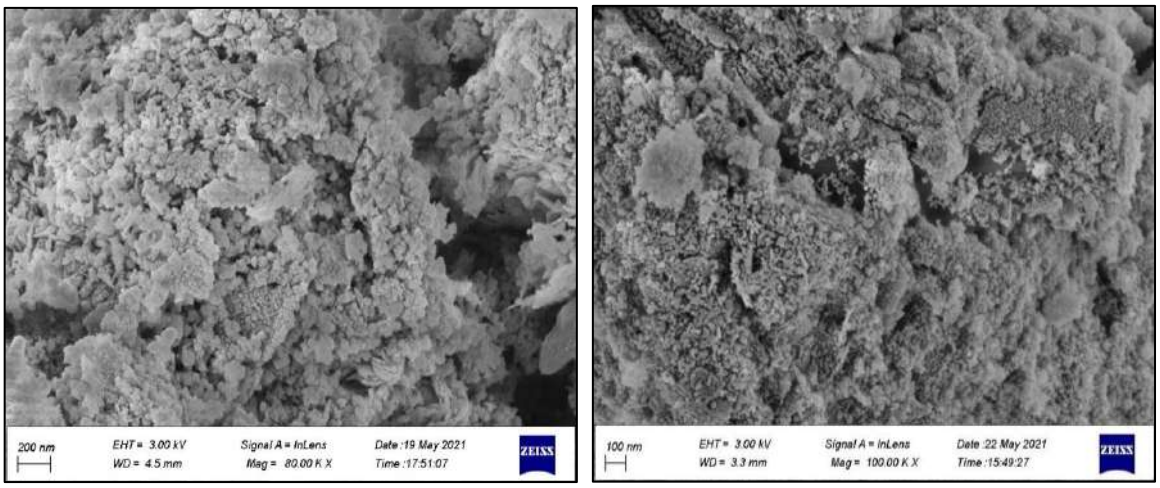

Figure 5. SEM images of Cu2Fe2O6 NPs

3.3 Corrosion Protection Performance:

The corrosion potential of CS coated with $Cu_2F_2O_6$ nanoparticles shifted towards more active values as the temperature increase from 298 to 328 K. The corrosion current density decreased from 168.72 µA/cm² for uncoated CS to 43.4 µA/cm² for coated CS at 298 K, indicating that the nanoparticles significantly reduce corrosion, the protection efficiency (PE) was calculated to be 76.038% at 308K. while the corrosion of potential values was slightly affected by temperature when increase from 298 to 328 K for CS coated by nanocomposite, therefor, return to (-718.2 µV) at 328K. Those indicate the mechanism of CS surface not change by high temperature. The equation below may be used to compute the Protection Efficiency (% PE):

$$\%PE = \frac{(Ic)un-(Ic)c}{(Ic)un} \times 100 \qquad (2)$$

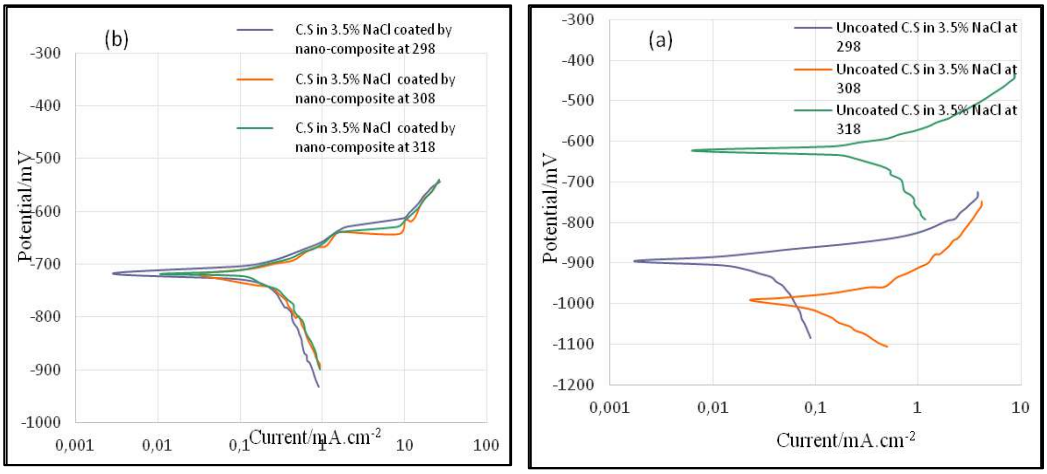

Figure 6. Polarization curves for C.S a) Uncoated, b) Coated by nanoparticles

Table 2. Corrosion Parameters for C.S Coated with Cu2Fe2O6 NPs at Different Temperature

Carbon steel	T/K	-ECorr /mV	ICorr /µA.cm-2	-bc /V.dec-1	Ba /mV.dec-1	PE%	θ
Uncoated	298	469.0	168.72	243.9	107.2	-	-
	308	573.5	201.57	179.1	104.2	-	-
	318	622.0	220.34	140.3	82.2	-	-
	328	693.1	260.45	117.6	80.2	-	-
With Nanoparticles	298	718.6	43.4	104	13.9	74.277	0.7427
	308	720.4	48.3	98.0	23.2	76.038	0.7604
	318	718.8	61.5	82.7	26.3	72.088	0.7208
	328	719.1	65.3	73.4	29.2	74.9	0.7493

3.4 Kinetic Parameters and Thermodynamic Analysis:

The activation entropy (ΔS*) during the corrosion process transition state was evaluated using the Arrhenius equation:

$$\text{Log}\left(\frac{Ic}{T}\right) = \log\left(\frac{R}{Nh}\right) + \frac{\Delta S*}{2.303R} - \frac{\Delta H*}{2.303RT} \qquad (3)$$

Here, I_C represents the corrosion current density of carbon steel, computed from Tafel extrapolation; h denotes Plank's constant, N is Avogadro number; ΔS* represents the activation entropy, and ΔH* is the activation enthalpy. The slope of (-ΔH* / 2.303 R) and the intercept of [(log (R/Nh) + (ΔS*/2.303 R)] were calculated using the log I_C/T against 1/T plot, and the values of ΔH* and ΔS* were approximated. The results in Table 3 demonstrate that the nanocomposite coating increased activation enthalpy and energy, enhancing corrosion resistance.

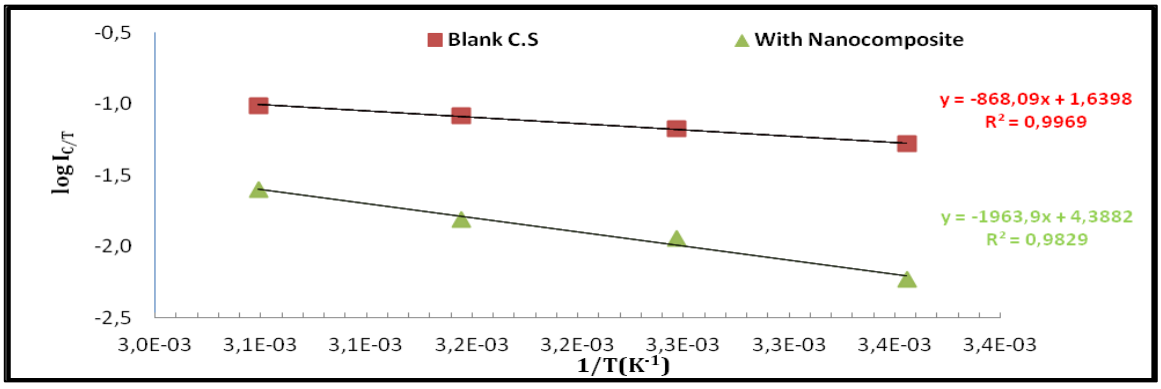

Figure 7. Kinetic and thermodynamic parameters for the corrosion Protective of C.S with and without Nanocomposite Coating at the Temperatures Range (298-328) K.

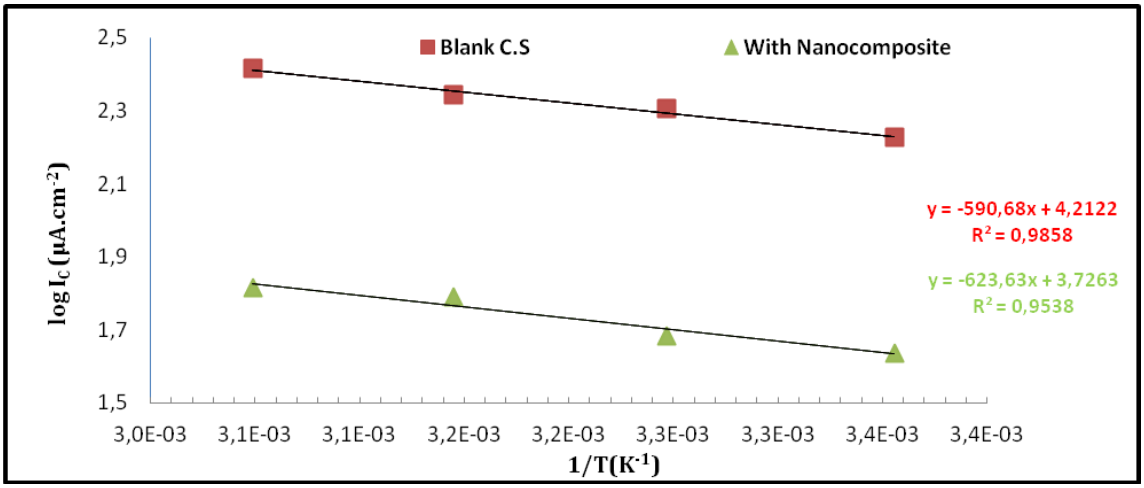

Figure 8. Arrhenius Plot of log IC. Versus 1/T for the corrosion for Protective of C.S with and without Nanocomposite Coating at the Temperatures Range (298-328) K

Table 3. Kinetic and thermodynamic parameters for the corrosion Protective o of C.S with and without Nanocomposite Coating at the Temperatures Range (298-328) K.

Temp. (K)		1/T (K^{-1})	Log I_{Corr}	ΔH ($kJ.mol^{-1}$)	ΔS ($J.K^{-1}.mol^{-1}$)	Ea ($kJ.\ mol^{-1}$)	A $Molecules.cm^{-2}.\ S^{-1}$
Uncoated	298	0.0034	2.23	8.712	-0.173	11.941	3.20551E+27
	308	0.0032	2.30				
	318	0.0031	2.34				
	328	0.0030	2.42				
With Composite	298	0.0034	1.64	9.171	-0.182	12.310	9.81288E+27
	308	0.0032	1.68				
	318	0.0031	1.79				
	328	0.0030	1.81				

4- Conclusıon

1. The photo-irradiation method effectively synthesized $Cu_2F_2O_6$ nanoparticles with an average size below 70 nm.

2. The $Cu_2F_2O_6$ nanoparticles demonstrated excellent corrosion protection for CS, achieving a 76% efficiency at 308 K

3. The nanocomposite coating increased activation enthalpy and energy, as well as the pre-exponential factor(A), implying that a greater energy barrier is required for corrosion to proceed, and these findings correlate well with the observed improvement in protection efficiency due to the nanocomposite coating.

References:

[1] Mukhopadhyay, S., Dasgupta, S., Roy, S., Mondal, A., Sukul, D., Ghosal, S., and Adhikari, U.: 'Corrosion Inhibition of Mild Steel by Aqueous Leaf Extract of Purple Hedge Plant: Experimental and Theoretical Investigation', Journal of Bio- and Tribo-Corrosion, 2021, 7, (4), 139, DOI:10.1007/s40735-021-00577-6

[2] Hussain, D.H., Abdulah, H.I., and Rheima, A.M.: 'Synthesis and characterization of ɣ-Fe2O3 nanoparticles photo anode by novel method for dye sensitized solar cell', International Journal of Scientific and Research Publications, 2016, 6, (10), 26-31

[3] Rheima, A.M., Mohammed, M.A., Jaber, S.H., and Hasan, M.H.: 'Inhibition effect of silver-calcium nanocomposite on alanine transaminase enzyme activity in human serum of Iraqi patients with chronic liver disease', Drug Invention Today, 2019, 12, (11), 2818-2821

[4] Rheima, A.M., Hussain, D.H., and Almijbilee, M.M.A.: 'Graphene-silver nanocomposite: synthesis, and adsorption study of cibacron blue dye from their aqueous solution', Journal of Southwest Jiaotong University, 2019, 54, (6), https://doi.org/10.35741/issn.0258-2724.54.6.14

[5] Poorbafrani, A., and Kiani, E.: 'Enhanced microwave absorption properties in cobalt–zinc ferrite based nanocomposites', Journal of Magnetism and Magnetic Materials, 2016, 416, 10-14, https://doi.org/10.1016/j.jmmm.2016.04.046

[6] Li, D., Horikawa, T., Liu, J., Itoh, M., and Machida, K.-i.: 'Electromagnetic wave absorption properties of iron/rare earth oxide composites dispersed by amorphous carbon powder', Journal of alloys and compounds, 2006, 408, 1429-1433 10.1016/j.jallcom.2005.04.109

[7] Khudhair, N.A., Kadhim, M.M., and Khadom, A.A.: 'Effect of Trimethoprim Drug Dose on Corrosion Behavior of Stainless Steel in Simulated Human Body Environment: Experimental and Theoretical Investigations', Journal of Bio- and Tribo-Corrosion, 2021, 7, (3), 124 https://doi.org/10.1007/s40735-021-00559-8

[8] Al-Mashhadani, H.A., Alshujery, M.K., Khazaal, F.A., Salman, A.M., Kadhim, M.M., Abbas, Z.M., Farag, S.K., and Hussien, H.F.: 'Anti-Corrosive Substance as Green Inhibitor for Carbon Steel in Saline and Acidic Media', in Editor (Ed.)^(Eds.): 'Book Anti-Corrosive Substance as Green Inhibitor for Carbon Steel in Saline and Acidic Media' (IOP Publishing, 2021, edn.), pp. 012128 10.3390/ma15062023

[9] AlMashhadani, H.A.: 'Corrosion Protection of Pure Titanium Implant by Electrochemical Deposition of Hydroxyapatite Post-Anodizing', in Editor (Ed.)^(Eds.): 'Book Corrosion Protection of Pure Titanium Implant by Electrochemical Deposition of Hydroxyapatite Post-Anodizing' (IOP Publishing, 2019, edn.), pp. 012071 10.24996/ijs.2020.61.11.1

[10] Almashhdani, H., and Alsaadie, K.: 'Corrosion Protection of Carbon Steel in seawater by alumina nanoparticles with poly (acrylic acid) as charging agent', Moroccan Journal of Chemistry, 2018, 6, (3), 6-3 (2018) 2455-2465 https://doi.org/10.48317/IMIST.PRSM/morjchem-v6i3.6214

[11] Rheima, A.M., Mohammed, M.A., Jaber, S.H., and Hameed, S.A.: 'Adsorption of selenium (Se4+) ions pollution by pure rutile titanium dioxide nanosheets electrochemically synthesized', Desalination and Water Treatment, 2020, 194, (2020), 187-193 : 10.5004/dwt.2020.25846

[12] Ismail, A.H., Al-Bairmani, H.K., Abbas, Z.S., and Rheima, A.M.: 'Nanoscale synthesis of metal (II) theophylline complexes and assessment of their biological activity', Nano Biomed. Eng, 2020, 12, (2), 139-147 10.5101/nbe.v12i2.p139-147

[13] Kumar, K., Bhadauria, S.S., and Singh, A.P.: 'Effect of Strain Loading on Stress Corrosion Cracking Susceptibility of 316L Stainless Steel in Boiling MgCl2 Solution', Journal of Bio- and Tribo-Corrosion, 2021, 7, (3), 123 https://doi.org/10.1007/s40735-021-00561-0

[14] Lavanya, M.: 'A Brief Insight into Microbial Corrosion and its Mitigation with Eco-friendly Inhibitors', Journal of Bio- and Tribo-Corrosion, 2021, 7, (3), 125 https://doi.org/10.1007/s40735-021-00563-y

[15] AlMashhadani, H.A.: 'Corrosion Protection of Pure Titanium Implant in Artificial Saliva by Electro-Polymerization of Poly Eugenol', Egyptian Journal of Chemistry, 2020, 63, (8), 2-3 10.21608/EJCHEM.2019.13617.1842

[16] Gangwar, S., Singh, R.K., Yadav, P.C., and Sahu, S.: 'Physical, Mechanical, and Tribological Properties of Industrial Waste Fly Ash Reinforced AA5083 Composites Fabricated by Stir Casting Process', Journal of Bio- and Tribo-Corrosion, 2021, 7, (3), 127 https://doi.org/10.1007/s40735-021-00560-1

[17] AlMashhadani, H.A., and Saleh, K.A.: 'Electrochemical Deposition of Hydroxyapatite Co-Substituted By Sr/Mg Coating on Ti-6Al-4V ELI Dental Alloy Post-MAO as Anti-Corrosion', Iraqi Journal of Science, 2020, 2751-2761 https://doi.org/10.24996/ijs.2020.61.11.1

[18] Abbas, H.A., Alsaade, K.A.S., and AlMAshhdan, H.A.Y.: 'Study the Effect of Cyperus Rotundus Extracted as Mouthwash on the Corrosion of Dental Amalgam', in Editor (Ed.)^(Eds.): 'Book Study the Effect of Cyperus Rotundus Extracted as Mouthwash on the Corrosion of Dental Amalgam' (IOP Publishing, 2019, edn.), pp. 012074 10.4081/ejtm.2018.7917

[19] Holzwarth, U., and Gibson, N.: 'The Scherrer equation versus the'Debye-Scherrer equation'', Nature nanotechnology, 2011, 6, (9), 534-534 10.1038/nnano.2011.145

[20] Jehad, M., and Salman, T.: 'Kinetic and inhibition effect studies of ecofriendly synthesized silver nanoparticles on lactate dehydrogenase and ferritin activity', Egyptian Journal of Chemistry, 2022, 65, (3), 627-635 10.21608/EJCHEM.2021.81194.4020.

Fingerprint Age Estimation based on CNN

Arwa Abdelsalam Arseel [1]

Zainab Mohammed Hussain [2]

Abstract

Fingerprints are used as the most widely proofs for individual identification. In this paper, human fingerprints have been used to determine and estimate the human age. The Principal Component Analysis (PCA) was used for the fingerprint feature extraction method, and a Convolutional Neural Network (CNN) was used for classification of the age. A final future vector result from feature extraction process on the tested fingerprint image goes to the CNN which classifies the fingerprint image to one of the group age classes by comparing final test future vector with the future vectors of database fingerprints. This proposed method is useful in many fields for example it used to reduce the search space of suspects in crime investigations.

Different age groups were formed for training (5-15), (15-25), (25-40), (40-65). All the fingers were used for testing and testing purposes. The performance and accuracy of the proposed system were tested on the “Sdumla fingerprint and aging databases”. This system achieves 96% accuracy as an average.

Keywords: *Fingerprint, Age Estimation, PCA, CNN.*

http://dx.doi.org/10.47832/RimarCongress04-7

[1] Ministry of Health Baghdad Al-Rusafa Health Department, Iraq

[2] College of Law And Political Science, Al-Iraqia University, Iraq zainabmohammadhussain@aliraqia.edu.iq

1. Introduction:

Biometric is the science of finding a person's from its physical or behavioral characteristics using many biometric techniques such as Fingerprints, Hand Geometry, etc. The identification or verification of a person can be find from fingerprint. A fingerprint is "the representation of the epidermis of a finger; it consists of a pattern of interleaved ridges and valleys. Fingertip ridges evolved over the years to allow humans to grasp and grip objects". Fingerprint ridges form through a combination of genetic and environmental factors, like everything in the human body. This is the reason of the difference of identical fingerprint twins [1].

Fingerprint biometric can be employed in commercial, civilian, military, and financial institutions. The pattern of ridges on a finger is imprinted to create a fingerprint. A ridge is defined as "a single curved segment" while a valleyis "a region that lies in between ridges", as depicted in Figure (1). The base elements in a fingerprint pattern, are ridges and valleys.

In practice, the obtained fingerprint images are rarely flawless. Many factors, such as differences in skin and impression conditions at the time of acquisition, can cause them to deteriorate and become corrupted with noise elements. Scars, breaks, and excessively dry or oily conditions can all be caused by these factors. [2].

Age estimation for fingerprint Images are used in many different contexts, such as border control, security and defense applications, ambient intelligence applications involving human-machine interaction, and recognition using soft biometric data. In this area, recent deep learning-based techniques have demonstrated encouraging results. The majority of these techniques make use of deep networks that have been especially created and trained to handle this issue. Regarding strategies for fine-tuning the main advantage consists of the post-processing step's ease of use and low computational cost. Using a series of pre-trained Convolutional Neural Networks (CNNs), the first age estimation study proposes post-processing methods for features retrieved using the pre-trained deep networks method from the input fingerprint image. After reducing the dimensionality of the feature space and performing a feature level fusion, the technique uses a Feed-Forward Neural Network (FFNN) to estimate the individual's age [3].

This work is aim to design and implementation of fingerprint age estimation system using PCA as a feature extraction method from the fingerprint images and the CNN for classifying and recognizing the age from these features. Working in collecting huge samples in each

category , gives better results of age estimation. The rest of this paper can be organized as: In part 2, a related work to this work will be described, part 3 describe the most important basics of the proposed work such as a CNN, fingerprint age estimation principles, PCA feature extraction, preprocessing method, and the performance measurements, part 4 illustrate the structure and the implementation of the proposed fingerprint age estimation, part 5 illustrate the final results from implementing this system, and finally the important conclusions explained in part 6.

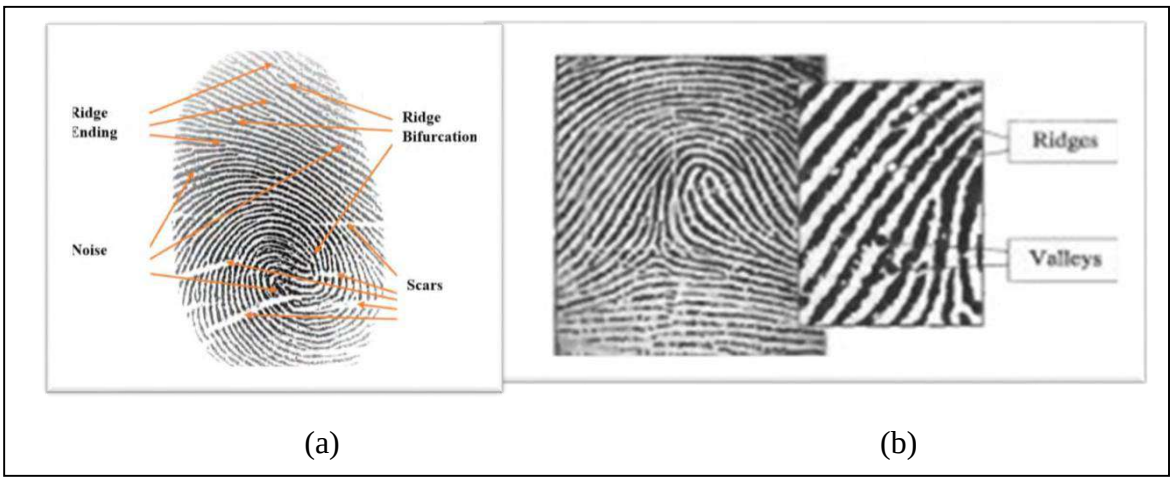

Figure 1. (a) Ridges and Valleys in fingerprint image, (b) a magnifiedpart from the fingerprint image

2. Related works

There are few researchers have worked on age estimation using fingerprints, some of these related to this work are:

In 2013 [4], T. Arulkumaran, Dr.P.E. Sankaranarayanan, Dr.G.Sundari , They suggested estimating a person's age using a fingerprint by combining Principal Component Analysis (PCA) and 2D-Discrete Wavelet Transform (DWT). The classifier that was employed was the minimum distance method. For analysis, 400 fingerprints from people ranging in age from 12 to 60 were collected. For a trained database, the experimental results are favorable. It was discovered that the system performs better when the database population in each category is increased.

In 2015 [5], Basavaraj Patil G.V and Mohamed Rafi provide a two-method approach for estimating the age of a finger print. These techniques include the use of support vector machines (SVM) as a classifier and the combination of 2D-Discrete Wavelet Transform (DWT) and Principal Component Analysis (PCA) to extract fingerprint features. After undergoing two

stages of feature extraction, the acquired fingerprint image yields distinct feature vectors that are subsequently fused to create a final future vector. By comparing the final future vector with the database fingerprints, the SVM assigns the fingerprint image to a recognized age class. This technique can help narrow down the suspect search area in criminal investigations.

In 2017 [6], M.Murali, S.Anusuriya, M.Pavithra, and G.Praveena Using feature points and a Convolution Neural Network (CNN), they had presented an enhanced damaged FP recognition algorithm. A fuzzy image of fingerprint feature points was proposed as the training sample for a fuzzy process of fingerprint feature points. It significantly streamlined the process of identifying a predetermined number of matched feature points, but it increased the recognition rate for damaged and blurry fingerprints.

3. Basics

Since people of different races age at different rates, age group estimation by automated systems has been considered a difficult problem by existing methods. Race and genetics are not the only factors that influence this; a variety of other factors, including living and working conditions, social interactions, and health status, are also important. Algorithms for fingerprint identification are widely used worldwide for both security and personal identification. Dermatoglyphics are ridges on the skin, such as fingerprints. Because fingerprints are unique and do not change over the course of a person's life, they have been used as a biometric for estimating age. The primary dermal ridges (ridge counts) in a fingerprint are created between weeks 12 and 19 of pregnancy. Fingerprints are static, and while their size and shape may change as people age, their fundamental pattern never changes. Furthermore, there is significant variation in the breadth of the human epidermis. There are statistical differences in dermatoglyphic features between age groups, ethnic groups, and sexes [7]. Determining the unknown's gender and age can help investigators choose the right person from the many potential matches.

3.1 CNN:

A revolutionary method for pattern recognition and object classification is the Convolutional Neural Network (CNN). It has made it possible for computers to outperform people in specific image recognition tasks. Prior art CNNs use a series of convolutional/non-linear layers stacked on top of a classifier to learn object features. CNN can be defined as class of deep NNs that is majorly utilized for doing image recognition, object detection, data classification, and so on [8].

Typically, CNN has three major layers (repeated layers): fully-connected layer, pooling layer and convolutional layer The main aim of convolution is extracting features from input. As programmers are going deep in the network, the network will identify extra complex features. A revolutionary method for pattern recognition and object classification is the Convolutional Neural Network (CNN). It has made it possible for computers to outperform people in specific image recognition tasks. Prior art CNNs use a series of convolutional/non-linear layers stacked on top of a classifier to learn object features. [9]. The pooling layer section can decrease the number of the parameters in a case when there are too large images, while spatial pooling referred to as down sampling or sub-sampling is reducing the dimensionality regarding each one of the maps, yet retaining significant information. SoftMax turn numeric output related to the last linear layer of multi class classification NN to probabilities via taking exponents regarding every one of the outputs and normalizing every one of the numbers via the summation of these exponents, thus the whole output vector will add up to one, all the probabilities must add up to one. Frequently, SoftMax was appended to the last layer of image classification network including those in CNNs [10].

$$softmax\ \sigma(\vec{z})_i = \frac{e^{z_i}}{\sum_{j=1}^{k} e^{z_j}} \qquad (1)$$

Where:

$\vec{z}$ The input vector to the SoftMax function, made up of (z_0, ..., z_k)

z_i The SoftMax function's input vector consists of all z_ivalues, which can have any real value—positive, zero, or negative.

e^{z_i} Every component of the input vector is subjected to the standard exponential function. If the input was negative, the resultant positive value above 0 would be very small; if the input was large, it would be very large. It is not, however, fixed in the range (0, 1), which is necessary for a probability.

$\sum_{j=1}^{k} e^{z_j}$ The term at the bottom of the formula is the normalization term. It ensures that the output value of each function will lie between 0 and 1 and add up to one, creating a valid probability distribution.

K The number of classes in the multi-class classifier.

The feature map matrix will be converted as vector (x_1, x_2, x_3 …). Features are combined for creating a model with fully-connected layers. Lastly, there is an activation function like

sigmoid or SoftMax used for classifying outputs like trucks, dogs, cats, cars, and so on. Also, fully-connected layer was simply, feed-forward NN. The fully-connected layers are forming the final few network layers, while the input of the fully-connected layer was an output from the final Pooling or the Convolution Layer, that has been flattened and after that fed to the fully-connected layer [11].

3.2 PCA Feature Extraction:

Principal Component Analysis (PCA) is one of the most effective tools for feature extraction and data visualization. Principal component analysis (PCA) is a "mathematical process that transforms a number of potentially correlated variables into a smaller number of uncorrelated variables known as principal components by mapping data from high dimensional space to low dimensional space using linear transformations". The first few principal components of the data contain the most variance. These are the main characteristics that classes are modeled after. The distances between eigenvalues during matching are used to compare a training and testing model. The total scatter matrix, given N sample images xk, is defined as [12]:

$$St = \sum_{k=1}^{n} (\mathrm{xk} - \mu)(\mathrm{xk} - \mu)\,\mathrm{T}\,, \qquad (2)$$

where m ∈ R n is the mean image obtained from the samples.

After mean centering the data for each attribute, PCA computes the eigenvalue decomposition of a data covariance matrix or the singular value decomposition of a data matrix. Typically, component scores and loadings are used to discuss PCA results. A vector that is multiplied by a constant known as the eigen value as a result of a specific linear transformation is known as an eigen vector. For positive eigenvalues, that transformation leaves the eigenvector's direction unaltered; for negative eigenvalues, it reverses the direction. To determine the eigenvector, each fingerprint in the database is subjected to PCA [13].

3.3 Median Filter for Preprocessing:

The acquired fingerprint image is subjected to image enhancement in order to improve the ridge and valley quality. The grayscale input image is transformed into binary. In order to improve the algorithms, low-quality fingerprints can be improved. The median filter was one of the most popular nonlinear filters for removing noise from fingerprint photographs. The noise

is removed by replacing the window center value with the center neighborhood median value [14].

3.4 Performance Measurements:

The performance of the proposed work can be assess, using the following standard performance indices are defined as follows:

3.4.1 Peak Signal to Noise Ratio (PSNR): is "an engineering term describing the ratio of a signal's maximal power to the power of corrupted noise that reduces the representation's fidelity." It is measured in decibel (dB).

Given a reference image f and a test image g, both of size M×N, the PSNR between f and g is defined by [14]:

$$\mathrm{PSNR}(f,g) = 10\log_{10}\frac{255^2}{\mathrm{mse}}\,(f,g) \qquad (3)$$

$$\mathrm{MSE}(f,g) = \frac{1}{mn}\sum_{i=1}^{m}.\sum_{j=1}^{n}(f-g)^2 \qquad (4)$$

Where MSE is “the mean square error between the original and the denoised image”.

3.4.2 **Accuracy:** Accuracy is defined as “the proportion of correctly categorized genders to all genders, as determined by the following formula” [15] , so a large value of accuracy indicates a higher classification rate:

$$\text{Accuracy} = \frac{\text{Total No.of correct prediction}}{\text{No.of input samples}} \qquad (5)$$

4. The Proposed System

A general block diagram of the proposed fingerprint age estimation based on CNN method is illustrated in figure (2). Pre-processing Module is to enhances and increases the fingerprint quality to improve the system performance using median filter. After preprocessing step the fingerprint image goes through one level of feature extraction algorithm using PCA. There are two stages to using CNN for fingerprint age estimation image classification: training and testing. CNN uses fingerprint image data with both positive and negative samples as input during training. The training algorithm solves the problem of separating a set of training vectors into two distinct classes.

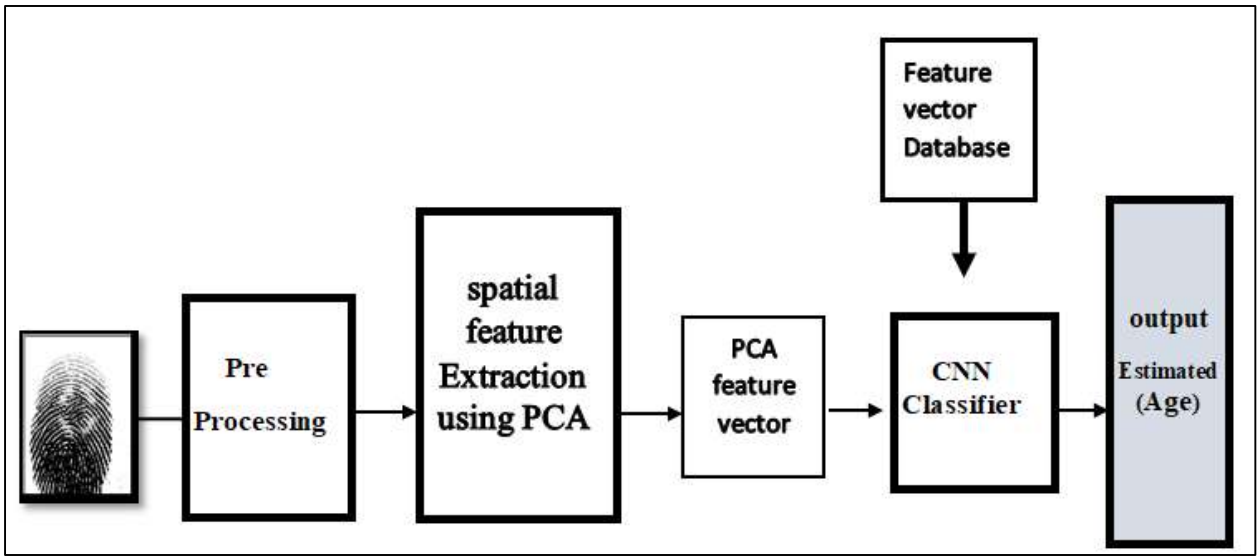

Figure 2. The proposed fingerprint age estimation system block diagram

The proposed system implemented using a laptop PC with the following properties: 2.2 GHz Intel (R) i5 (R) CPU, 8 GB RAM and NVIDIA Get Force GT 640M GPU, and using a MATLAB 2017 software running on 64 bit Windows 10 professional. The total execution time needed to estimate the age from each image was (4.59 - 14.50) s.

Five fingerprint vein images and fingerprint images taken with five different sensors make up the SDUMLA-HMT database used in this system. The database contains actual multimodal data from one hundred people. In the summer of 2010, SDUMLA-HMT was gathered at Shandong University in Jinan, China. 106 participants of various ages—61 men and 45 women—participated in the data collection process. Furthermore, research on the sensor interoperability of fingerprint recognition—a hotspot in fingerprints—will be enhanced by the fingerprint database collected using five sensors [16]. This database contains digital fingerprints from four age groups for training and testing purposes.

5. Results

The proposed system has been provided with an interface that contains all the tools and resources so it will be easy to use by users. The fingerprints database is the source of fingerprint age estimating system which are grouped based on the ages. Four age groups are formed for testing (5-15), (15-25), (25-40), (40-65). These four groups with the fingerprint images of these ages are made to go through the feature vector extraction steps. With the exception of the database's groups changing, every step stays the same. The feature vector of the query fingerprint also is obtained after the feature extraction process. Such that the feature vectors of the query fingerprint are now prepared for the CNN classification procedure.

In the next step the obtained PCA feature vectors was used to create a single fingerprint's final feature vector. In a similar manner, all of the fingerprint image feature vectors in the database are compiled into a database feature vector.

The fingerprint images experimented using median filter, The quantitative results have been given in Table (1) for four sampled images. From table (1) it can be seen that the PSNR value of four images are tested, and as seen in figure (3), fingerprint images are best suited for applying the median filter.

The main goal of using a Principal Component Analysis (PCA) is to reduce dimension and enhance class separability, such that to gives an improved performance in age estimation. The implementation of feature extraction algorithm using PCA can be illustrated as shown in figure (4).

Table 1. PSNR value for 4 types of age group images

Fingerprint image more than one sample	**Age Groups**			
	5-15	15-25	25-40	40-65
PSNR value	53.505%	54.234%	55.364%	55.163%

Figure 3. PSNR value comparison for four types of age group images

The time of the database feature vector extraction process is short time (From 2-4 second). Part of the fingerprints image database were used for training purpose and the rest was used for testing purpose.

The experiment results for this work can be obtained after pass the following steps:

Step One – Training: From the fingerprint image database, thirty (30) images has been selected. The proposed system was trained using the PCA approach, to obtain the Training Feature Vector.

Step Two - testing images: Twenty-five (25) images has been selected for each class (5-15), (15-25), (25-40) and (40-65) from the (100) fingerprint image database. To obtain the Testing Feature Vector, the images has been processed using PCA approach.

In the testing phase, fingerprint images are used to extract core points and candidate core points. A feature vector is then extracted for each point.

Step Three - Classification: The CNN classifier was used to enhance class separability as shown in figure(4).

Table (2) show the results of samples for the selected of 10 fingerprint images from the age group of (5-15), (15-25), (25-40) and (40-65) years such that the proposed system can estimate the age group. The time function in MATLAB is used to determine the execution time in seconds for the system's processes. Each fingerprint image has a different execution time for any given process; Tables (2) show that the database's execution time is short.

To evaluate the age classification accuracy the accuracy equation is implemented for training and testing the algorithm on in Sdumla database, such that 30% was used for training and 70% for testing arranged in four age groups: 5–15 → (25 fingerprints), 15–25 → (25 fingerprints), 25–40 → (25 fingerprints), 40–65 → (25 fingerprints). The result showed in table (3) and in table (4).

The maximum success rate is 98% achieved for the age group (15-25) years and is therefore helpful for investigating crimes because the crime rate for this group is higher than that of other groups. Tables (3), and (4) shows the descriptive statistics of sample dataset. 28 fingerprints has been used for training and 100 for testing. The little fingers, ring finger, middle finger, index fingers and thumbs are used for training and testing purpose.

Finally, system was used to classify the images into one of four major groups. The groups are: Group1 is (5 to 15 years), Group2 is (15 to 25 years), Group3 is (25 to 40 years) and Group4 is (40 to 65 years). The robustness and the accuracy of the proposed system was tested on the Sdumla, fingerprint and aging databases. Figure (5) shows the diagram for all the four age groups classification. According to experimental results, there may be instances where

fingerprint growth is out of proportion to age, resulting in an overlap between the fingerprints of the various age groups.

Table 2. Results of using CNN classifier for a sample person for age groups (5-15), (15-25), (25-40), and (40-65)

input Fingerprint image	Age Group	Age Estimation	Time (second)
	5-15	(5-15) year	9.45s
	15-25	(15-25) year	6.933s
	5-15	(5-15) year	6.45s
	15-25	(15-25) year	4.664s
	15-25	(15-25) year	4.627s
	15-25	(15-25) year	4.75s
	25-40	(25-40) year	5.668s
	25-40	(25-40) year	5.73s
	25-40	(25-40) year	6.627 s
	40-65	(40-65) year	4.668s
	40-65	(40-65) year	5.661s
	40-65	(40-65) year	5.730s

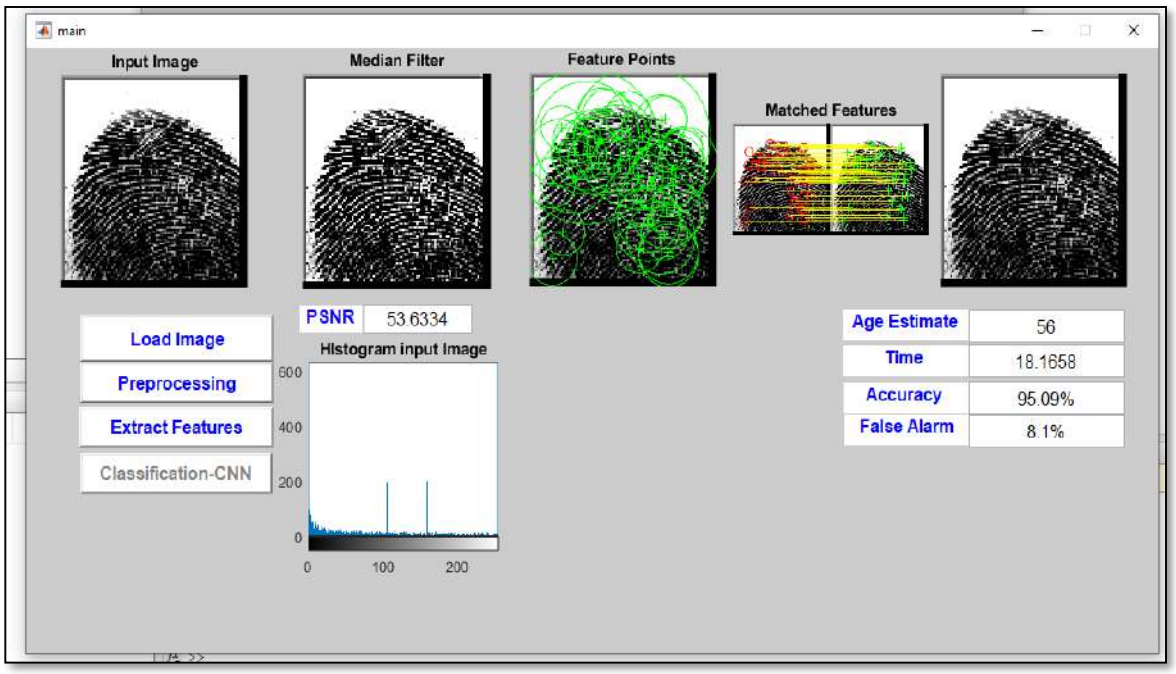

Figure 4.The result of the age estimation process PCA and (Classification CNN) in GUI

Table 3. Statistics of the samples (Training):

Descriptive Statistics	Age groups			
	5-15	15-25	25-40	40-65
Accuracy	95.02%	95.05%	95.03%	93.09%
No of Images	7	7	7	7

Table 4. Statistics of the samples (Testing):

Descriptive Statistics	Age groups			
	5-15	15-25	25-40	40-65
Accuracy	96.02%	98.08%	95.04%	95.07%
No of Images	25	25	25	25

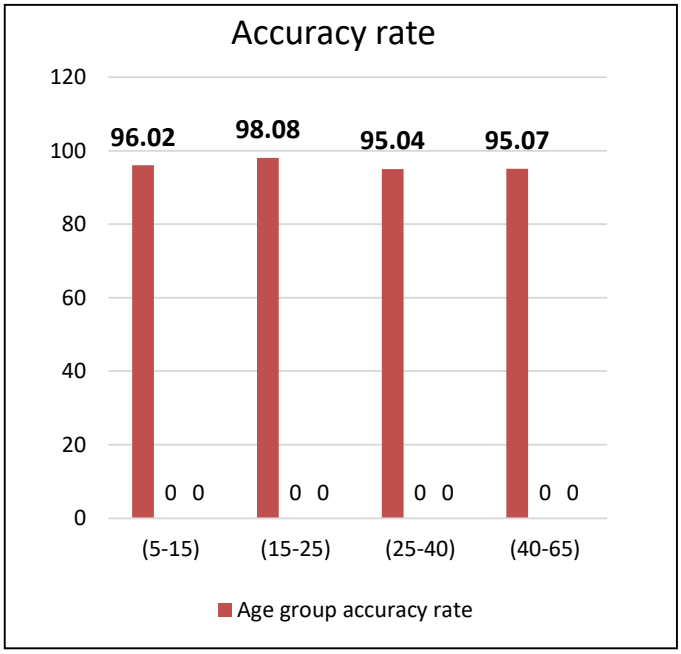

Figure 5. The graph of the Accuracy to age classification

6. Conclusions

In this paper, a system for estimating the person age through their fingerprint's images was proposed. The fingerprint goes through one level of PCA feature extraction, and using CNN for age classification. From experimental results it can be conclude that, after using the median filter, the PSNR values of images are properly similar group **(5-15)** 53.505, **(15-25)** 54.234, **(25-40)** 55.364, **(40-65)** 55.163. Also the results show that the proposed system achieved satisfactory performance for fingerprint images dataset, and the maximum success rate is 98% that achieved for one of the age groups and 96% as an average. Finally a short execution time (from 4-15 s) can be obtained from experiments.

References:

[1] M. Lourde R and D. Khosla," Fingerprint Identification in Biometric Security Systems", International Journal of Computer and Electrical, Vol. 2, No. 5, October 2010.

[2] C. Gottschlich, "Curved-region-based ridge frequency estimation and curved Gabor filters for fingerprint image enhancement", IEEE Transactions on Image Processing 21 (4) (2012) 2220–2227.

[3] A. Khan, A. Sohail, U. Zahoora, and A. S. Qureshi, "A survey of the recent architectures of deep convolutional neural networks," *Artif. Intell. Rev.*, vol. 53, no. 8, pp. 5455–5516, 2020.

[4] T.Arulkumaran,Dr.P.E.Sankaranarayanan,Dr.G.Sundari **,"** Fingerprint Based Age Estimation Using 2D Discrete Wavelet Transforms and Principal Component Analysis", *International Journal of Advanced Research in Electrical, Electronics and Instrumentation Engineering Vol. 2, Issue 3, March 2013*

[5] Gnanasivam, P., and S. Muttan. 2015. "Estimation of Age Through Fingerprints Using Wavelet Transform and Singular Value Decomposition." *International Journal of Biometrics and* (6):58 67.

[6] M. Murali, S. Anusuriyu, M. Parithra and G. Praveena," Fault Fingerprint Identification Using Convolution Neural Networks", International Journal of Computer Trends and Technology (IJCTT), Special Issue April – 2017.

[7] P. Gnanasivam & Dr. S. Muttan , "Estimation of Age Through Fingerprints Using Wavelet Transform and Singular Value Decomposition", International Journal of Biometrics and Bioinformatics (IJBB), Volume (6) : Issue (2) : 2012

[8] A. Khan, A. Sohail, U. Zahoora and A. Qureshi, "A survey of the recent architectures of deep convolutional neural networks". Journal of Computer Vision and Pattern Recognition, pp:1-62, 2020.

[9] S. Albawi, T. Mohammed and Saad ALZAWI, "Understanding of a Convolutional Neural Network", Conference on Neural Information Processing Systems (NIPS), Antalya, Turkey, 2017.

[10] S. Kanai, "Sigsoftmax: Reanalysis of the Softmax Bottleneck". 32nd Conference on Neural Information Processing Systems, Montréal, Canada, 2018.

[11] H. Nakahara, T. Fujii, and S. Sato, "A fully connected layer elimination for a binarizec convolutional neural network on an FPGA". 27th International Conference on Field Programmable Logic and Applications (FPL), Ghent, 2017.

[12] Suganthy, M. and P. Ramamoorthy "Principal Component Analysis Based Feature Extraction, Morphological Edge Detection and Localization for Fast Iris Recognition." Journal of Computer Science 8 (9): 1428-1433, 2012 ISSN 1549-3636: pp 1-6.2012.

[13] http://www.unilorin.edu.ng/step-b/biometrics.

[14] D. Maheswari et. al. '' NOISE REMOVAL IN COMPOUND IMAGE USING MEDIAN FILTER (IJCSE) International Journal on Computer Science and Engineering Vol. 02, No. 04, 2010(Ragavan et al. 2016).

[15] Radha ShankarMani and Vijayalakshmi,"Big Data Analytics", 2nd Edition, Wiley India Pvt.Ltt, ISBN 978- 81-265-6575-7, 2017.

[16] [16] Yilong Yin, Lili Liu, and Xiwei Sun, "SDUMLA-HMT: A Multimodal Biometric Database", School of Computer Science and Technology, Shandong University, Jinan, 250101, China, January 2011.

Alternative Medical Uses of beneficial Microorganisms (Probiotics) on Digestive System

Zainab Abdulkhaliq Ahmed [1]

Marwa Amer Ali [2]

Zahraa Hussein Kadhim [3]

Areej Ghazy Al-Charrak [4]

Abstract

Many scientific studies have demonstrated and supported the efficacy of probiotic bacteria as a preventative measure and a treatment for gastrointestinal problems in both people and animals. These bacteria find application in both clinical and veterinary settings. Nutritional intolerances (such as lactose intolerance) can be alleviated, macro and micronutrient bioavailability can be increased, and allergy reactions in vulnerable individuals can be reduced with the help of probiotics. The digestive tract was vital for nutritional absorption and digesting, as well as for keeping the mucosal barrier intact. The physiology of the animal was severely disrupted when a population of commensal bacteria was found in its gastrointestinal system. In the gut, probiotics make it harder for infections to survive by competing with them for resources and receptor-binding sites. And, bacteriocins, probiotics can also serve as anti-microbial agents, lowering pathogenic bacteria. However, probiotics help gut's immunological response and tight junction protein expression (such as blocking and claudin 1), which in turn improves barrier of the mucosa. Increasing the use of probiotics in digestive illnesses, there are several conditions that can be avoided or reduced, such as Irritable Bowel Syndrome (IBS), Small Intestinal Bacterial Overgrowth (SIBO), Pseudomembranous colitis, Inflammatory Bowel Disease (IBD), diarrhea, and the eradication of *Helicobacter pylori.*

Keywords: *Probiotics, Digestive System, IBS, Microorganisms.*

http://dx.doi.org/10.47832/RimarCongress04-8

[1] Department of Technologies Anesthesia Techniques, College of Medical & Health Technologies, Ahlulbait University Zainab8@abu.edu.iq

[2] Department of physiology, pharmacology and Biochemistry, and Veterinary Medicine Collage, Al-Qasim Green University, Iraq

[3] Department of physiology, pharmacology and Biochemistry, and Veterinary Medicine Collage, Al-Qasim Green University, Iraq

[4] Department of physiology, pharmacology and Biochemistry, and Veterinary Medicine Collage, Al-Qasim Green University, Iraq

1. Introduction

The term "probiotic" was initially coined by Kollath in 1953. He was described probiotics as living organisms that serve vital roles in enhancing several parts of health. According to the (FAO) and (WHO), these bacteria can provide health benefits to the creatures that they inhabit when properly handled (1).

By looked examined several bacteria that may be probiotics, including those from the Pediococcus, Lactococcus, Enterococcus, Streptococcus, Propionibacterium, and Bacillus genera. Common strains include those of the bacterial families Bifidobacterium and Lactobacillus, which have different but complementary effects on human health. They bio transform mycotoxins into riboflavin and food, produce vitamin K and folate (2), and digest undigested fiber in the colon (3), among other things. They detoxify xenobiotics and environmental contaminants. By teaching the host immune system to regulate its reaction and limiting the binding sites on mucosal epithelial cells, probiotics protect the intestinal barrier from harmful bacteria (4). The benefits of probiotics have been associated with changes in gut flora, alleviation of food intolerances (such as lactose intolerance), increased macro and micronutrient absorption, and a decrease in allergic reactions in people who are prone to them (5). The digestive tract was essential for nutritional absorption and processing, as well as for keeping the mucosal barrier intact (6). Possible methods of modifying the gut microbiota include antibiotics, prebiotics, fecal transplant management, and probiotics (7).

The host's health was negatively and positively affected by the metabolic function of the gut microbiome. Irritable bowel syndrome, ulcers, antibiotic-associated diarrhea, and inflammatory bowel disease are many chronic and acute clinical illnesses that can arise from an imbalance in the microflora, often known as eubiosis (8). Furthermore, other studies have provided evidence that suggests microbial dysbiosis play a crucial role in the development some malignancies in humans. (9), especially GI cancers (10). Revitalizing Gut Health Managing gastrointestinal illnesses with microbiota might be a feasible method. Potential benefits of probiotics include a more robust immunological microenvironment, increased enzyme (Lactase) synthesis, and a more diverse and abundant microbial community (11). An alternate medicinal application of beneficial probiotics on the digestive system is briefly discussed in this article.

2. Reviews of the literature

2.1. Probiotics

Élie Metchnikoff, a Russian Nobel laureate, popularized the term "probiotic" to describe her theory that introducing certain beneficial bacteria into the gut microbiome might have health benefits and even extend life expectancy (12). The concept reflected what probiotics are all about: bacteria that are practical, good to health, and inclusive of a wide variety of uses (13). In a position statement, (14). The name "probiotic" was used interchangeably in the food and supplement industries, leading to some confusion, therefore it was crucial to define the principles for probiotics. There are specific requirements that a probiotic strain must meet before it can be considered for use.

These include having been shown to be safe in at least one human research, and the product must be able to give the dose that was examined and be viable until it expires. Now that new "biotic" has entered the world language, it was especially helpful to clarify the basic requirements necessary for this term (15). Figure 1 shows that several disorders, including cancer, and other disorders. Included a variety of research on the use of probiotics in various illnesses. Probiotics were initially characterized by Lilly and Stillwell, though they had likely been around for decades (17,18). Live bacteria that, when administered in adequate doses, benefit the host's health are known as probiotics, according to the Food and Drug Administration (19).

An additional International Scientific Association for Probiotics and Prebiotics (ISAPP) panel revisited the word "probiotic" and reached a consensus in support previous definitions (20). They discussed the regulatory implications of four categories of composites or products that included living microbes and were designed for human consumption:1. Products that claim to include living or active cultures, such yogurts, do not necessarily give any health benefits unless proof of such a benefit is supplied 2. An unlabeled probiotic supplement or meal items of this kind boast that they "contain probiotics." Assuming they are safe, they have shown promise for improving human health in general. According to certain authorities, the word "probiotic" was considered an implicit health claim based on the criteria given above.

As a result, it was illegal to be used until there was satisfactory evidence of a health benefit (21). Important for the definitions. To be considered for this category, a product must provide strong proof of a certain health (22; 23). a. Information on the strain or strains used in a probiotic blend b. Recording of the association between health and what was thought to be a

positive physiological impact on the intended audience c. Proof the biological activity of the body. This must now meet all regulatory standards to be licensed as a medication in the US and internationally. In the USA, at 1994 classified probiotics as foods if their intended use was as dietary supplements (category 1-3 above) and not as drugs.

The DSHE Act of 1994 exempted dietary supplements from FDA review prior to marketing, provided they met the standards of Current Good Manufacturing Practice and provided evidence of safety. It is mandatory to notify the Food and Drug Administration of any serious adverse events (24). Other regulatory forms' approaches to nonfood probiotics ranged widely, from labeling them as biological agents or medications to functional foods. There was hardly any error in the others (25).

There were outcomes according to the present probiotic definition. The emphasis on "live" creatures and the insistence on consulting "a health advantage on the host" were two subjects that received extra attention. First, although it was widely accepted that some animal studies had shown that dead bacteria or even bacterial components or products (26-28) might produce a variety of anti-inflammatory and anti-infective benefits in people, this was not always the case.

This part of the definition will need to be clarified or the word will have to be left unregulated altogether because it looked unlikely that the effects of probiotics on people will be restricted to living organisms. All biologically active components originating from the microbiota were originally going to be referred to as pharmabiotics. Secondly, it was clear from the definition's later section that reliable clinical trial results are required to support any clinical claims in humans, whether they pertain to health enhancement or illness treatment (29).

Synbiotic

A "synbiotic" refers to a blend of prebiotics which are a group of nutrients that are degraded by gut microbiota. and probiotic microorganisms. The goal is to enhance the efficacy of the probiotic and promote the growth of the beneficial bacteria that were already present (29).

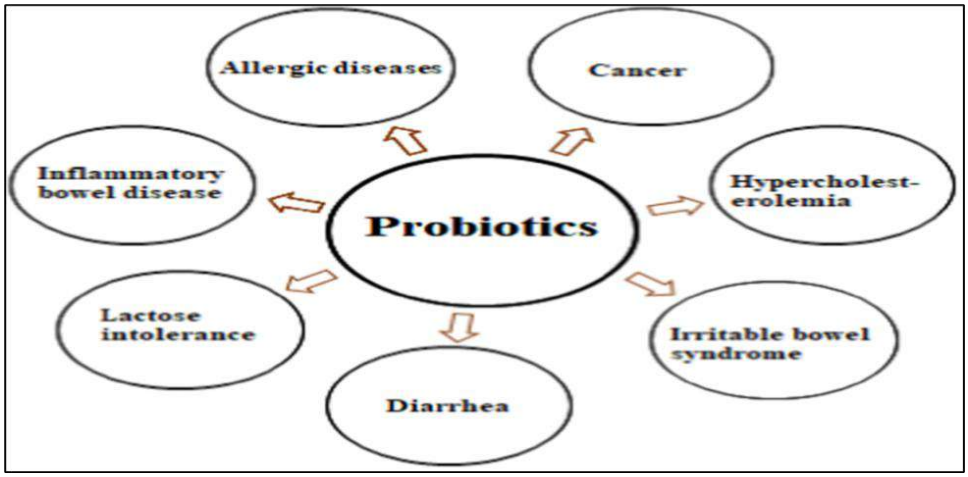

Figure 1. Benefits of probiotics for health (20).

2.2. Mechanisms of action

Although probiotic research had progressed, a significant step toward understanding how they work remained unmet. By enhancing intestinal barrier functioning, producing neurotransmitters, competitively excluding pathogens, and modulating the host's immune system, probiotics good for human body. Pathogens have a harder time surviving in the gut when probiotics compete with them for nutrition and sites of binding (30). Probiotics reduced harmful gut bacteria by acting as anti-microbial agents and invasion of pathogenic bacteria (31), and bacteriocins (32).

Additionally, probiotics boost the function of barriers by modulating the gut immune response, increasing mucin protein synthesis (33) (34). Dendritic cells (DC), macrophages (M), and B and T lymphocytes were all influenced by probiotic regulation of the immune response, both innate and adaptive (35). In addition, these microbes may be involved in the production of neurotransmitters by probiotics. Some probiotic stains may alter levels of serotonin, GABA, and dopamine, which in turn may influence gastrointestinal motility, stress circuits, behavior, and mood (36). Fig 2 (37)

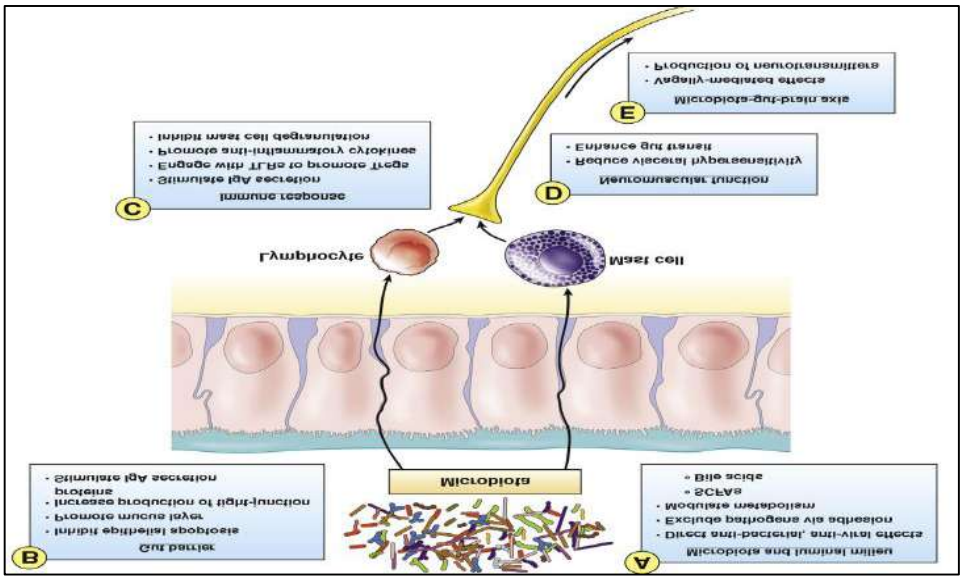

Figure 2. Probiotics mechanisms of action (37).

2.3. Microorganisms used as probiotics

In addition to preventing gastric ulcers, inhibiting the progression of disease, and stimulating the immune system both locally and systemically, probiotics have many effects, such as influencing the incidence of colorectal cancer and infectious diseases and allergies.

The manufacturing and preservation of foodstuffs, particularly dairy products, also made use of probiotics (38). Lactobacillus and Bifidobacterium are two types of microbes that should be addressed. These were of utmost importance because of their bacteriostatic action and their capacity to modulate the immunological function of the intestines. They produce enzymes including glucose-6-phosphate and lactate dehydrogenase, which enhance the bioavailability of dietary items. They also participate in the production of vitamin K and B vitamins (39).

2.4. Sources of probiotics

To improve consumer health and create novel probiotic products, it was necessary to isolate probiotic microbes from food. Many criteria determine whether microorganisms isolated from food have probiotic potential. These include the microbes' capacity to survive in the GI tract, colonize the intestinal tract, and create health-promoting metabolites (40).

The sources of probiotic bacteria in food were illustrated in Figure 3. Human probiotics often originate in dairy products, while animal probiotics were derived from the animals' own digestive systems (41). It was thought that probiotics derived from "unconventional sources" would gain in popularity. More and more people were looking for alternatives to dairy products to avoid consuming probiotics. In search of possible probiotics, we looked for bacteria in

unusual places, including the air, soil, and non-intestinal sources of fermentation, as well as in unfermented foods (fruits and vegetables) (42). A few writers have also noted the critical importance of collecting wild-type bacterial strains to diversify the library of LAB strains used in innovative product development (43).

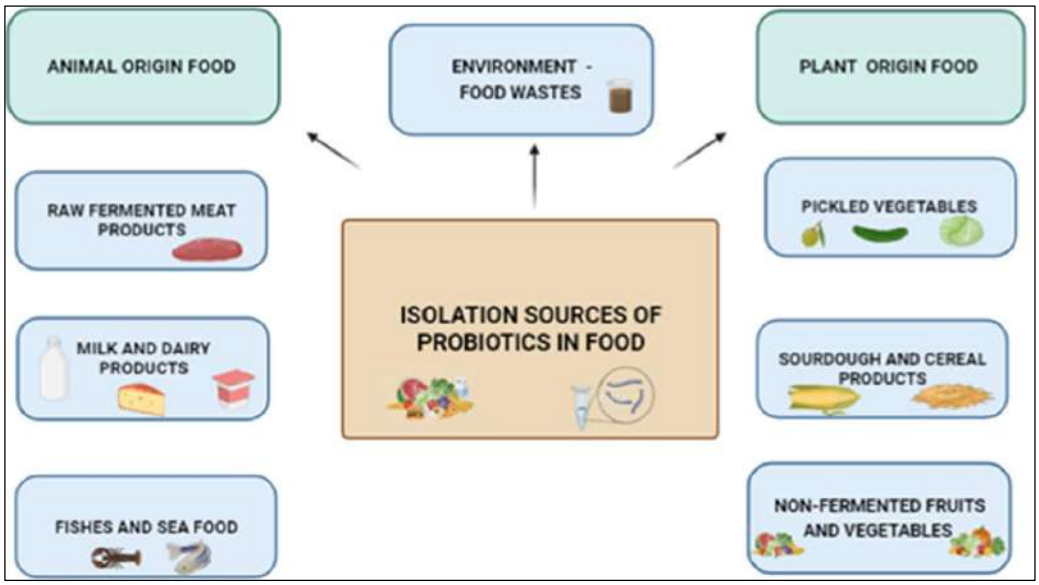

Figure 3. Probiotic microorganisms' source in food (41).

2.5. Repercussions in GI Disorders and Symptoms

While there is compelling data suggesting that the microbiota contributes to the development of several gastrointestinal illnesses and that prebiotic and probiotic qualities may be advantageous in treating these problems, the effectiveness of these interventions in clinical trials is presently only supported by limited evidence. Although there is an abundance of research, the lack of a standardized clinical design and the fact that studies differ in the products and formulations utilized, the study populations, and the outcomes have made it difficult to draw meaningful conclusions. This review does not aim to include all research on prebiotics, probiotics, and symbiotics for all gastrointestinal illnesses (44).

Systematic reviews of randomized trials or n-of-1 trials provided one degree of evidence, while mechanism-based reasoning provided the lowest level. In order to construct this grading system, the Oxford Centre for Evidence-Based Medicine (45). Level 1 indications for a specific probiotic or probiotic cocktail included avoiding antibiotic related diarrhea in different clinical evidence, lowering Helicobacter pylori eradication therapy side effects, preventing after operative sepsis in patients having high gastrointestinal disorder, keeping pouchitis in reduction, and reducing lactose maldigestion symptoms. Level 1 was obtained by lactulose in the therapy of liver encephalopathy, the only indication for prebiotics. Even though there are

additional systematic evaluations that supported the perfect effects of probiotics across a range of clinical situations, most of them are cautious when it comes to recommending them or cannot distinguish between species in terms of effectiveness because of data constraints (44).

2.5.1. Irritable bowel syndrome

When the make-up of the GIT microbiota changes, it can lead to (IBS). These case affects 10–20% of the people in developing nations. A person's style of life is greatly affected by the produced bain, which is abdominal pain due to decreased bowel activity, and frequent bloating (46). Constipation or diarrhea, bloating, gas, an increased need to defecate. Separation of (IBS) into types based on stool consistency study revealed three main manifestations: constipation, diarrhea, and a mixed type, unclassified type. The best approach to treating irritable bowel syndrome (IBS) is a multidisciplinary team effort that incorporates pharmaceutical and non-pharmaceutical measures.

Diastolic and antidiarrheal medications, gas-limiting agents, laxatives (lactulose), and spasmolytic and cholinolytic medications are all part of the pharmacological therapy (47). Patients were educated and encouraged to adjust their lifestyle, diet, and psychotherapy as part of the non-pharmacological treatment.

Due to a beneficial impact on the digestive system and makes defecation easier, modest, personally adjusted physical exercise should be the first thing modified after an irritable bowel syndrome diagnosis. Exercising regularly also lowers stress levels, which plays a role in illness onset and progression (48). Probiotics have been recognized as an increasingly important factor in combating symptoms of (IBS). Small intestinal bacterial overgrowth (SIBO) occurs when there is an excessive proliferation of primarily anaerobic bacteria in the jejunum of the small intestine.

This happens because the protective systems in the digestive tract are weakened. Furthermore, an elevated gastric pH is no longer able to sustain the optimal equilibrium of bacterial colonization in both the stomach and intestines. One factor contributing to the retention of an overabundance of germs in the small intestine is disorders of gastric motility. An imbalance in the production of immunoglobulin A (IgA) and mucus, together with ileocecal valve failure that allowed colonic bacteria to enter the small intestine, resulted in an absence of substances that strengthened microorganisms, leading to overgrowth of bacteria in the intestines. Gas, bloating, diarrhea (often watery or fatty), stomach discomfort, and weight loss were common clinical signs. Additional symptoms of the condition due to vitamin deficiencies

include neurological abnormalities, oedema, rickets, osteomalacia, and tetany. Issues with the immune system can lead to the development of parenteral symptoms such as redness, ulcers, inflammation of the osteochondral system, dermatitis, and inflammation of the kidneys and liver (49).

2.5.2 Excessive proliferation of microbes in the small intestine

An overabundance of mostly anaerobic bacteria in the jejunum because of compromised gastrointestinal defense systems is known as small intestinal bacterial overgrowth (SIBO). It is a breakdown in the delicate equilibrium between the bacterial colonization of the stomach and intestines due to an elevated gastric pH. Retentive extreme bacteria in the small intestine were influenced by disorders of stomach motility. Overgrowth of bacteria in the small intestine can be attributed to ileocecal valve malfunction, an imbalance in the production (IgA) and mucus, and a lack of substances that strengthen bacteria (50). Diarrhea (which can be either watery or fatty), gas, bloating, decreased appetite, and stomach discomfort are common clinical manifestations.

Vitamin shortages are another complication of the condition that can lead to rickets, osteomalacia, tetany, swelling, and neurological abnormalities. Ulcers, redness, inflammation of the osteochondral system, dermatitis, and inflammation of the kidneys and liver are all symptoms that might manifest as parenteral infusions when there is an immunological imbalance (51). Treatment for SIBO includes antibiotic medication, dietary changes, probiotics, supplementation with missing nutrients, and a reduction in the overabundance of bacteria in the intestines. Since there is a wide variety of microbes that might cause gastrointestinal problems, it is important to target both aerobic and anaerobic bacteria with antimicrobial treatment.

A wide range of medications should be used for this purpose. A low-lactose diet was frequently suggested to patients as a means of easing common gastrointestinal issues. Reducing dietary fat and, if desired, supplementing with medium-chain triglycerides fatty acids (MCT) were both essential. Deficiency supplementation with iron, fat-soluble vitamins, and vitamin B12 was another critical part of the therapy. Considering nutritional supplements is a good idea in cases of severe malnutrition and weight loss. An integral part of illness therapy is the use of probiotics, particularly Lactobacillus strains, which have been shown to successfully back up normal flora following antibiotic therapy and extend the duration of disease (52).

2.5.3 Pseudomembranous colitis

C. diff induced pseudomembranous colitis; whereby antibiotic therapy disrupted normal gut flora. Because of their surroundings', hospitalized patients were more likely to get C. diff, which most frequently caused distress for these patients. Once within the body, Clostridium difficile causes diarrhea and pseudomembranous colitis by multiplying and releasing toxins. Risk factors for the condition include being older, having surgery on the gastrointestinal system, having chronic inflammatory bowel disease, using rectal thermometers, or being on enteral nutrition (53). Pseudomembranous colitis is the most severe kind of C. diff infection; its main symptoms, consequences, and clinical picture are as follows: Another treatment option that was considered throughout the later illness decreases was fecal microbiota transplant (FMT). After the normal therapy failed, this kind of treatment was suggested.

The goal of FMT, an alternate treatment for C. diff infections, was to reestablish healthy microbiota and intestinal function by inoculating patients with fresh bacteria from a healthy donor. Bowel illnesses characterized by inflammation Ulcerative colitis (UC) and Crohn's disease (CD) were forms of (IBD) whose causes remained unclear. Acute exacerbation and remission are common features of the illness progression. IBS and its sequelae have gut microbiota problems as a contributing factor. Therapy efficacy and reduction maintenance were both enhanced by avoiding pathogenic alterations in microbiota (54).

2.5.4. *Helicobacter pylori* eradication

A ubiquitous resident of the stomach mucosa, Helicobacter pylori has been linked to gastric ulcers and gastric malignancies. On the other hand, H. pylori served a dual purpose: it was discovered that children who were in touch with the bacterium had a lower chance of developing atopic dermatitis (55). It has been designed that eliminating H. pylori due to associated with a higher likelihood of developing obesity (56).

Eliminating carriers was necessary due of its infectious nature. Research on the antagonistic effects of probiotics, especially Lactobacillus, on H. pylori in animals and in vitro has not been confirmed in human trials. Therefore, probiotics should not be thought of as a substitute for conventional treatment (57). Given the possible beneficial function of the organism, it may be better to use strains such *Lactobacillus johnsonii* La1 (58), which has been found to decrease H. pylori populations and activity. While not a cure-all, research shows that probiotics can improve traditional medication by lowering adverse effects, increasing compliance, and increasing success rate (72% vs. 82%) (59). In their consensus report on H.

pylori therapy, the experts at Maastricht IV also recommended this (60). Using *S. boulardii* is recommended (with a recommendation grade of D) in the Maastricht IV report. Similar processes to those for autoimmune Addison's disease (AAD) risk reduction may explain the beneficial impact of some probiotics on H. pylori eradication, but other variables appear to be involved as well.

2.6. Prebiotics

Essential in the battle against pathogens, prebiotics alleviated symptoms of allergies, decreased the likelihood of contracting *Clostridium difficile*, and eased the symptoms of travelers' diarrhea. IBS illness was also treated with prebiotics (61). Functional foods were the most prevalent source of prebiotics in the food supply. Every part must be just right for it to be considered a prebiotic food. To begin, foodstuffs must be impervious to the digestive enzymes found in the mouth, pancreas, and intestines. In addition, the gut microbiota might ferment it, which would promote the expansion and activity of the host's beneficial bacteria and aid in maintaining the host's health (62). Vegetables, fruits, cereals, nuts, seeds, and legumes are good sources of dietary fiber, which includes plant cell wall components such cellulose, hemicellulose, pectin, gums, and non-starch polysaccharides like lignin (63).

There were two types of dietary fiber, soluble and insoluble, each with its own unique role. The proper functioning of the digestive system is mostly impacted by insoluble dietary fiber (64). It increased the amount of stomach contents by binding water, which in turn enhanced peristalsis by irritating the walls of the large intestine. However, soluble dietary fiber helped treat diarrhea by releasing intestinal channel mucus and delivering energy to colonocytes through prolonged bacterial fermentation. The metabolism of lipids was also positively affected by dietary fiber (65). Numerous foods, including wheat, chicory, sunchoke, onions, garlic, tomatoes, and bananas, contain fructose polymers called fructtooligosaccharides (FOS).

One of the key prebiotics in these foods is oligofructose. Many "light" goods employ FOS as a sweetener alternative because of their subtle sweetness. In addition, fermented milk products include them. Oligofructose decreases the water activity of goods due to its hygroscopic qualities. According to estimates, the amount of Bifidobacteria in feces increases 5-10 times when 4-15 g of this drug is given to the body. This is because the proliferation of Bifidobacteria in the colon is caused by their digestion of fructooligosaccharides. Furthermore, Bifidobacteria dominance in gut microbiota was achieved even after a brief period of consuming a diet high in these components (66).

2.7. Novel Approaches Improving Probiotic Stability

Biofilms and lipid membranes are two novel approaches that can enhance the probiotics' stability (67). The formation of biofilms can be triggered by a variety of mechanisms governed by components of the extracellular matrix, which in turn are impacted by environmental variables and the reactions of bacterial communities (68). Biofilms are a promising new material for probiotic coatings due to their dual role as a physical adhesion enhancer and protective barrier. Applying a Bacillus subtilis biofilm on the surface of probiotics increased their distribution by 125 times, suggesting that bacterial biofilms might be utilized for gastrointestinal administration (67).

Currently, there exist uncomplicated and efficient methods for preserving probiotics, enabling the expedited creation of probiotic formulations in a significantly reduced timeframe, while safeguarding them from harsh conditions. Past research has shown that bacterial lipid membranes may be produced by vortexing E. coli and Staphylococcus aureus with a mixture of dimethyl benzoic acid and cholesterol (69). Their intestinal bioavailability rose fourfold, and the self-assembly process had no effect on the bacteria's bioactivity.

The results show that bacteria covered with supramolecular self-assembly are effective, and this method has promise for delivering probiotics. Intriguingly, the application of edible nanoparticles which did not harm the food matrix in any way—restored the bioavailability of the food's bioactive components and improved the compatibility of those components (67). Nanostructured particles offered an alternative to traditional methods of creating individualized probiotic delivery systems by allowing for the customization of pore size and breadth, which slowed the pace of release inside the digestive tract's hostile environment (68).

Conclusion

The articles propose that probiotics have health advantages in terms of preventing and decreasing the occurrence of various diseases, such as IBS, SIBO, Pseudomembranous Colitis, IBD, diarrhea, and the reduce of Helicobacter pylori in relation to the use of probiotics in digestive disorders.

References:

[1] Munir, A., Javed, G. A., Javed, S., and Arshad, N. (2022). *Levilactobacillus brevis* from carnivores can ameliorate hypercholesterolemia: *in vitro* and *in vivo* mechanistic evidence. *J. Appl. Microbiol.* 133, 1725–1742. doi: 10.1111/jam.15678

[2] Hamad, G. M., Amer, A., el-Nogoumy, B., Ibrahim, M., Hassan, S., Siddiqui, S. A., et al. (2022). Evaluation of the effectiveness of charcoal, Lactobacillus rhamnosus, and *Saccharomyces cerevisiae* as aflatoxin adsorbents in chocolate. *Toxins* 15:21. doi: 10.3390/toxins15010021

[3] Warman, D. J., Jia, H., and Kato, H. (2022). The potential roles of probiotics, resistant starch, and resistant proteins in ameliorating inflammation during aging (inflammaging). *Nutrients* 14:747. doi: 10.3390/nu14040747

[4] Fusco, A., Savio, V., Cimini, D., D'Ambrosio, S., Chiaromonte, A., Schiraldi, C., et al. (2023). *In vitro* evaluation of the most active probiotic strains able to improve the intestinal barrier functions and to prevent inflammatory diseases of the gastrointestinal system. *Biomedicine* 11:865. doi: 10.3390/biomedicines11030865

[5] Roobab, U., Batool, Z., Manzoor, M. F., Shabbir, M. A., Khan, M. R., and Aadil, R. M. (2020). Sources, formulations, advanced delivery and health benefits of probiotics. *Curr. Opin. Food Sci.* 32, 17–28. doi: 10.1016/j.cofs.2020.01.003

[6] Shehata, A. A., Yalçın, S., Latorre, J. D., Basiouni, S., Attia, Y. A., Abd el-Wahab, A., et al. (2022). Probiotics, prebiotics, and phytogenic substances for optimizing gut health in poultry. *Microorganisms* 10:395. doi: 10.3390/microorganisms10020395

[7] Shahverdi, E. (2016). Probiotics and gastrointestinal diseases. *Int. J. Dig. Dis.* 2, 1–2. doi: 10.4172/2472-1891.100022

[8] Saber, A., Alipour, B., Faghfoori, Z., and Yari Khosroushahi, A. (2017). Cellular and molecular effects of yeast probiotics on cancer. *Crit. Rev. Microbiol.* 43, 96–115. doi: 10.1080/1040841X.2016.1179622

[9] Su, S.-C., Chang, L. C., Huang, H. D., Peng, C. Y., Chuang, C. Y., Chen, Y. T., et al. (2021). Oral microbial dysbiosis and its performance in predicting oral cancer. *Carcinogenesis* 42, 127–135. doi: 10.1093/carcin/bgaa062

[10] Pereira-Marques, J., Ferreira, R. M., Pinto-Ribeiro, I., and Figueiredo, C. (2019). *Helicobacter pylori* infection, the gastric microbiome and gastric cancer. *Adv. Exp. Med. Biol* 1149, 195–210. doi: 10.1007/5584_2019_366

[11] Jang, W. J., Lee, J. M., Hasan, M. T., Lee, B. J., Lim, S. G., and Kong, I. S. (2019). Effects of probiotic supplementation of a plant-based protein diet on intestinal microbial diversity, digestive enzyme activity, intestinal structure, and immunity in olive flounder (*Paralichthys olivaceus*). *Fish Shellfish Immunol.* 92, 719–727. doi: 10.1016/j.fsi.2019.06.056

[12] Metchnikoff, E.; Mitchel, P.C. The Prolongation of Life: Optimistic Studies; G.P. Putnam's Sons: New York, NY, USA; London,UK, 1910

[13] Hill, C.; Guarner, F.; Reid, G.; Gibson, G.R.; Merenstein, D.J.; Pot, B.; Morelli, L.; Canani, R.B.; Flint, H.J.; Salminen, S.; et al. The International Scientific Association for Probiotics and Prebiotics consensus statement on the scope and appropriate use of the term probiotic. Nat. Rev. Gastroenterol. Hepatol. 2014, 11, 506–514.

[14] ISAPP. Minimum Criteria for Probiotics. Sacramento, CA: International Scientific Association for Probiotics and Prebiotics. Available online: https://isappscience.org/minimum-criteria-probiotics/ (accessed on 22 April 2023).

[15] Binda, S.; Hill, C.; Johansen, E.; Obis, D.; Pot, B.; Sanders, M.E.; Tremblay, A.; Ouwehand, A.C. Criteria to qualify microorganisms as "probiotic" in foods and dietary supplements. Front. Microbiol. 2020, 24, 1662. [CrossRef]

[16] Grom, L. C., Coutinho, N. M., Guimarães, J. T., Balthazar, C. F., Silva, R., Rocha, R. S., et al. (2020). Probiotic dairy foods and postprandial glycemia: a mini-review. *Trends Food Sci. Technol.* 101, 165–171. doi: 10.1016/j.tifs.2020.05.012

[17] Lilly DM, Stillwell RH. Probiotics. Growth promoting factors produced by micro-organisms. Science 1965; 147:747–748.

[18] Schrezenmeir J, de Vrese M. Probiotics, prebiotics, and synbiotics—approaching a definition. Am J Clin Nutr 2001; 73(Suppl):361S–364S.

[19] Food and Agriculture Organization of the United Nations and World Health Organization. Health and nutritional properties of probiotics in food including powder milk with live lactic acid bacteria. World Health Organization. 2001. Available at: http://www.who.int/foodsafety/publications/fs_management/en/ probiotics.pdf. Accessed October 29, 2018.

[20] Hill C, Guarner F, Reid G, et al. Expert consensus document. The International Scientific Association for Probiotics and Prebiotics consensus statement on the scope and appropriate use of the term probiotic. Nat Rev Gastroenterol Hepatol 2014; 11:506–514.

[21] Food Safety Authority of Ireland. Probiotic health claims. Available at: http://www.fsai.ie/faq/probiotic_health_claims.html: Accessed October 29, 2018.

[22] Salminen S, van Loveren H. Probiotics and prebiotics: health claim substantiation. Microb Ecol Health Dis 2012; 23:40–42.

[23] van Loveren H, Sanz Y, Salminen S. Health claims in Europe: probiotics and prebiotics as case examples. Annu Rev Food Sci Technol 2012; 3:247–261.

[24] Venugopalan V, Shriner KA, Wong-Beringer A. Regulatory oversight and safety of probiotic use. Emerging Inf Dis 2010; 16:1661–1665.

[25] Arora M, Baldi A. Regulatory categories of probiotics across the globe: a review representing existing and recommended categorization.Indian J Med Microbiol 2015;33(Suppl):2–10.

[26] Rachmilewitz D, Kayatura, Karmeli F, et al. Toll-like receptor 9 signaling mediates the anti-inflammatory effects of probiotics in murine experimental colitis. Gastroenterology 2004; 126:520–528.

[27] Kamiya T, Wang L, Forsythe P, et al. Inhibitory effects of Lactobacillus reuteri on visceral pain induced by colorectal distension in Sprague-Dawley rats. Gut 2006; 55:191–196.

[28] Gibson GR, Brummer RJ, Isolauri E, et al. The design of probiotic studies to substantiate health claims. Gut Microbes 2011; 2:299–305.

[29] Binnendijk KH, Rijkers GT. What is a health benefit? An evaluation of EFSA opinions on health benefits with reference to probiotics. Benef Microbes 2013; 4:223–230.

[30] Plaza-Diaz, J., Ruiz-Ojeda, F. J., Gil-Campos, M., and Gil, A. (2019). Mechanisms of action of probiotics. *Adv. Nutr.* 10, S49–S66. doi: 10.1093/advances/nmy063

[31] Ahire, J., Jakkamsetty, C., Kashikar, M. S., Lakshmi, S. G., and Madempudi, R. S. (2021). *In vitro* evaluation of probiotic properties of *Lactobacillus plantarum* UBLP40 isolated from traditional indigenous fermented food. *Probiotics Antimicrob Proteins* 13, 1413–1424. doi: 10.1007/s12602-021-09775-7

[32] Fantinato, V., Camargo, H. R., and Sousa, A. L. O. P. (2019). Probiotics study with Streptococcus salivarius and its ability to produce bacteriocins and adherence to KB cells. *Rev Odontol UNESP* 48, 1–9. doi: 10.1590/1807-2577.02919

[33] Chang, Y., Jeong, C. H., Cheng, W. N., Choi, Y., Shin, D. M., Lee, S., et al. (2021). Quality characteristics of yogurts fermented with short-chain fatty acid-producing probiotics and their effects on mucin production and probiotic adhesion onto human colon epithelial cells. *J. Dairy Sci.* 104, 7415–7425. doi: 10.3168/jds.2020-19820

[34] Bu, Y., Liu, Y., Liu, Y., Wang, S., Liu, Q., Hao, H., et al. (2022). Screening and probiotic potential evaluation of bacteriocin-producing *Lactiplantibacillus plantarum in vitro*. *Foods* 11:1575. doi: 10.3390/foods11111575

[35] Petruzziello, C., Saviano, A., and Ojetti, V. J. V. (2023). Probiotics, the immune response and acute appendicitis: a review. *Vaccines* 11:1170. doi: 10.3390/vaccines11071170.

[36] Gangaraju, D., Raghu, A. V., and Siddalingaiya Gurudutt, P. J. N. S. (2022). Green synthesis of γ-aminobutyric acid using permeabilized probiotic *Enterococcus faecium* for biocatalytic application. *Nano Select* 3, 1436–1447. doi: 10.1002/nano.202200059

[37] Quigley EMM. Bifidobacteria as probiotic organisms. An introduction. In: Floch MH, Ringel Y, Walker MA, eds. The Microbiota in Gastrointestinal Pathophysiology. London: Elsevier Academic Press, 2017:125–126.

[38] Masood MI, Qadir MI, Shirazi JH, et al. Beneficial effects of lactic acid bacteria on human beings. Crit Rev Microbiol 2011; 37: 91-98.

[39] Steinka I. Wybrane aspekty stosowania probiotyków. Ann Acad Med Gedan 2011; 41: 97-108.

[40] Cristofori, F.; Dargenio, V.N.; Dargenio, C.; Miniello, V.L.; Barone, M.; Francavilla, R. Anti-inflammatory and immunomodulatory effects of probiotics in gut inflammation: A door to the body. Front. Immunol. 2021, 12, 178.
[41] Sornplang, P.; Piyadeatsoontorn, S. Probiotic isolates from unconventional sources: A review. J. Anim. Sci. Technol. 2016, 58, 26.
[42] Schoster, A.;Weese, J.S.; Guardabassi, L. Probiotic use in horses—What is the evidence for their clinical efficacy. J. Vet. Intern. Med. 2014, 28, 1640–1652. [CrossRef]
[43] Poltronieri, P.; Rossi, F.; Cammà, C.; Pomilio, F.; Randazzo, C. Genomics of LAB and Dairy-Associated Species. In Microbiology in Dairy Processing: Challenges and Opportunities; Poltronieri, P., Ed.; Wiley and Sons: Hoboken, NJ, USA, 2017; pp. 71–95. Available online: https://www.wiley.com/enus/Microbiology+in+Dairy+Processing%3A+Challenges+and+Opportunities-p-97811191 14987 (accessed on 20 April 2023).
[44] Guarner F, Sanders ME, Eliakim R, et al. Probiotics and prebiotics. World Gastroenterology Organisation Global Guidelines. 2017. Available at: http://www.worldgastroenterology.org/User Files/file/guidelines/probiotics-and-prebiotics-english-2017.pdf. Accessed October 29, 2018.
[45] Goldenberg JZ, Lytvyn L, Steurich J, Parkin P, Mahant S, Johnston BC. Probiotics for the prevention of pediatric antibiotic-associated diarrhea. Cochrane Database Syst Rev 2015;12:CD004827.
[46] OCEBM levels of evidence. Available at: http://www.cebm.net/ index.aspx?o¼5653; 2016:Accessed October 29, 2018.
[47] Staudacher HM, Lomer MCE, Anderson JL, et al. Fermentable carbohydrate restriction reduces luminal Bifidobacteria and gastrointestinal symptoms in patients with irritable bowel syndrome. J Nutr 2012; 142: 1510-1518.
[48] Mulak A, Waszczuk E. Zaburzenia czynnościowe jelit, zespół jelita nadwrażliwego. In: Paradowski L (ed.). Zaburzenia czynnościowe przewodu pokarmowego. Cornetis, Wrocław 2012; 105-117.
[49] Gugała-Mirosz S. Zespół jelita nadwrażliwego – leczenie multidyscyplinarne. Żyw Człow Metab 2013; 40: 47-53.
[50] Gugała-Mirosz S. Wpływ różnych składników żywności na dolegliwości zespołu jelita drażliwego. Żyw Człow Metab 2013; 40: 39-45.
[51] Mrukowicz JZ. Choroby jelita cienkiego – zespół przerostu flory bakteryjnej jelita cienkiego. In: Konturek SJ (ed.). Gastroenterologiai hepatologia kliniczna. Vol. 5. PZWL, Warszawa 2006; 270-271.
[52] DiBaise JK. Nutritional consequences of small intestinal bacterial overgrowth. Pract Gastroenterol 2008; 12: 15-28.
[53] Gerding DN. Choroba związana z zakażeniem Clostridium difficile wraz z rzekomobłoniastym zapaleniem jelit. In: Rydzewska G (ed.). Gastroenterologia i hepatologia. Vol. 1. Czelej, Lublin 2012; 283-287.
[54] Jarosz M, Kożuch M. Wrzodziejące zapalenie jelita grubego, choroba Leśniowskiego-Crohna. In: Jarosz M (ed.). Praktyczny podręcznik dietetyki. Instytut Żywności i Żywienia, Warszawa 2010; 242-248.
[55] Seiskari T, Kondrashova A, Viskari H, et al; EPIVIR Study Group. Allergic sensitization and microbial load – a comparison between Finland and Russian Karelia. *Clin Exp Immunol*. 2007;148(1):47–52.
[56] Nwokolo CU, Freshwater DA, O'Hare P, Randeva HS. Plasma ghrelin following cure of Helicobacter pylori. *Gut*. 2003;52(5):637–640.
[57] Franceschi F, Cazzato A, Nista EC, et al. Role of probiotics in patients with Helicobacter pylori infection. *Helicobacter*. 2007;12(Suppl 2):59–63.
[58] Cruchet S, Obregon MC, Salazar G, Diaz E, Gotteland M. Effect of the ingestion of a dietary product containing Lactobacillus johnsonii La1 on Helicobacter pylori colonization in children. *Nutrition*. 2003; 19(9):716–721.
[59] Zhang MM, Qian W, Qin YY, He J, Zhou YH. Probiotics in Helicobacter pylori eradication therapy: a systematic review and meta-analysis. *World J Gastroenterol*. 2015;21(14):4345–4357.

[60] Malfertheiner P, Megraud F, O'Morain CA, et al; European Helicobacter Study Group. Management of Helicobacter pylori infection – the Maastricht IV/Florence consensus report. *Gut*. 2012;61(5):646–664.
[61] Rastall RA, Gibson GR. Recent developments in prebiotics to selectively impact beneficial microbes and promote intestinal health. Curr Opin Biotech 2015; 32: 42-46.
[62] Scheid MMA, Moreno YMF, Junior MRM, et al. Effect of prebiotics on the health of the elderly. Food Res Int 2013; 53: 426-432.
[63] Górska S, Jarząb A, Gamian A. Bakterie probiotyczne w przewodzie pokarmowym człowieka jako czynnik stymulujący układ odpornościowy. Postepy Hig Med Dosw 2009; 63: 653-667.
[64] Kordyl M, Libudzisz Z. Mikroflora jelitowa – znaczenie i modulacja. Żyw Człow Metab 2006; 33: 266-278.
[65] Cao, Z.; Wang, X.; Pang, Y.; Cheng, S.; Liu, J. Biointerfacial Self-Assembly Generates Lipid Membrane Coated Bacteria for Enhanced Oral Delivery and Treatment. Nat. Commun. 2019, 10, 5783. [CrossRef] [PubMed]
[66] Tolker-Nielsen, T. Biofilm Development. Microbiol. Spectr. 2015, 3, 51–66. [CrossRef]
[67] Wang, X.; Cao, Z.; Zhang, M.; Meng, L.; Ming, Z.; Liu, J. Bioinspired Oral Delivery of Gut Microbiota by Self-Coating with Biofilms. Sci. Adv. 2020, 6, eabb1952. [CrossRef]
[68] Sampathkumar, K.; Tan, K.X.; Loo, S.C.J. Developing Nano-Delivery Systems for Agriculture and Food Applications with Nature-Derived Polymers. iScience 2020, 23, 101055. [CrossRef]
[69] McClements, D.J. Nanotechnology Approaches for Improving the Healthiness and Sustainability of the Modern Food Supply. ACS Omega 2020, 5, 29623–29630. [CrossRef]

Natural and Artificial Radioactivity Estimation for Different types of Pasta Samples in Baghdad City

Hiba Al-Hameed [1]

Huda Abdul Jabbar Hussein [2]

Abstract

Pasta is a dry, hollow pastry, made from cereals such as wheat, rice, barley. It is a diet rich in carbohydrates for various age groups. Pasta's natural and synthetic radionuclide concentrations measured four samples from various locations were selected from the Baghdad city markets. The uranium - radium and thorium series ^{40}K and ^{137}Cs gamma emitter radionuclides have been measured for concentration using the high purity Germanium detector (HpGe). Every sample's spectrum was examined for two hours. The following was the range of particular activity for the radionuclides under study: ^{238}U, ^{232}Th, ^{40}K, and ^{137}Cs have average concentrations of 15.58 Bq/kg, 0.63 Bq/kg, 12.93 Bq/kg, and 0.22 Bq/kg, respectively. The amounts of ^{238}U, ^{232}Th, ^{40}K, and ^{137}Cs that correspond to the yearly effective dosage external AEDE are 7.9 mSv.y^{-1}, 2.6 mSv.y^{-1}, 1.6 mSv.y^{-1}, and 0.306 mSv.y^{-1}.

Keywords: *Natural radioactivity, Gamma spectroscopy, Annual effective dose, Thorium, Uranium* .

http://dx.doi.org/10.47832/RimarCongress04-9

[1] Department of Physics, College of science for Women, University of Baghdad, Baghdad, Iraq
heba.musadek @csw.uobaghdad.edu.iq

[2] Department of Physics, College of science for Women, University of Baghdad, Baghdad, Iraq
huda.a@csw.uobaghdad.edu.iq

Introduction:

Natural and man-made radioactivity are the two main categories. Natural radioactivity can be generated by either Earth's crustal radioactive elements or alien sources. Research centers, industrial facilities, and nuclear power plants all emit a substantial amount of artificial radioactivity. [1]. Numerous radioisotopes can be found in nature; they were created both during solar system formation and as a result of cosmic rays interacting with atmospheric molecules. The ionizing radiation that permeates the natural world continuously is known as background radiation. Food and drinking water both naturally contain trace levels of radioactive materials. For example, radioactive materials are commonly found in soil and ground water used for vegetable cultivation. These minerals cause internal exposure to natural radiation once consumed.

The chemical and biological characteristics of naturally occurring radioactive isotopes, including ^{40}K and ^{14}C, are identical to those of their non-radioactive counterparts. Our bodies are constructed and maintained with the help of these radioactive and non-radioactive materials. Naturally occurring radioisotopes are ubiquitous in many foods and cause us to be exposed to radiation all the time. Activities involving radioactive material and medical procedures also expose people to radiation created by humans. Nuclear reactors produce radioisotopes as a by-product, and devices like cyclotrons can also make radioisotopes.

The domains of nuclear medicine, biochemistry, manufacturing, and agriculture all make extensive use of man-made radioisotopes [2]. To provide humans with an adequate level of protection, the radioactivity level would be monitored and the radiation threats would have to be assumed. This study's objective is to determine the radioactivity of commonly used pasta samples in Baghdad and assess the potential health risks associated with them. Pasta samples were gathered and the activity of ^{238}U, ^{232}Th, ^{40}K and ^{137}Cs content have been measured by using γ-ray spectroscopy [3].

Material and Methods

1. Sample collection and preparation

For this investigation, a total of six pasta samples were taken from the local market in Baghdad, Iraq, and their natural and artificial radioactivity was analysed. Since pasta is originally dry and moisture-free because it is vacuum-packed, the samples were first ground into powder and sieved to create homogenous samples. Each sample was then weighed and put

into a bag with a corresponding label, and the samples were then measured and put into plastic flasks, with a final weight of 0.5 kg.

2. Sample counting

The natural and artificial activity of pasta samples were measured by using detector high purity germanium (HPGe) with efficiency 40% and the spectra for each sample were analysed for (3600 sec) [4].

The system was calibrated for energy by using isotope ^{60}Co with resolution of (2.0 keV) at 1173, 1332 keV respectively. The energy calibration of spectrum for isotope ^{60}Co of the detector system is displayed in Figure 1 [5, 6].

The activity concentration can be calculated by using equation:

$$A = \frac{c}{m.I.\varepsilon.t} \quad \ldots\ldots\ldots\ldots\ldots \quad (1)$$

In this context, A represents the specific activity concentration in Bq/kg, C stands for the net area under the curve, m for the mass of the sample in kg, I for the efficiency and emission possibility of γ-ray, and ε for the absolute efficiency at energy intake. The units of measurement are E and t. (sec).

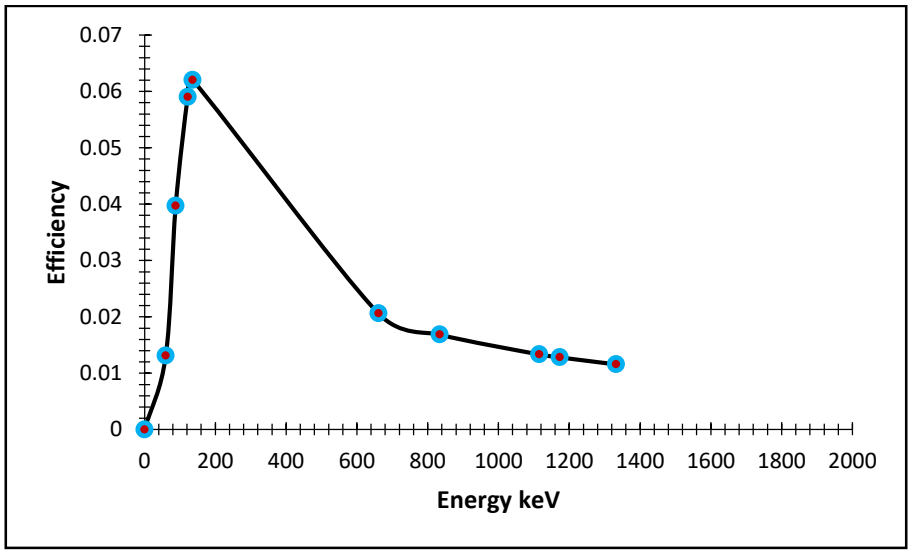

Figure 1. A calibration spectrum for ^{60}Co source

Results and Discussion

The pasta samples exhibit low and high levels of radioactivity for various detected radionuclides; the activity concentration of the pasta has been measured, and the findings have been organized in Table 2, 3 correspondingly. The coding samples of various local sites are displayed in Table 1. According to the results, sample A2 had the highest radioactivity of ^{28}U

at 17.34 Bq / kg, while sample A1 had the lowest activity concentration at 13.4 Bq / kg. The average mean value of radioactivity levels was 15.58 Bq / kg. For ^{238}Th, sample A1 had the highest value at 0.92 Bq / kg, and sample A3 had the lowest value at 0.34 Bq / kg with an average mean value of 0.63 Bq / kg. With an overall mean value of 12.93 Bq / kg, the activity for ^{40}K varied from 10.3 Bg / kg in sample A3 to 14.43 Bq / kg in sample A1. In sample A2, the activity concentration of ^{137}Cs was as low as 0.14 Bq / kg, while sample A4 had the highest value of 0.35 Bq / kg, with an average of 0.22 Bq/ kg. Figures 2, 3, 4 and 5 show sample numbers in relation to activity concentration.

Table1. Coding of sampling Location

No	Sample Code
1	**A1**
2	**A2**
3	**A3**
4	**A4**

Table 2. Activity concentration of different natural and artificial isotopes^{238} U, ^{232}Th, ^{40}K, ^{137}Cs in (Bq/kg) for the pasta samples

Sample's Code	^{238} U Bq / kg	^{232}Th Bg/ kg	^{40}K Bq / kg	^{137}Cs Bq / kg
A1	**13.4**	**0.92**	**14.43**	**0.27**
A2	**17.34**	**0.58**	**13.2**	**0.11**
A3	**15.54**	**0.38**	**10.3**	**0.14**
A4	**15.62**	**0.63**	**13.82**	**0.35**
Average	**15.58**	**0.63**	**12.93**	**0.22**

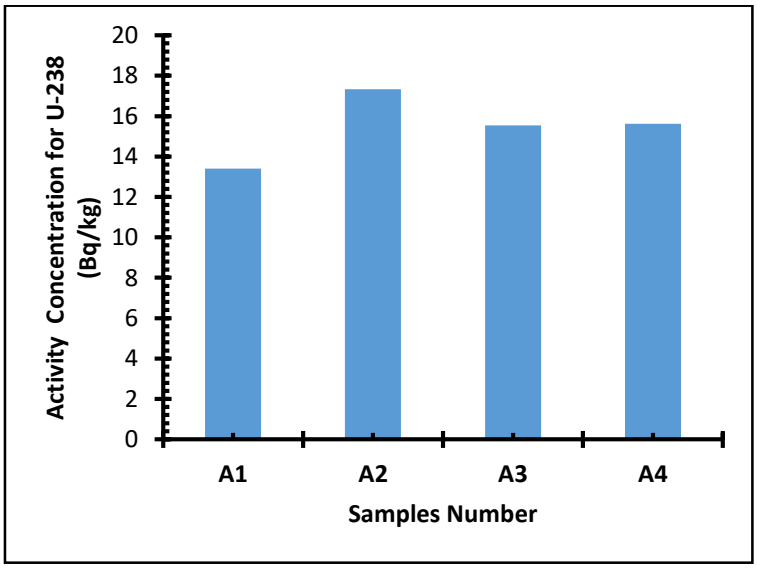

Figure 2. Activity concentration of ^{238}U

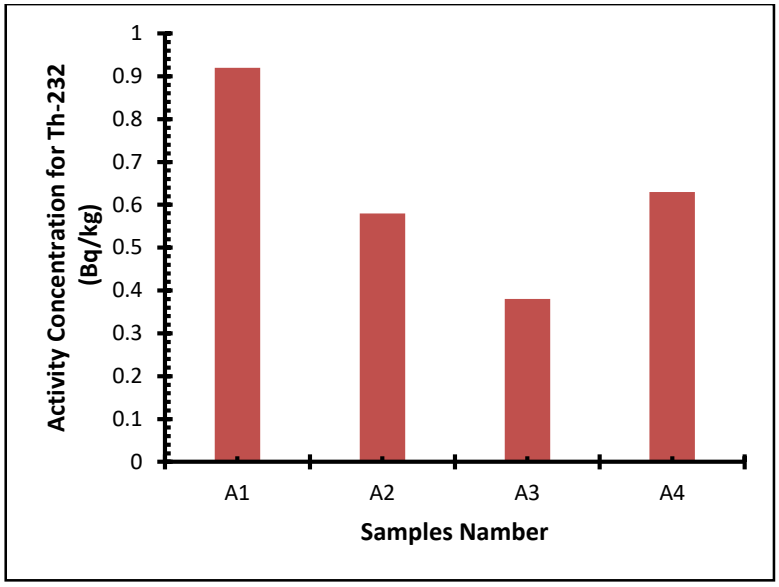

Figure 3. Activity concentration of ^{232}Th

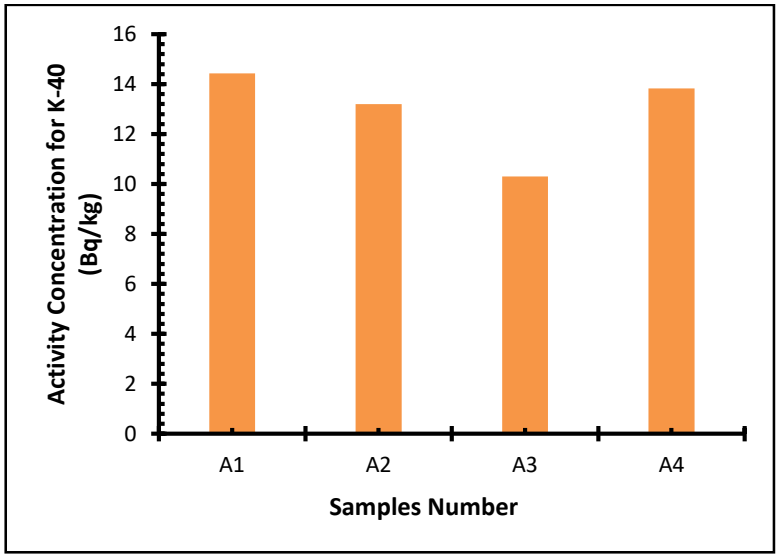

Figure 4. Activity concentration of ^{40}K

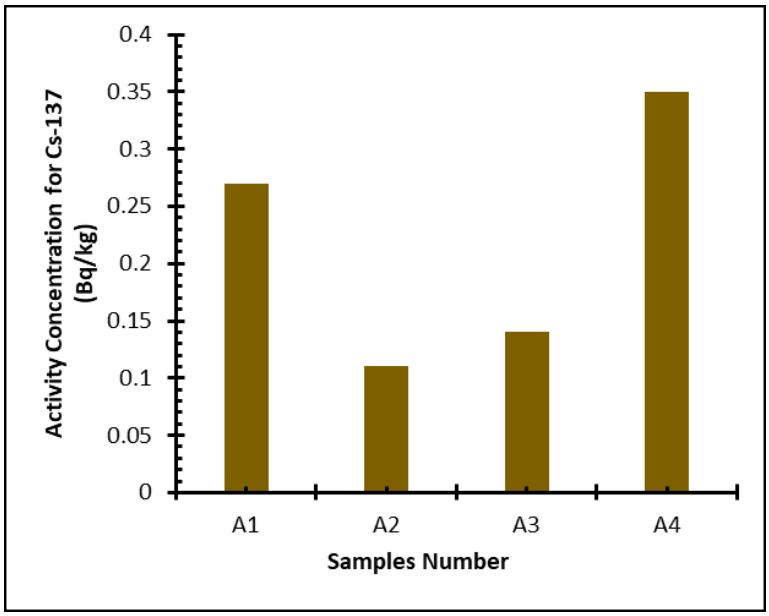

Figure 5. Activity concentration of ^{137}Cs

Table 3. Absorbed dose rate in pasta samples of different natural isotopes

Sample's Code	AEDE ^{238}U	AEDE ^{232}Th	AEDE ^{40}K
A1	**6.84**	**3.86**	**1.56**
A2	**8.85**	**2.43**	**1.63**
A3	**7.94**	**1.59**	**1.49**
A4	**7.98**	**2.64**	**1.79**
Average	**7.9**	**2.6**	**1.6**

The average value of ^{232}Th 2.6 mSv/y with range between 1.59-3.86 mSv/y and the average value of ^{40}K 1.6 mSv/y with range between 1.49-1.63 mSv/y are all measurements with the natural limits. Compute the Annual Effective Dose Equivalent, or AEDE, internal using equation 2 and is shown in Figure 6 Table 4 displays the average value of ^{234}U 7.9 mSv/y with the highest value of 8.85 and the lowest value of 6.84.

$$\boldsymbol{AEDE(Sv.y^{-1}) = Absorbed\ dose(nGy/h) \times 8760\,h/y \times 0.7(Sv/Gy) \times 0.8 \times 10^{-6}} \quad \text{..... (2)}$$

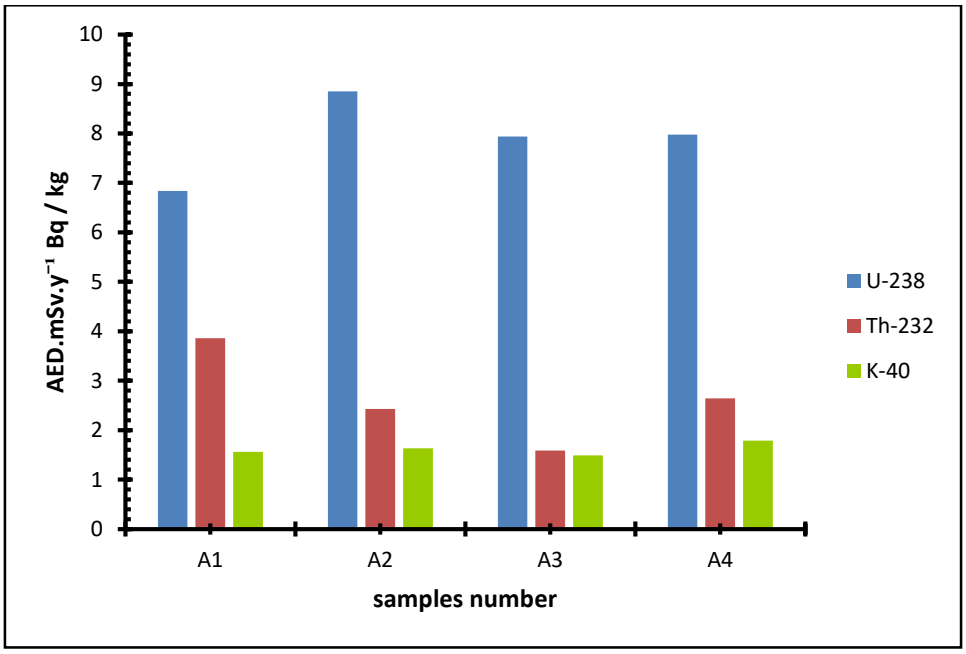

Figure 6. The Annual Effective Dose Equivalent AEDE internal of ^{238}U, ^{232}Th, ^{40}K for pasta samples

The estimated ^{137}Cs values in 4 samples of pasta with average value 0.306mSv/y and the range of measurements between 0.142-0.492 mSv/y as shown in table 4 and Fig 7 [8, 9, 10, and 11].

Table 4. Absorbed dose rate in pasta samples of ^{137}Cs

Sample's Code	AEDE ^{137}Cs
A1	**0.335**
A2	**0.492**
A3	**0.142**
A4	**0.256**
Average	**0.306**

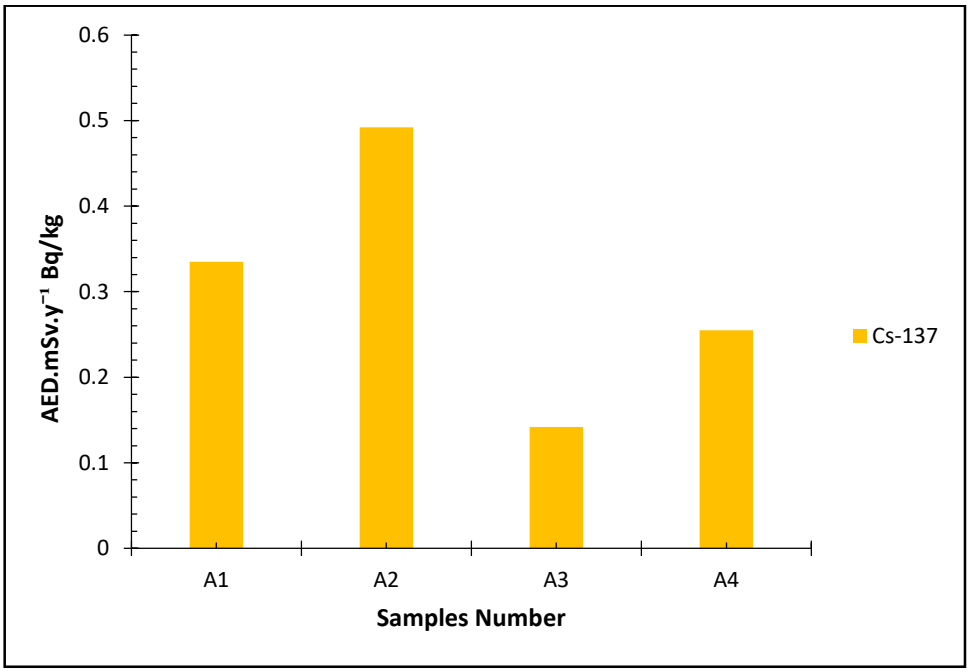

Figure 7. The Annual Effective Dose Equivalent AEDE internal of ^{137}Cs for pasta samples

Conclusion

The following is a list of the most important discoveries:

1. The results might be seen as an indication of the amounts of natural background radiation that have been monitored.
2. The activity concentrations of ^{238}U, ^{233}Th, ^{40}K, and ^{137}Cs sample locations were found to be within the global range, and the yearly effective doses were found to be within the world median ranges during examination.
3. The measurements were conducted with utilizing of a HpGe detector.
4. The maximum effective dosage per year that remains within the international safety standards.

References:

[1] K. A. Kabir, S. M. A. Islam and M. M. Rahman, "Distribution of Radionuclides in Surface Soil and Bottom Sediment in the District of Jessore, Bangladesh and Evaluation of Radiation Hazard," Journal of Bangladesh Academy of Science, Vol.33, No.1, 2009.

[2] Introduction to Radiation , Canadian Nuclear Safety Commission, 2012

[3] A. B.Mavi, H. Akyildirim and K.Gunoglu, Natural radioactivity of coals and its risk ,assessment, International journal of Physical Science, 2009.

[4] IAEA, "Generic procedures for monitoring in a nuclear or radiological emergency, IAEA-TECDOC-1092, 2000.

[5] M.S.Aswood , M.SC Physics , University of Babylon , 2003.

[6] K. Abbas, F. Simonelli, F. D. Alberti, M. Forte and M.F. Stroosnijder, Reliability of two calculation codes for efficiency calibrations of HPGe detectors, Applied Radiation and Isotopes, 2002.

[7] T.A.El-Daly and A.S. Hussein, Natural radioactivity levels in environmental samples in north western desert of Egypt, Environmental Physical Conference, Aswan, Egypt, 2008.

[8] IAEA, International Atomic Energy Agency, Measurement of Radionuclides in Food and Environment, a Guidebook, Technical Reports. 1989; 295 (230).

[9] Maitham S. Radiation Hazard Index of Common Imported Ceramic Using for Building Materials in Iraq. Aust J Basic Appl Sci. 2017; 11(10): 94-102.

[10] Hiba M. Salim Al-Hameed, Measurement of Radioactivity in Marsh Sediments of South Iraq, IOSR Journal of Applied Physics,2018,10(3) :43-49

[11] Basim Khalaf Rejah, Specific Activities of Natural Radionuclides and Annual Effective Dose Due to the Intake of Some Types of Children Powdered Milk Available in Baghdad Markets, Baghdad Science Journal, 2017.


150

مؤتمر ريمار الدولي الرابع للعلوم الصرفة والتطبيقية

IV. International Rimar Congress of Pure, Applied Sciences

ISBN 978-625-95642-9-6

Rimar Academy Publishing House